Streamer branching: conformal mapping and regularization

Bernard Meulenbroek

Streamer branching:
conformal mapping and regularization

PROEFSCHRIFT

door

Bernardus Joannes Meulenbroek

geboren te Voorburg

Dit proefschrift is goedgekeurd door de promotor:

prof.dr. U.M. Ebert

Copromotor:
prof.dr. J. Hulshof

Contents

Chapter 1

Introduction

The spontaneous formation of patterns occurs in nature on all lengthscales; the inhomogeneous distribution of galaxies in the universe and the shape of a single snowflake are extreme examples. Moving ionization fronts that create the plasma body of sparks are on a scale somewhere inbetween. One of the striking aspects of pattern formation is that completely different systems may give rise to similarly looking patterns, the spiral shapes observed in chemical reaction patterns and galaxies are well known examples. This can be exploited in the analysis of those patterns, since it allows the use of similar mathematical techniques. This thesis will focus on so-called moving boundary problems: two bulk phases separated by an interface. Determining the motion of the interface is usually the most challenging aspect of the problem. Well known examples of moving boundary problems are dendritic growth, combustion fronts, growth of bacterial colonies and viscous fingering. A moving boundary approximation for streamers will be derived in this thesis. The investigation is inspired by the literature on viscous fingering. Since we will restrict the study to two dimensions, conformal mapping can be applied.

A major problem in such a moving boundary approximation is the regularization mechanism; it took several decades to prove that surface tension was the appropriate mechanism in viscous fingering. We have derived a new, possibly regularizing mechanism for our moving boundary problem. The important question whether this condition is indeed regularizing will be investigated.

1.1 Organization of this thesis

The first chapter of my thesis is dedicated to the physical problem: streamer propagation and branching. A minimal PDE model for streamers is introduced; results of numerical simulations of the full model are given. The main mathematical question of this thesis is formulated: can the minimal model describe streamer propagation and branching? The computations suggest a certain approach for the analysis: the derivation of a moving boundary problem from the

PDE model. We will study the problem in 2D; this allows us to use conformal mapping. The general description of this method is given in Chapter 3. A moving boundary approximation has been used in many problems, mentioned in the previous section. Especially the problem of viscous fingering is well studied in the literature. A short review of a part of the literature on this subject is given at the end of Chapter 3. The application of the machinery developed earlier leads to the problem of finding the temporal behaviour of the so-called mapping function. This mapping function contains all information about the temporal evolution of the interface. In this thesis, the boundary will be between the ionized and the non-ionized regions.

An equation of motion for the mapping function is studied in Chapter 4. Cusp formation is inevitable; this is not due to the mathematical method, but signals the fact that something is missing in the moving boundary approximation. A mechanism is required to regularize the short lengthscales and prevent the formation of cusps. In viscous fingering, surface tension is used as a regularization mechanism. It is more difficult to find the correct regularization mechanism for the ionization fronts.

In Chapter 5 a possible regularization is derived, namely a boundary condition which is streamer specific and derived from the microscopic PDE's. This condition depends on the width ϵ of the interface. Implementation of this condition turns out to be difficult. In the two following chapters of my thesis I try to answer the question whether this new condition is indeed regularizing the problem or not.

First I decide to look close to the cusps; suppose the interface starts near a cusp, is the condition enough to prevent the formation or not. The unregularized case from Chapter 4 is revisited briefly; cusp formation is shown to be inevitable. If the new condition is imposed, regularization can happen, but further investigation is required.

This is done in Chapter 7. Uniformly translating circles are found to be solutions, both for the regularized and the unregularized problem. Will a small perturbation of the circle cause a breakdown of the solution or not? The stability of the unregularized circle is studied, and we see that the unregularized circle is unstable, as expected. We learn more from this case, though. It is not possible to use an expansion in temporal eigenmodes to get the correct information regarding the stability. This turns out to be the case in the regularized problem as well. A truncated expansion in Fourier modes leads to the incorrect conclusion that only purely imaginary eigenvalues exist. If a PDE is derived and solved a different result is obtained. The circle is linearly convectively stable: perturbations may grow initially, but are convected away to the back where they are damped out. In viscous fingering this convective stability has been observed numerically and experimentally; we can get further since we are able to solve the PDE analytically for a particular value of the regularization parameter ϵ, $\epsilon = 1$. The analytical solutions are a gauge point for the numerical code which needs to be developed to study the case $0 < \epsilon < 1$. The last section of Chapter 7 is devoted to the comparison of the numerical results to the analytic solution for the linear stability analysis.

In the last chapter, results of the planar fronts are given. A different regularization mechanism containing the same physical information is derived. Whether this mechanism will regularize and/or give the same outcome as the boundary condition derived in Chapter 5 is an open question and requires further investigation. Furthermore, the dispersion relation for an ionization front with electron diffusion is derived that could be embedded in a stronger regularizing boundary condition than investigated in the rest of the thesis.

Chapter 2

The physical problem: streamer propagation and branching

This section will guide you from natural phenomena in the atmosphere via experiments to simulations of the minimal streamer model. Physics is typically reductionistic; this is already clear from the 'minimal': reality is modelled which a few (essential) processes. The question is of course whether a model is reduced too far.

Starting from the particle level, PDE's for the densities have been derived. Those PDE's can be solved numerically, but I will try to reduce the model one step further in this thesis. I will use a moving boundary approximation to describe the streamer.

This means that we have gone through two model reductions; from the particles to the PDE's and from the PDE's to a moving boundary approximation. Describing experiments would require a third model reduction in order to describe the total pattern. The question is of course whether the model reductions are too severe and whether all essential processes are taken into account: does the minimal model still capture the correct physics. Is the minimal streamer model able to describe branching?

2.1   Discharges in nature

Lightning is one of the most impressive phenomena in nature. It was not earlier than 1990 that many phenomena above thunderstorms were recorded, although their possible existence was already predicted in 1925 by Wilson [1]. Those events have been named transient luminous events (TLE's); this term covers a variety of phenomena. An overview is given in figure 2.1.
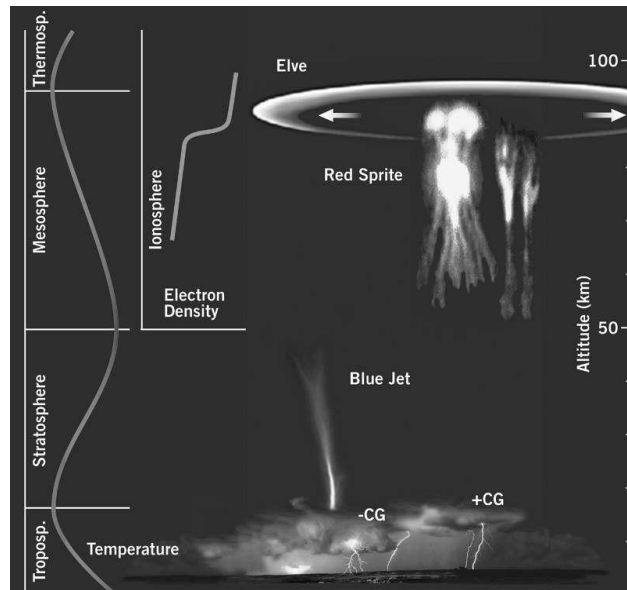
Figure 2.1: An overview of the different Transient Luminous Events

On top of a thundercloud, between 10 and 40 km, so called blue jets, fountains of blue light, can be observed. Sprites, propagating downwards toward the thundercloud and upwards toward the base of the ionosphere (at 90 km) and elves spreading in the lateral direction in the ionosphere have been recorded. Gigantic jets propagating upwards from the cloud were reported only a few years ago by Pasko [3], [4].
A lightning stroke occurs after the charge separation in the cloud and removes a considerable part of the charge, leaving a net charge with can be either positive or negative. The charge creates an electric field above the cloud, which allows TLE's if it is larger than some threshold value. Based on those arguments, sprites would be expected after both positive and negative cloud to ground lightning but have been reported (almost) exclusively after positive lightning. This is one of the (many) unsolved problems.
It is natural to wonder why those events were reported and recorded only in the last two decades and not before, especially since the possibility of the existence of sprites was already put forward eighty years ago. Observation of those effects from the ground is difficult due to the presence of clouds and the brighter lightning flashes: they can easily be missed if you do not know exactly where to look. Furthermore, one needs a clear sky to be able to look above the thunder cloud.
All those phenomena form an essential part of the global electric circuit, which can be seen as a capacitance consisting of two concentric spheres: the conducting surface of the earth and the ionosphere can be considered as the two plates

of a capacitance. Since TLE's contribute to charge transport between the plates
of the capacitance, they should be taken into account when describing the global
electric circuit [2].

All the phenomena described above are examples of gas discharges: a non-
conducting medium is exposed to a strong electric field, which accelerates a few
electrons. Those are able to either ionize neutral molecules, thus generating
more free electrons and causing a chain reaction, or to excite molecules. The
excited molecules return to the ground state by emission of a photon. Those
photons can be observed and allow us to actually see the gas discharge. This
is the basic idea of the local process, but an attempt to describe or explain the
rich variety of gas discharges which are observed on top of thunderclouds needs
some model reductions. An important picture towards a better understanding
was made by Gerken, who took pictures of sprites showing more details about
the structure.
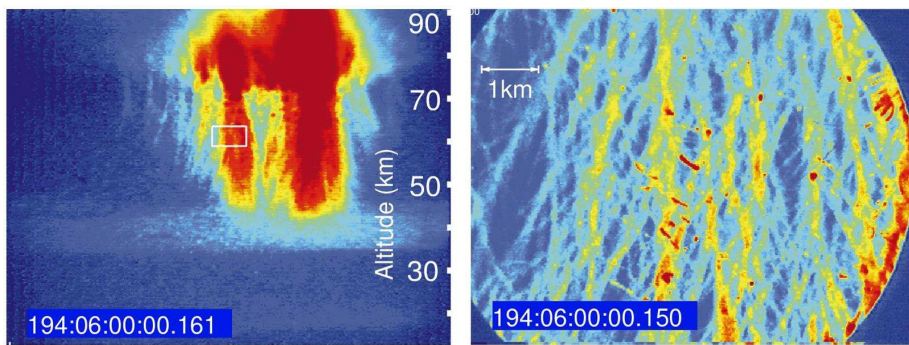
Figure 2.2: Telescopic images of sprites [5].

Figure 2.2 was published in [5] and reveals that the sprite contains a lot of
channels. Those channels are probably similar to so called streamer channels. A
precise definition of a streamer will be given later, for now it suffices to see it as
an ionized channel, which is conducting, with a propagating head containing the
charge. Those streamers can be considered as the building blocks, understanding
them is imperative if one wants to understand the full phenomenon. The study
of those streamers, starting from the microscopic theory, is the purpose of this
thesis.

2.2 Towards the experiments: scales and results

When studying a physical phenomenon, it is desirable to have accurate exper-
imental data. The observations of sprites do not fullfill this requirement for
obvious reasons; it is difficult to measure e.g. partical densities or electrical
fields, one can not change the experimental parameters (e.g. gas composition)

and the events can not be deliberately triggered, but only observed from a distance. At first sight, lab experiments seem an impossible task due to the huge scales (of order kilometers) involved in sprite discharges. But the experimentalist is saved by the scaling of space, as will be explained in the next section.

2.2.1 Scaling space and time

At the heights on which sprites are observed, the density of air is much lower than on the ground. Geophysicists usually use the empirical formula:

$$N = N_0 10^{-h/14km}, \tag{2.1}$$

where N and N_0 are densities at height h and at ground pressure. This means, that at typical sprite heights of about 70 km, the density is a factor of 10^5 lower. (Exact values are not important for this argument.) This means that an electron can travel much further before colliding with a molecule; the mean free path is much longer. Distances should be measured in terms of the mean free path, they become much shorter on the ground, a streamer of 1 km at 70 km would correspond to a streamer of 1 cm on the ground. Energy is measured in terms of the ionization energy for nitrogen (so does not scale); this means that the electric potential and the kinetic energy, thus the velocity of the electrons are not scaling. But this is wonderful for the experimentalist; the values of the electrical potential (in order of kV) are easily attainable so streamers should be observed when applying those voltages to air. And indeed, anyone can generate sparks with e.g. a van de Graaf generator. There is one problem though concerning good observation of the streamers: the time scales. The velocity does not scale, which means that time has to scale with a factor 10^5, too: streamers become much 'shorter' in time as well. Their lifetime is in the nano (10^{-9}) second regime. This poses experimental problems; one has to use a fast camera to be able to record the streamer and one has to know exactly where and when to look.

2.2.2 Experimental setup and results

As an example I will give a sketch of experiments on streamers which have been recently performed in Eindhoven by Tanja Briels and Eddie van Veldhuizen. A schematical picture of their setup is given in figure 2.3:
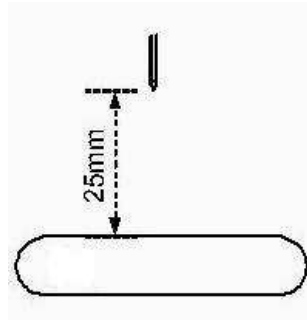
Figure 2.3: A schematic picture of the experimental setup: streamers are initiated at the needle electrode above and propagate downwards to the plate electrode [6].

The width of the gap, the electric field, gas composition and the pressure can be varied. The streamer starts after a fast increase of the voltage from the point of a needle, so place and time of occurence are known. The results are recorded with a fast CCD-camera. An example is shown in figure 2.4.
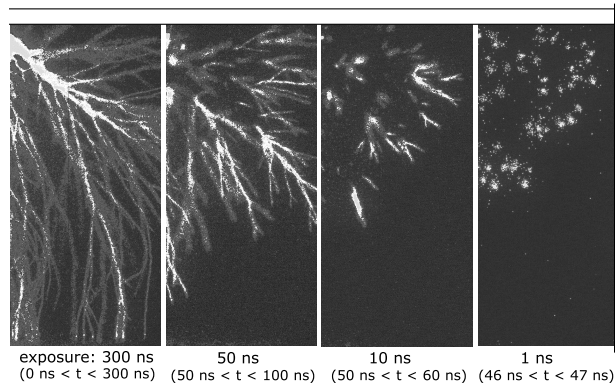
Figure 2.4: Experimental results; when the exposure time of the camera is decreased, one observes that only the tips of the streamers are emitting light.

Those pictures are taken from [6]; see this ref. for more details on the experiments. I will focus on those aspects that are the most important for comparison with theory.
If the exposure time of the camera is large, one observes a highly branched structure; reducing the exposure time reveals that only the tips of the channels

are actually emitting light. This means that the streamers consist of two parts: an active head with a lot of energetic ionizing electrons and an ionized tail.

2.3   Modelling streamers: the minimal streamer model

When describing a physical phenomenon, one usually uses a model which neglects certain processes. If one wants to include all possible chemical reactions in air and all electrodynamic effects in a model, there are two major problems. The number of points from the spatial discretization is simply too large for the CPU of a computer. Even when much more sophisticated computers or algorithms would be used (in the future), another more fundamental problem is encountered. A lot of reaction rates are not known. It is possible to get any outcome if you are allowed to use many fit parameters; the physical meaning is doubtful. Such an approach is based on brute (computational) force and fails to clarify which processes are the essential ones.

We would like to study the streamer problem with a minimal number of physical parameters in order to be able to study the essential features of propagation of negative streamers in non-attaching gasses. It is very important to realize which assumptions are made; I will discuss and justify those assumptions in the next section. The translation of the model in mathematical terms is standard and will be done in section 2.3.2.

2.3.1   Discussion of the model

The minimal model includes only two charged species, electrons and ions. The electron density will be denoted by σ and the ion density by ρ. An electron can create another electron and an ion by impact ionization:

$$e^- + N_2 \rightarrow 2e^- + N_2^+. \tag{2.2}$$

This means that attachment of electrons is neglected and no negative ions can be formed. Experimentally, this models a non-attaching gas like nitrogen or argon. The density of nitrogen is assumed to be constant, which is valid since the amount of ionized molecules is only about 10^{-5}; the change in density of neutral nitrogen is indeed negligible. The increase in electron density depends strongly on the local electric field; the electrons need to be fast enough to be able to ionize a molecule. This functional dependence is measured experimentally and fit with a function $f(E)$. We will use this function; as we will see later on, the exact functional form is not very important anyway. The approximation made is called the Townsend approximation.

The electrostatic Maxwell equations are used to describe the time evolution of the charged species and the electric field. This means that magnetic effects are neglected; there is a magnetic field, since there are currents, but it does not couple back to the dynamical equations since it is too weak. See ref. [9] for an

estimate of the magnetic field.

The most important point is, that this is a model for a negative streamer (propagating in the direction of the anode). In nature, both positive and negative streamers occur.

After the discussion of the assumptions, the introduction of the model in mathematical terms is straightforward and will be given in the next section.

2.3.2   The model in mathematical terms

First of all there are continuity equations for the electrons and the ions:

$$\partial_t \sigma + \nabla \cdot \mathbf{j}_e = \text{source}, \tag{2.3}$$

$$\partial_t \rho + \nabla \cdot \mathbf{j}_+ = \text{source}, \tag{2.4}$$

where σ denotes the electron density and ρ the ion density. The source terms are equal since electrons and ions are created in pairs. Since the electrons move much faster than the ions, the latter are considered immobile:

$$\mathbf{j}_+ = 0 \tag{2.5}$$

and the electrons drift and diffuse:

$$\mathbf{j}_e = -\sigma \mathbf{E} - D\nabla\sigma. \tag{2.6}$$

The source term is given by the Townsend approximation, as discussed before:

$$\text{source} = \sigma|\mathbf{E}|e^{-1/|\mathbf{E}|}. \tag{2.7}$$

Additional electrons are only created if both electrons and an electric field are present ($\sigma|\mathbf{E}|$). Furthermore, the electric field has to exceed a certain treshold, $|\mathbf{E}| > 1$ in dimensionless units; it has to overcome the ionization energy. The Poisson equation for the electrical field:

$$\nabla \cdot \mathbf{E} = \rho - \sigma \tag{2.8}$$

completes the model, which is now fully deterministic. Given an electron and ion density, the electric field is determined via the Poisson equation. This in term determines the right hand side of the dynamical equations for the electrons and ions. Notice, however, that those equations are strongly nonlinear as soon as a non-negligible charge density is present. For future reference it is convenient to introduce the electric potential ϕ and to summarize the minimal streamer model:

$$\partial_t \sigma - \nabla(\sigma \mathbf{E} + D\nabla\sigma) = \sigma|\mathbf{E}|e^{-1/|\mathbf{E}|}, \tag{2.9}$$

$$\partial_t \rho = \sigma \mathbf{E} e^{-1/|\mathbf{E}|}, \tag{2.10}$$

and

$$\nabla \cdot \mathbf{E} = \rho - \sigma, \quad \mathbf{E} = -\nabla \phi. \tag{2.11}$$

Numerical analysis of the full PDE-model is discussed in Section 2.4 and analysis of so called planar solutions is presented in Chapter 8.

Finally I note that all variables are non-dimensionalized. The natural scales are mean free path of the electrons l_{ion} and the ionization energy E_{ion}. The velocity scale is the electron drift velocity at this field, $v_0 = \mu_e E_{ion}$, leading to a time unit $t_0 = \frac{l_{ion}}{v_0} = \frac{l_{ion}}{\mu_e E_{ion}}$ and a charge unit $q_0 = \epsilon_0 E_{ion}/l_{ion}$. For N_2 at normal (ground) pressure, the values are listed as:

$$\begin{array}{ll} l_{ion} \approx 2.3 \ \mu \ \mathrm{m}, & v_0 \approx 7.56 \cdot 10^7 \ \mathrm{cm/s} \\ t_0 \approx 3 \cdot 10^{-12} \ \mathrm{s} & q_0 \approx 4.7 \cdot 10^{14} \ \mathrm{e} \ /cm^3 \\ E_{ion} \approx 200 \ \mathrm{kV/cm} & \mu_e \approx 380 \ cm^2/\mathrm{Vs}. \end{array} \tag{2.12}$$

2.4 Numerical analysis of the minimal streamer model

A method to solve the PDE's (2.9)-(2.11) is as follows: discretize space in N^3 points, where N needs to be large enough, fix the potential at $z = 0$ and $z = L$ to mimic the electrodes. Since we want to eliminate the effect of lateral boundaries, the boundary conditions at $x, y = 0$ and $x, y = L_{x,y}$, L_x and L_y should be taken large enough. Take as an initial condition e.g. a single electron close to the cathode ($z = 0$) and calculate the electric potential on the whole computational domain. The electric potential yields the electric field which in turn gives you the right hand side of the continuity equations for electrons and ions. Take a timestep, update the position of the space charges and repeat the whole procedure. This turns out to be difficult in 3D after space charge effects become important and sharp fronts are formed, since too many points are required. To get (partly) rid of this problem, one can solve the equations in 2D instead. In high fields with steep fronts, even this becomes inaccurate on uniform grids. Carolynne Montijn imposed cylindrical symmetry on the solutions, which means that they become essentially 2D and she furthermore implemented adaptive grid refinement within her thesis [7] that allows for very accurate computations. I did some numerical simulations in 2D, which means that the variation in the densities and the electric field in one direction, e.g. the x-direction, are neglected. Most of the numerical results are on the cylindrical case; the results and pictures are from the thesis of Carolynne [7].

2.4.1 Boundary conditions and initial conditions

The equations are transformed from (x, y, z) to (r, ϕ, z) and assumed to be independent of ϕ. Results can be plotted in the (r, z) plane but keep in mind that all of them are radially symmetric around $r = 0$. Electrodes are set at $z = 0$ and $z = L$, which means that the potential is specified. The streamer

propagation should not be influenced by the (artificial) boundary conditions for $r = \pm R$, which means that R should be taken large enough: the streamer should not approach R. The numerical routine requires boundary conditions on the electron and ion density as well. Usually Neumann conditions are imposed on the cathode, allowing inflow of electrons. The other conditions do not matter, since we stop the computation before the streamer and thus the electrons reach the anode. The initial condition is a small package of electrons close to the cathode. For a detailed discussion about the numerical procedure, see ref. [7].

2.4.2   Avalanche and streamer phase: branching?

Initially, the electric field is not altered by the presence of the space charge; this means that equations (2.9) and (2.10) are essentially linear. Electrons drift toward the anode, generating more ion-electron pairs. An avalanche of electrons is created, moving toward the anode. This can be seen in the numerical simulation, see figure 2.5. The increasing space charge will generate its own elecric field; at a certain point, the effect of the space charge on the total field is not negligible anymore. A thin space charge layer at the tip of the streamer arises and the electric field behind the head is effectively screened by the presence of the charge: the streamer becomes a conductor with a head surrounded by a thin negative space charge layer (and a tail with positive charge). From now on, the problem is strongly nonlinear, since the electric field couples, via the source term and the drift term, in a very nonlinear way back to the continuity equations for the electrons and ions. The simulation can be continued further, and one observes that the head of the streamer becomes unstable and branches, shown in figure 2.7. Simulations in 2D instead of 3D with cylindrical symmetry have been done as well; the results are shown in figures 2.8 and 2.9. The branching instability is observed in this case as well.

The problem is, of course, whether this is instability is numerical or whether there is a real physical instability within this model. This question was particularly pressing as many streamer experts believed that streamer branching in our deterministic fluid model was a numerical artifact. Actually the numerical approach in the thesis of C. Montijn and the present analytical study have been developed in parallel. Meanwhile the numerics convincingly demonstrates that the branching instability persists on finer grids. This approch is complemented by the present thesis that studies streamer evolution analytically in a reduced interfacial approach. Furthermore analytical results can easily be extended to larger systems where computations again might break down. The central question which I try to answer in this thesis is: can I formulate and solve an interfacial model that gives us complementary reliable information on streamer evolution and branching?
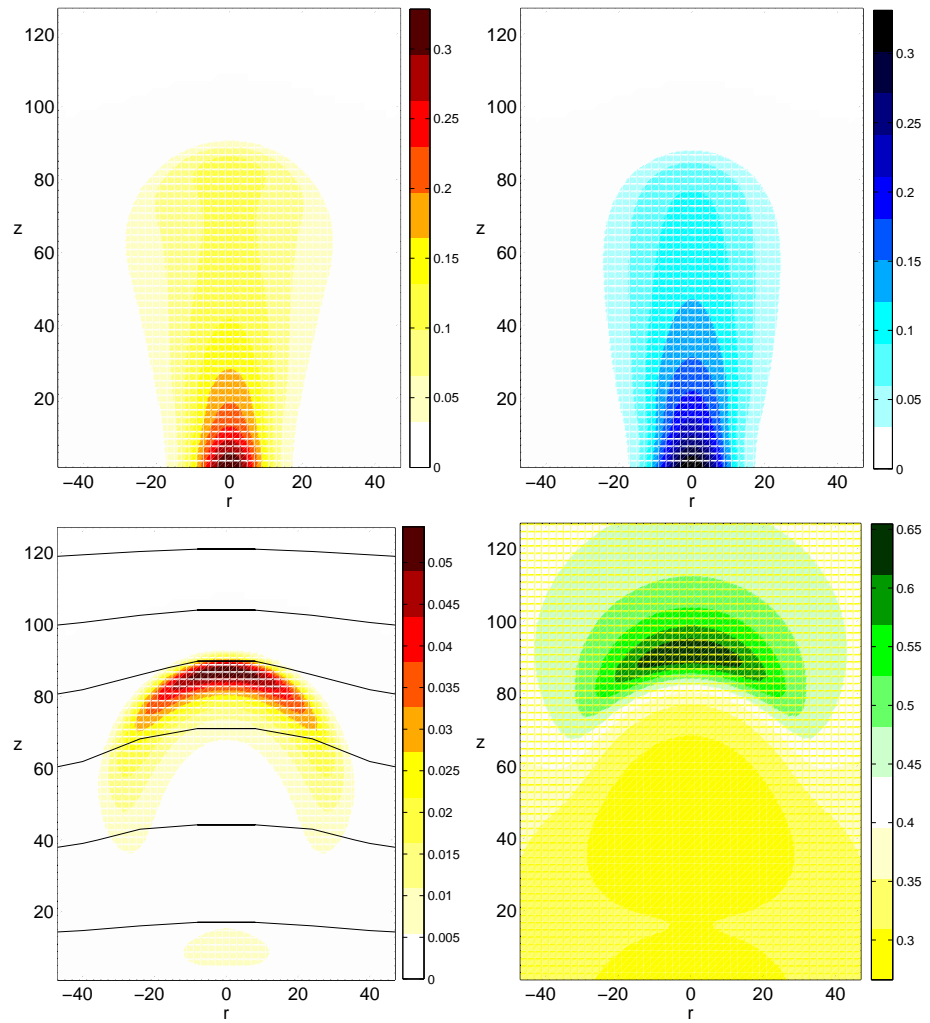
Figure 2.5: The first stage: the formation of a streamer out of the avalanche phase [7]; the density of the electrons and ions are presented in the upper part of the figure, the net charge with the equipotential lines and the electric field in the lower part.
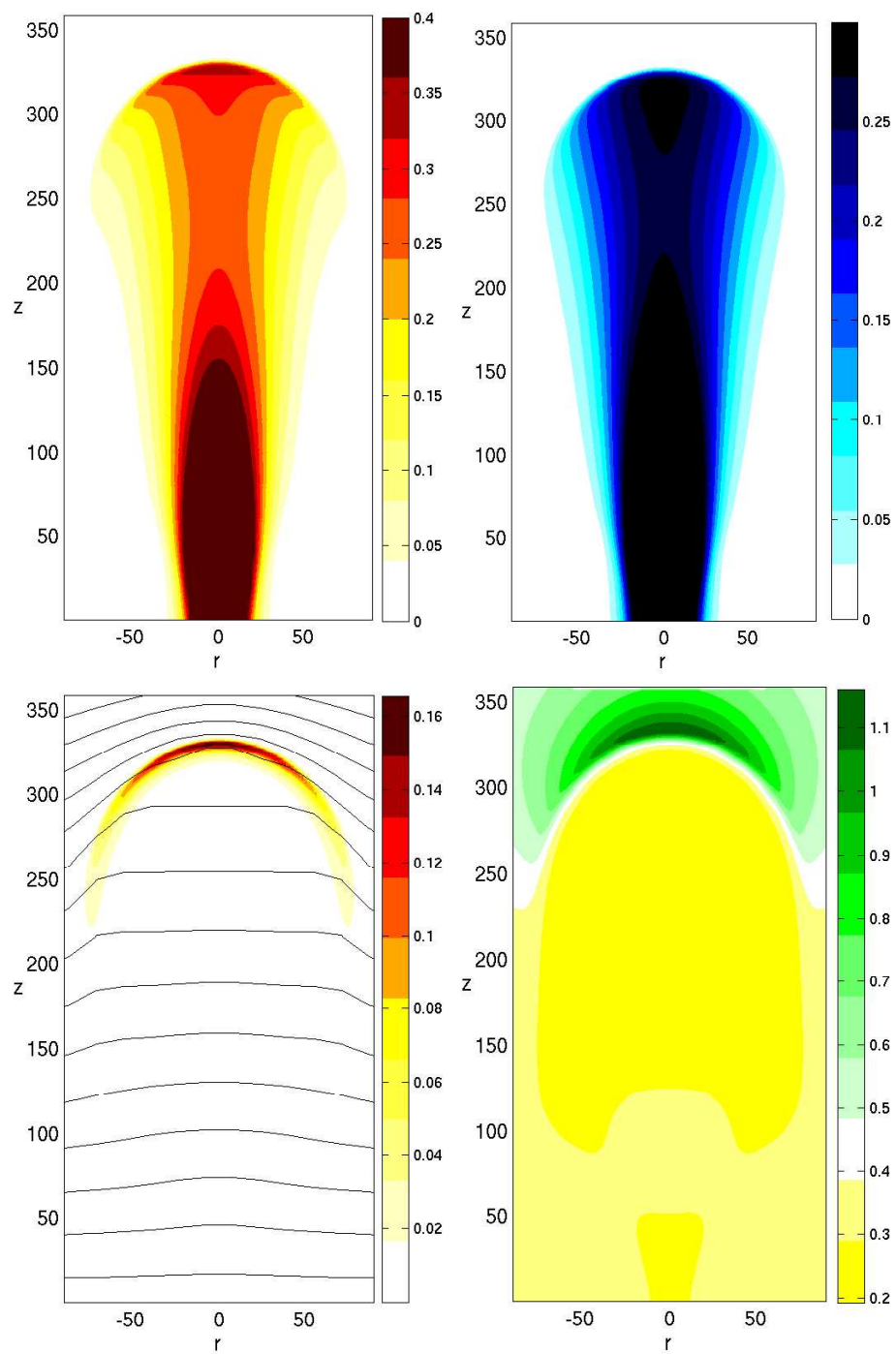
Figure 2.6: The second stage: the streamer phase: electric field is changed due to the formation of a thin space charge layer at the streamer tip [7].
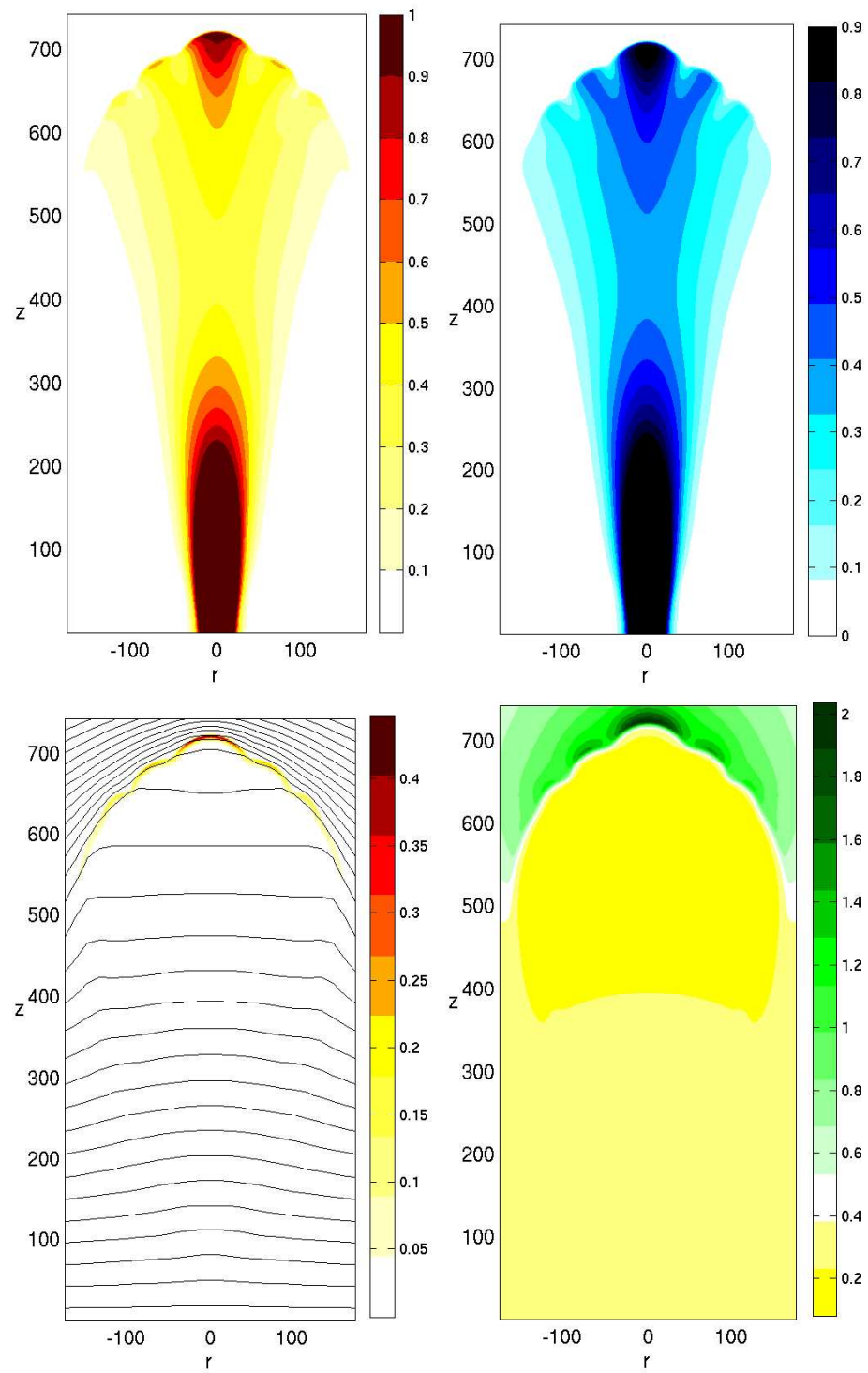
Figure 2.7: The final stage: branching of the streamer.
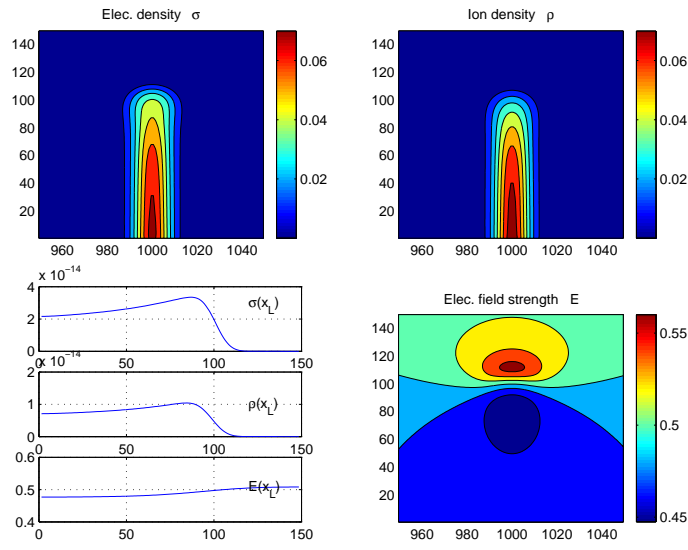
Figure 2.8: Simulations in 2D in a background field of $E = 0.5$; $T = 200$ electron and ion density are shown in the upper panels, the electric field in the lower panel on the right. Below: $T = 300$.
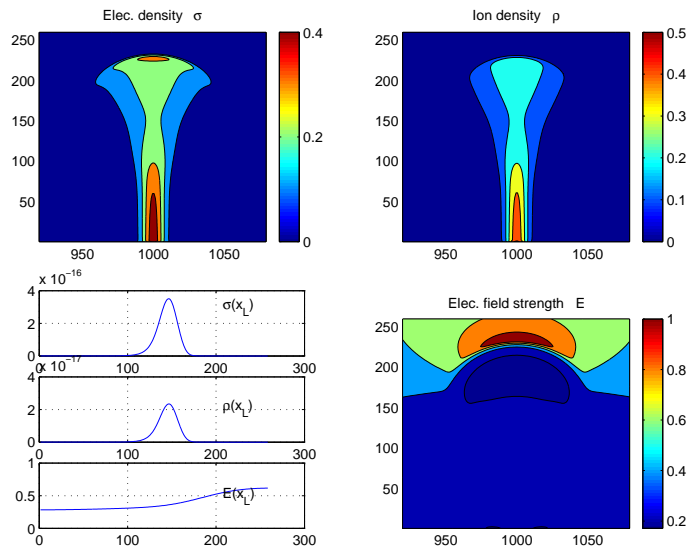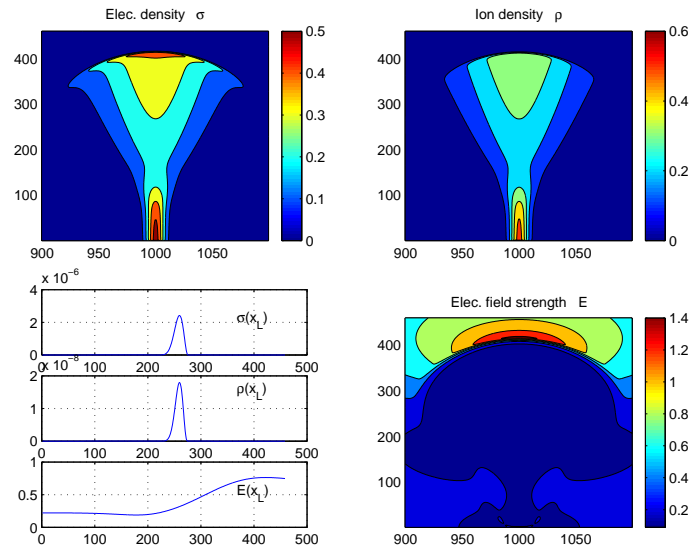
Figure 2.9: The same simulations, now $T = 400$ above and $T = 500$ below; branching is observed.
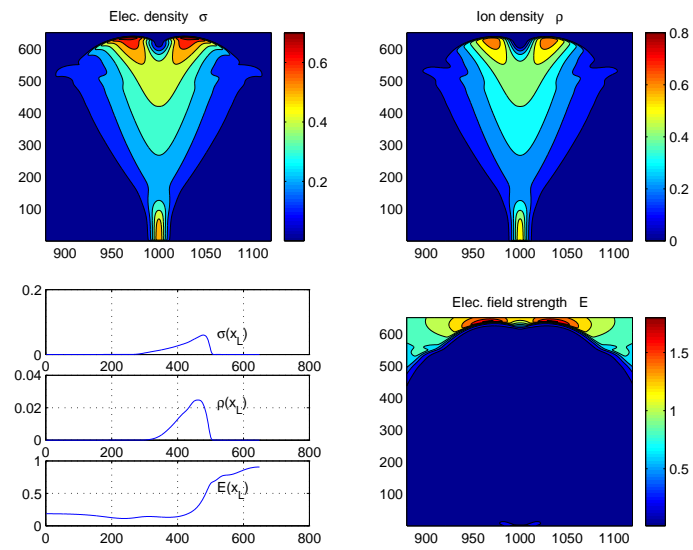
Chapter 3

The mathematical problem

The essential tools of the mathematical analysis will be presented in this chapter. The central idea is the separation of the problem in two scales; the so called inner and outer scale of the problem. Examining the numerical simulations reveals that there are essentially two regions, separated by a narrow boundary layer. If we zoom in on the charge layer, we can neglect the curvature from the global structure. This means that the geometry is greatly simplified, which allows a full analysis. This analysis of the inner scale was already done in [9] and results in an effective dynamical condition for the outer scale. On the outer scale, the boundary layer becomes infinitely thin and will be taken as a mathematical line. The information about the structure of the inner scale is transferred into an effective dynamical condition for the outer scale.

The analysis of the inner scale will be given in section 3.2. In section 3.3 the outer scale is analyzed and a moving boundary problem (MBP) is derived. Conformal mapping is a very powerfull tool to analyze the MBP; this concept will be introduced in section 3.4. The form of the mapping function and an equation of motion for the mapping function are derived.

The MBP is similar to a well studied MBP: viscous fingering. A literature study of this problem will be presented in the last section of this chapter.

Since the whole chapter relies heavily on complex analysis, I will give a short review of the results used in this thesis first.

3.1 General complex analysis

In this section we will summarize some important properties from complex analysis. We will give some theorems too (without proof), since we will use them extensively in this chapter.

Let us define the complex variable $z = x + iy$ in the usual way. We will study complex functions $f(z) : G \to \hat{\mathbb{C}}$, where G is some open subset of $\hat{\mathbb{C}}$. Notice that G corresponds to some open subset in $\mathbb{R}^2$ as well, we will denote this set

by G'. In general, $f(z)$ will have a real and imaginary part:

$$f(z) = u(x, y) + iv(x, y), \tag{3.1}$$

where $u(x, y)$ and $v(x, y)$ are real functions from G' into $\mathbb{R}$.

3.1.1 Analytic functions

Definition $f(z)$ is analytic if it has a derivative for all $z_0 \in G$.
To illustrate the importance of analytic functions, we will list some of the properties.

Theorem 1 *Let $f(z)$ be analytic in a simply connected region G and let C be a closed contour in G:*

$$f^{(n)}(z) = \frac{n!}{2\pi i} \int_C \frac{f(\zeta)}{(\zeta - z)^{n+1}}. \tag{3.2}$$

Notice that one retrieves Cauchy's integral formula by substiting $n = 0$. Theorem 1 implies that an analytic function can be written as a Taylor series:

$$f(z) = \sum_{k=0}^{\infty} a_k (z - z_0)^k, \tag{3.3}$$

where

$$a_k = \frac{f^{(n)}(z_0)}{n!}. \tag{3.4}$$

Equation (3.3) follows directly from equation (3.2).
A composition of analytic functions is analytic:

Theorem 2 *If $f(z) : G_1 \rightarrow G_2$ and $g(z_1) : G_2 \rightarrow G_3$ are analytic, $h(z) = g(f(z)) : G_1 \rightarrow G_3$ is analytic.*

We are now ready to turn our attention to a smaller class of analytic functions, to the conformal mappings.

3.1.2 Conformal mappings

Definition An analytic function $f(z)$ is conformal in G if $f'(z) \neq 0 \ \forall z \in G$.
We will use the following property of conformal mappings:

Theorem 3 *$f(z)$ is conformal and injective if and only if $f(z)$ is biholomorphic.*

(biholomorphic: bijective, analytic and analytic inverse).
Notice that all our definitions are valid only for open sets. We have a theorem though which allows us to extend conformal mappings continuously to the boundary:

Theorem 4 *Let G be an open subset of $\hat{\mathbb{C}}$ and $f(z)$ a conformal mapping from G to $\hat{\mathbb{C}}$, then $f(z)$ can be extended continuously and bijectively to the boundary of G.*

It is quite difficult to prove theorem 4; a proof can be found in [57]. Finally we want to mention the famous Riemann mapping theorem:

Theorem 5 *Let $G \subset \hat{\mathbb{C}}$ be an open simply connected region such that $\hat{\mathbb{C}} - G$ contains at least two points. There exist a biholomorphic mapping*

$$f : G \rightarrow D,$$

where D is the open unit disc.
One can require for some $z_0 \in G$ that $f(z_0) = 0$, and $f'(z_0) \in \mathbb{R}^+$. Then f is unique.

3.1.3   Harmonic functions

A function $u(x, y) : \mathbb{R}^2 \rightarrow \mathbb{R}$ is called harmonic if it satisfies the Laplace Equation:

$$u_{xx} + u_{yy} = 0. \tag{3.5}$$

We state two fundamental theorems without proof:

Theorem 6 *If $f(z) = u(x, y) + iv(x, y)$ is analytic in G, then $u = u(x, y)$ and $v = v(x, y)$ are harmonic in G'.*

Theorem 7 *If $u(x, y)$ is harmonic in G', then it is possible to construct $v(x, y)$ harmonic in G', such that $f(z) = u(x, y) + iv(x, y)$ is analytic.*

Combining these theorems, we see that solving for a harmonic function in a certain region is equivalent to finding an analytic function in that region viewed as a function of z. Moreover, due to Cauchy's integral formula, we only need the real part of an analytic function on the boundary to determine the function. If the region G is the unit disc, one can calculate $f(z)$ explicitly once $u(\theta) = f(z = e^{i\theta})$ is given:

$$f(z) = iv(0) + \frac{1}{2\pi} \int_0^{2\pi} u(\theta) \frac{e^{i\theta} + z}{e^{i\theta} - z} d\theta \tag{3.6}$$

3.2   Analysis of the inner scale

If we zoom in on the streamer head we see the following picture (3.1):
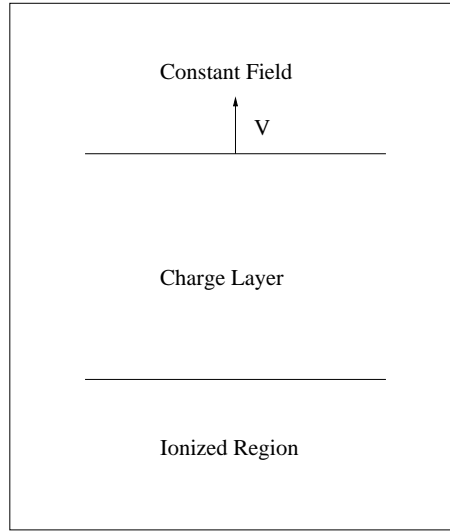
Figure 3.1: Sketch of the inner problem

The width of the charge layer is much smaller than the local radius of curvature of the streamer; this means that the streamer is approximately planar on this scale. But this simplifies the analysis a lot. Propagation of planar fronts was studied in [9] and [8]. The analysis shows that fronts with $D \neq 0$ are so-called pulled fronts that are difficult to handle [Ebert, van Saarloos, Phys. Rep. 2000]. We therefore examine fronts with $D = 0$ in most of the thesis, and return to $D \neq 0$ in the last chapter.

A result of these papers was the aforementioned effective boundary condtion: the velocity a planar front is given by the local electric field

$$\mathbf{v} = -\mathbf{E}. \tag{3.7}$$

Furthermore, (almost) analytic expressions for the charge density and electric field strength were found. Plots for zero diffusion can be found in Figure 5.1 in Chapter 5. Notice that the asymptotes show the expected (imposed) behaviour: zero densities far in front of the front and zero net charge behind the front, constant electric field in front and behind the front. These explicit analytic results will be used later in the derivation of a new boundary condition, Chapter 5.

Finally we note that planar fronts are interesting in itself; the (in)stability of planar fronts will be the subject of Chapter 8.

3.3   The analysis on the outer scale

If we zoom out, we obtain the following picture 3.2:
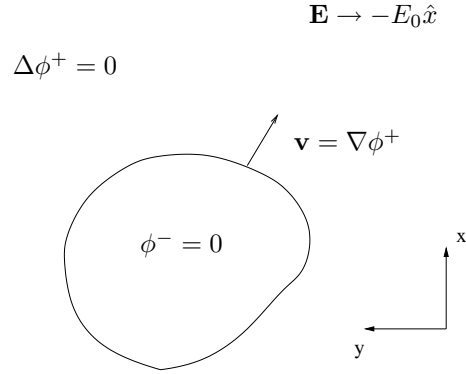
Figure 3.2: Sketch of the moving boundary problem

The charge layer has shrunk to a line which separates the ionized region and the air. This line will be called the interface; our problem is reduced to the dynamics of the interface. This is an example of a so called moving boundary problem (MBP).
We choose the electric field far from the streamer to be homogeneous; this yields the boundary condition (3.8):

$$\mathbf{E} \to -E_0 \hat{x} \quad \text{for} \quad x \to \infty, \tag{3.8}$$

where $\hat{x}$ is the unit vector in the x-direction. Notice the peculiar choice of coordinates; this choice will be convenient in the future. From the inner analysis a condition for the normal component of the velocity of the interface is derived (3.9):

$$\mathbf{v} = -\mathbf{E} = (\nabla \phi) \tag{3.9}$$

If the shape of the interface is initially specified, the electric field and the velocity can be calculated; one can take a timestep and use the updated interface to calculate the updated electric field. There is however a more efficient way to study these MBP's if the system is two-dimensional.

3.4   Conformal mapping

The idea of our approach is illustrated in figure 3.3; in the region outside the streamer in the z-space, we have to solve $\Delta \phi = 0$. Solving the Laplace equation in a region G' is equivalent to finding an analytic function in a region G. Let us therefore define $\Phi(z)$:

$$\Phi(z) : G \to \hat{\mathbb{C}}, (analytic) \tag{3.10}$$

$$\text{Re } \Phi(z) = \phi(x, y). \tag{3.11}$$

Instead of finding a harmonic function $\phi(x, y)$ we have to find an analytic function with a prescribed real part on the boundary. We still have a problem: we have a moving boundary.
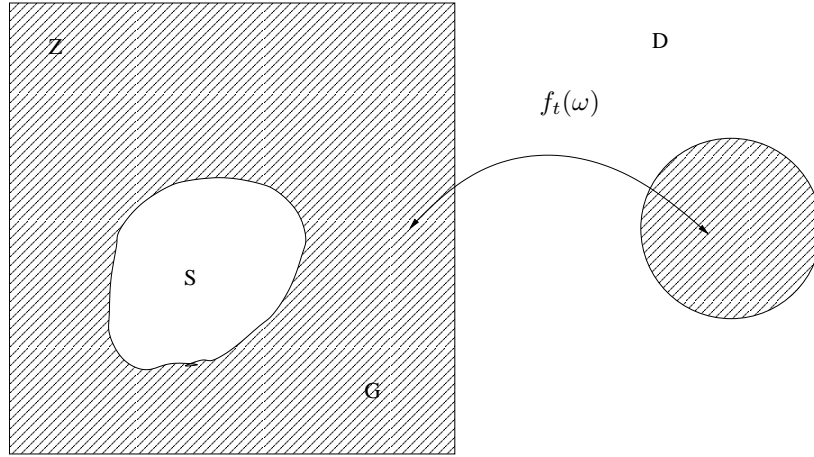
Figure 3.3: Conformal mapping

We will use a conformal map which maps the moving domain onto the unit disc D. Since a conformal map is biholomorphic, its inverse is conformal as well and we will try to find a mapping

$$f_t(\omega) : D \to G, \tag{3.12}$$

where

$$G = \hat{\mathbb{C}} - S; \tag{3.13}$$

S is the streamer with its boundary in the complex plane. We assume $S \subset \hat{\mathbb{C}}$, therefore $\infty \in G$; the electrodes in figure 3.3 will be moved to infinity. Since both $\Phi(z)$ and $z = f_t(\omega)$ are analytic, their composition is analytic and we can try to find $\hat{\Phi}(\omega)$ instead:

$$\Phi(z) = \Phi(f_t(\omega)) = \hat{\Phi}(\omega). \tag{3.14}$$

This is a relatively easy problem, since we have a fixed boundary instead of a moving boundary. This will be done in section 3.6. The problem is transferred to the problem of finding a conformal mapping. Tracing the time evolution of the mapping function at the boundary is equivalent to tracing the interface. Since the conformal mapping $f_t(\omega)$ can be continuously and bijectively extended to the boundary of the unit disc, the unit circle, we know that the unit circle maps to the boundary of the streamer: it maps to the interface. This means that we can track the time evolution of the interface by evaluating the conformal mapping at $|\omega| = 1$.

3.5   Deriving the form of the mapping function

In this section we will prove the existence of a conformal mapping which maps the area outside the streamer onto the unit disc. We will use the complex coordinate z to denote the 'streamer space'; the complex variable ω is defined on the unit disc. Let us define the region G in the 'streamer space', describing the space outside the streamer:

$$G = \hat{\mathbb{C}} - S, \tag{3.15}$$

where S is the streamer with its boundary. We assume $S \subset \hat{\mathbb{C}}$, therefore $\infty \in G$. Since we include the point at infinity, G is an open, simply connected subset of $\hat{\mathbb{C}}$.

It is usefull to define a third complex space, in which points are given by the complex variable w. Define the biholomorphic mapping g:

$$g : \hat{\mathbb{C}} \to \hat{\mathbb{C}}, \tag{3.16}$$

where

$$z = g(w) = \frac{1}{w}. \tag{3.17}$$

This allows us to define G' as the image of G; G' is an open, simply connected subset of $\hat{\mathbb{C}}$:

$$G' = \{ w \in \hat{\mathbb{C}} : g(w) \in G \}. \tag{3.18}$$

Remark: $0 \in G'$, because we assumed that $\infty \in G$.
We define the subset D, the open unit disc, in the following way:

$$D = \{ \omega \in \mathbb{C} : |\omega| < 1 \}. \tag{3.19}$$

The Riemann-mapping theorem gives us the existence and uniqueness of a function $f_t(\omega) : D \to G$. The theorem is not constructive. Since we would like to find such an analytic form of such a function f, it turns out to be more convenient to apply Riemann mapping theorem to the region G'. It is clear that G' satisfies the conditions in the theorem. This means that we have a function g_1

$$g_1 : D \to G', \tag{3.20}$$

where g_1 is biholomorphic. We require

$$g_1(0) = 0, \quad g_1'(0) \in \mathbb{R}^+. \tag{3.21}$$

This implies that $g_1(\omega)$ is the unique biholomorphic function which maps D onto G' with the properties given in equation (3.21). Since g_1 is analytic on D, we can expand it around 0:

$$g_1 = a_1 \omega (1 + \alpha_1 \omega + ..). \tag{3.22}$$

Since g_1 is biholomorphic, it has only one zero inside the unit disc, $\omega = 0$, which means that the expression between the brackets in equation (3.22) is nonzero for all ω in the unit disc. Furthermore, $a_1 \in \mathbb{R}^+$, since we put $g_1'(0) \in \mathbb{R}^+$. We can define a biholomorpic mapping from G to D composing the mappings g and g_1:

$$f_t(\omega) = \frac{1}{g_1} = \frac{1}{a_1\omega} + \frac{p(\omega)}{1 + \alpha_1\omega + ..}, \tag{3.23}$$

where $p(\omega)$ is some polynomial in ω. The right hand side of equation (3.23) can be rewritten in the following form:

$$f_t(\omega) = \frac{a_{-1}(t)}{\omega} + h_t(\omega), \tag{3.24}$$

where $a_{-1}(t) \in \mathbb{R}^+$ and $h_t(\omega)$ analytic since it is a quotient of analytic functions with nowhere zero denominator:

$$h_t(\omega) : D \to \mathbb{C} \tag{3.25}$$

and

$$a_{-1}(t) \in \mathbb{R}^+. \tag{3.26}$$

Remark Note that $f_t(\omega)$ is analytic for all ω, including $\omega = 0$, because of the definition of analyticity around the point ∞.

3.6   Calculation of the complex potential

In this section we would like to derive an equation for the complex potential $\Phi(z)$ such that

$$\text{Re } \Phi(z) = \phi(x, y), \tag{3.27}$$

where we have taken $z = x + iy$ in equation (3.27). From equation (3.27) we will obtain an equation for the potential in the ω domain,

$$\hat{\Phi}(\omega) = \Phi(f_t(\omega)). \tag{3.28}$$

Let us focus on the large x regime first. The physical potential $\phi(x, y)$ has to satisfy the following property:

$$\nabla\phi = E_0\hat{x} \quad \text{for large } x. \tag{3.29}$$

This means that we have

$$\Phi(z) = E_0 z \quad \text{for large z.} \tag{3.30}$$

In section 3.5 we derived

$$z = f_t(\omega) = \frac{a_{-1}(t)}{\omega} + h_t(\omega),$$ (3.31)

which gives us

$$\hat{\Phi}(\omega) = \Phi(f_t(\omega)) = \frac{E_0 a_{-1}(t)}{\omega}$$ (3.32)

if ω is small. This singular part of the potential describes the behavior for large z. The structure of the mapping $f_t(\omega)$ will not change this behavior, since the mapping describes the changing shape of the interface. This implies that the singular part of the potential is the one given in equation (3.32), and:

$$\hat{\Phi}(\omega) = \frac{E_0 a_{-1}(t)}{\omega} + \text{analytic terms.}$$ (3.33)

In order to determine the analytic terms of equation (3.33) we need a boundary condition on the streamer.

3.7   The equation of motion for the mapping

In order to derive the equation of motion for the mapping, we shall follow the guidelines of [11]. In our problem the relationship between the velocity of the interface and the potential is the following:

$$v_n = (\hat{n} \cdot \nabla \phi),$$ (3.34)

where $\hat{n}$ is the unit normal vector. Eq. (3.34) is extended to the complex plane in the following way. Introduce the complex normal to the interface $n = n_x + i n_y$, and a complex velocity $v = v_x + i v_y$. Then the left hand side of (3.34) becomes

$$v_n = v_x n_x + v_y n_y = \text{Re}(v n^*),$$ (3.35)

the star denotes the complex conjugate. Use equation (3.34) to obtain

$$\text{Re}(v n^*) = (\hat{n} \cdot \nabla \phi),$$ (3.36)

where the right hand side has to be expressed as a complex number in the same way. Introduce α to parametrize the boundary of the unit disc:

$$\omega = e^{i\alpha}.$$ (3.37)

Functions depend on α via ω; the argument of the function determines which variable is used, i.e.

$$f(\omega) = f(e^{i\alpha}) \equiv f(\alpha).$$ (3.38)

Now, the complex velocity can be related to the mapping as:

$$v = \dot{z} = \frac{df_t(\alpha)}{dt} = \frac{\partial f_t(\alpha)}{\partial t} + \frac{\partial f_t(\alpha)}{\partial \alpha}\frac{d\alpha}{dt}. \tag{3.39}$$

This is because the parametrization of the interface may in principle change in time. Then the equation of motion for the mapping becomes

$$\text{Re}\left\{\left(\partial_t f_t(\alpha) + \partial_\alpha f_t(\alpha)\frac{d\alpha}{dt}\right)n^*\right\} = (\hat{n}\cdot\nabla\phi) \tag{3.40}$$

Using the expression for the normal, as in [11],

$$n = n_x + in_y = i\frac{\partial_\alpha f_t(\alpha)}{|\partial_\alpha f_t(\alpha)|}. \tag{3.41}$$

we obtain:

$$\text{Re}\left\{\frac{-i\partial_\alpha f_t^*(\alpha)\partial_t f_t(\alpha)}{|\partial_\alpha f_t(\alpha)|} - i|\partial_\alpha f_t(\alpha)|\frac{d\alpha}{dt}\right\} = (\hat{n}\cdot\nabla\phi) \tag{3.42}$$

which means

$$\text{Re}\left\{\frac{-i\partial_\alpha f_t^*(\alpha)\partial_t f_t(\alpha)}{|\partial_\alpha f_t(\alpha)|}\right\} = (\hat{n}\cdot\nabla phi), \tag{3.43}$$

since the parametrization of the interface is a real quantity. Let us calculate now the term $(\hat{n}\cdot\nabla\phi)$:

$$(\hat{n}\cdot\nabla phi) = (n_x\partial_x\phi + n_y\partial_y\phi) = \text{Re}(n\partial_z\Phi), \tag{3.44}$$

where $z = x + iy$, $\Phi = \Phi(z)$ is the complex potential defined in section 3.4 and the property $\partial_z\Phi \equiv \partial_x\Phi$ has been used. Going to the ω-domain, and using the chain differentiation rule,

$$\frac{\partial}{\partial z} = \frac{\partial\omega}{\partial z}\frac{\partial}{\partial\omega} \equiv \frac{\partial_\omega}{\partial_\omega z}, \tag{3.45}$$

we obtain:

$$(\hat{n}\cdot\nabla\phi) = \text{Re}\left(\frac{n\partial_\omega\hat{\Phi}(\omega)}{\partial_\omega z}\right)\Bigg|_{\omega=e^{i\alpha}}, \tag{3.46}$$

where $\hat{\Phi}(\omega)$ corresponds to the complex potential mapped onto the ω-plane. Now, recalling Eq. (3.41), it is a simple matter to show that

$$(\hat{n}\cdot\nabla\phi) = \text{Re}\left(\frac{i\partial_\alpha\hat{\Phi}(\alpha)}{|\partial_\alpha f_t(\alpha)|}\right). \tag{3.47}$$

Using this, we finally obtain:

$$\text{Re}\left(i\partial_\alpha f_t^*(\alpha)\partial_t f_t(\alpha)\right) = \text{Re}\left(-i\partial_\alpha\hat{\Phi}(\alpha)\right), \tag{3.48}$$

which is our basic interfacial equation. This is the fundamental mapping equation already reported in [11].

3.8   Comparison to viscous fingering

In this section I will discuss the viscous fingering problem, since the underlying mathematical is similar to our moving boundary problem. The physical system consists of a so called Hele-Shaw (HS-) cell, two parallel plates which are very close to each other, filled with two fluids. When a pressure gradient is applied, the interface between the two fluids will become (un)stable depending on whether the more viscous fluid is driving or not. If the less viscous fluid is driving, one usually observes the emergence of one or more fingers. The prediction of the width of the finger became a classical problem: the selection problem.

There are of course some generalizations of this experimental setup; one can study bubbles of air in a HS-cell, or injection from air in the center of the fluid from above.

I will describe a general setup of the problem in section 3.8.1 and discuss the early contributions in section 3.8.3. The selection problem is solved in those papers. In section 3.8.4 I will discuss the later contributions, which are from a dynamical systems point of view. Similarities and differences with the streamer problem will be discussed in section 3.8.5. In the last section I will discuss some mathematical papers concerning the complex moments.

3.8.1   General statement of the problem

The 'classical' viscous fingering is shown in figure 3.4:
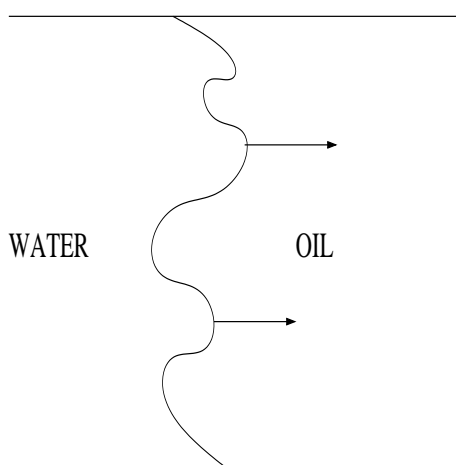
Figure 3.4: Classical viscous fingering in a thin Hele-Shaw cell, seen from above.

The water-oil interface is unstable if the less viscous fluid of the two is driving the more viscous. One usually observes a 'fingered' pattern in this case, which is the reason for the name of the phenomenon, 'viscous fingering'. This problem was already known by engineers, trying to push oil with water and ending up with oil-water mixtures due to the instability of the interface. From

now on, I will use air to denote the less viscous and water to denote the more
viscous fluid for convenience.

When air is injected from one side into a long stretched Hele-Shaw cell filled
with water, usually a finger is observed with width $\lambda = \frac{1}{2}$ (where the width
of the channel is set to one). In 1958 Saffman and Taylor analyzed this prob-
lem and derived a family of exact finger shapes in absence of surface tension
parametrized by their width λ in [15]. They showed that their analytically
predicted shape fitted the experimental one very well, provided they imposed
$\lambda = \frac{1}{2}$. They conjectured and checked experimentally that the width of the
finger could only depend on a dimensionless combination of the surface tension.
The selection of the width of the finger by surface tension was called the 'selec-
tion problem'.

Their work was originally motivated by penetration of a fluid into a porous
medium, the aforementioned engineering problem. They wanted to model this
problem with a HS-cell, where air instead of water, water instead of oil and the
cell instead of a porous rock is used to study the instability.

In a later paper, [16], they studied the shapes of bubbles in a Hele-Shaw cell.
They were able to calculate the shapes of the bubbles analytically but encoun-
tered again a similar selection problem; a family of solutions exists.

3.8.2   Derivation of the moving boundary problem

The idea of the moving boundary approximation is given in figure 3.5. The
interface separating the air region from the water region is taken infinitely thin;
this means that we end up with two regions. In both regions the pressure
has to satisfy the Laplace equation, since overdamped motion ($\mathbf{v} = -\nabla p$) and
incompressibility ($\nabla \cdot \mathbf{v} = 0$) are assumed. The viscosity of air can be neglected
with respect to oil/water, so the pressure is constant in the air region to the
left.

$$\Delta p_+ = 0 \quad \text{in the water region} \tag{3.49}$$

and

$$p_- = \text{constant in the air region} \tag{3.50}$$

The pressure determines the local normal component of the velocity on the
interface via Darcy's law:
(**Remark**: This law can be obtained directly from integration of the Navier-
Stokes equations)

$$-(\nabla p_+)_n = v_n \tag{3.51}$$

which means that the local velocity of the interface is determined by the pres-
sure; the tangential component is just a reparametrization of the interface and
can not be seen.
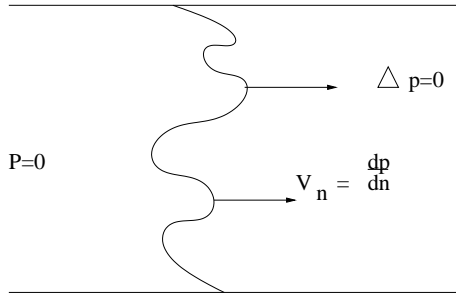
Figure 3.5: A moving boundary approximation for the viscous fingering problem

Furthermore, one usually takes a constant extraction rate of the fluid at $x = \infty$, which means that the velocity is fixed: $\mathbf{v} \to U\hat{x}$ if $x \to \infty$. At the sidewalls, the velocity of the fluid is parallel to the walls, which means:

$$\frac{dp}{dy} = 0 \quad \text{at the walls.} \tag{3.52}$$

This means that the problem is fully determined once some initial shape of the interface is given and if the jump condition for $p_+ - p_-$ is given. The simplest (unregularized) case is

$$p_+ - p_- = 0 \tag{3.53}$$

and the regularized case

$$p_+ - p_- = T\kappa, \tag{3.54}$$

where T is the dimensionless surface tension and κ the curvature. Notice that equation (3.54) reintroduces the third dimension into the problem; there are actually two radii of curvature. Analysis shows that both smoothen out the sharp cusps in the interface and one usually uses the two dimensional curvature from the interface in equation (3.54). Let me formulate the ST-problem in channel geometry for future reference:

$$\Delta p = 0, \quad \text{in the water} \tag{3.55}$$

$$\frac{dp}{dy} = 0 \quad \text{on the walls and} \quad -\frac{dp}{dx} \to U \quad \text{as} \quad x \to \infty \tag{3.56}$$

$$p = T\kappa \quad \text{on the interface} \tag{3.57}$$

and

$$v_n = -(\nabla p)_n \quad \text{on the interface} \tag{3.58}$$

The problem (3.55)-(3.58) with $T = 0$ will be denoted as the unregularized problem.

3.8.3   Discussion of early papers

A class of solutions of the unregularized problem was already found in [15]: the finger (ST1). The width λ was a free parameter though and could not be obtained.

McLean included surface tension [17] and found a unique solution, which appeared to be linearly unstable. Romero and Vandenbroeck [18] showed that McLean had only found the smallest possible λ; a whole family of solutions exists. In the meantime, the smallest finger was observed in experiments and numerical solutions of the full problem; perturbations seemed to grow first but were convected away to the side of the finger and elongated (larger k, more stable) in [26] and [27]. The stability and the selection problem was finally solved at the same time by Bensimon [22] and (independent) Kessler and Levine [24], [25]; the fingers of [17] are indeed stable, but extremely sensitive to noise if T is small; this leads to a nonlinear (subcritical) instability for small T. The higher values of λ, reported in [18] are unstable and thus unobservable. Instabilities imposed on the selected λ are convected away to the back. The breakdown of the stability analysis of [17] is due to the role of exponentially small terms which can not be captured by a linear stability analysis, although such an analysis appears to be consistent. This means that a complete picture for the finger selection is achieved.

The unregularized problem exhibits some nice features; one can use an ansatz like:

$$f_t(\omega) = \sum_{k=0}^{N} a_k(t)\omega^k; \qquad (3.59)$$

on the conformal map. If the initial shape of the interface can be described by N modes a_k, no higher modes will be generated. This means that the equation of motion for the mapping function, a PDE, can be reduced to N ODE's. All those polynomial initial conditions will lead to cusps, points on the interface with infinite curvature. When an ansatz like

$$f_t(\omega) = \frac{a_0(t)}{\omega} + \sum_{m=1}^{M} \alpha_M \ln(\omega - a_m(t)), \qquad (3.60)$$

a sum of logarithms is inserted instead, no cusps will occur. This seems to be a nice property, but the mappings can describe initial conditions which are arbitrarily close to each other. This means that cusp formation is a generic feature of the problem which can not be cured properly by a different ansatz on the mapping function.

3.8.4   The later contributions

The idea is to use the known exact solutions, add a small amount of surface tension and see whether the right finger width is selected and whether the cusps are regularized away. This turns out to be the case, but not in the way it was

expected. Terms of all order need to be kept in a perturbative expansion in T in order to obtain the right λ. Furthermore, solutions for $T = 0$ and $T \neq 0$ which are originally close to each other can differ even qualitatively at time of order unity. This is due to the emergence of so called daughter singularities. The way the surface tension is selecting the right width is called microscopic solvability; microscopic since a microscopic property selects a macroscopic property and solvability since solvability integrals are involved.

Casademunt wrote an interesting paper [41] which highlights all subtleties of the problem. In a setup with multiple fingers, unequal fingers are a solution of the unregularized problem, the planar interface is unstable and a single finger is a solution as well. Addition of surface tension changes the full phase space: only the equal fingers fixed point is left, but this has become a saddle point. The single finger with $\lambda \approx \frac{1}{2}$ is the attractor of the problem. Even an addition of a small amount of surface tension is able to change the phase space in regions far away from the fixed points (and far away from the regions with high curvature, where it is supposed to work). This means that a different ansatz on the mapping function will not cure the sensitivity to cusp formation; an additional lengthscale is needed, which is surface tension in the viscous fingering case.

3.8.5 Comparison with the streamer

Let me compare the unregularized streamer problem to the bubble in the HS-case; those two are very similar. The inner region of the streamer is fully ionized which means $\phi = 0$, corresponding to the air bubble of constant pressure. The chargeless outer region $\Delta\phi = 0$ corresponds to the water region where $\Delta p = 0$. The geometry is the same in this case (no effects of the side walls). Since the problem is not regularized, the jump condition on the interface, $\phi = 0$ is the same in both cases as well. The only difference is in the constant field at infinity (streamer) instead of a prescribed potential, which is usually $\sim Q \log z$ (injection of air in the center of the bubble) in the HS-case. Nevertheless it is not surprising to find very similar results in both cases, i.e. polynomials are solutions but develop cusps in finite time. Although this could probably be 'cured' using the logarithms instead, this would not be the correct approach. The emphasis should be on the regularization of the problem.

The comparison of the regularized cases is more interesting, especially since both regularization mechanisms can be compared directly (independent of global topology). A regularization mechanism for the streamer was derived from the inner problem:

$$\phi = \epsilon(\nabla\phi)_n, \qquad (3.61)$$

where ϵ is the width of the boundary layer. This boundary condition was already mentioned by Howison [34], he derived the correct dispersion relation for the planar front.

Although the conditions (3.57) and (3.61) look very different, they both penalize regions of large curvature. The first one explicitly, the latter one as well, since

high curvature corresponds to high electric fields.

The inclusion of surface tension indeed regularizes the HS-problem; perturbations can be amplified but are finally convected away. This is exactly what we observe as well. We got even further, since we were able to derive analytic solutions of the regularized problem which exhibit this feature. Furthermore we were able to show that only a shift remains from any perturbation as $t \to \infty$. I want to conclude this section with a remark made by Tanveer: this should be a 'cautioning tale' for physicists. It is an example where a perturbative approach failed completely due to the singular nature of the perturbation.

3.8.6   An alternatitive approach: the complex moments

The moving boundary can be solved in a different way; instead of solving the PDE for the mapping function, the complex moments of the domain can be used. This idea was introduced by Richardson in [42]. I will discuss three papers and make a comparison with my own work in the last part.

Summary of Richardson's paper

His motivation came from an industrial application; injection moulding. A molten polymer is forced into a mould of an appropriate shape through a hole. It would be desirable to understand the shape of the growing domain, since air has to escape at the points where the polymer arrives last. The same problem, injection moulding, happened to be the subject of my master thesis [45], [46]. In [42], the polymer is replaced by a compressible Newtonian fluid; all the complicating rheology is removed from the problem. Since he assumes furthermore that the boundaries of the mould are infinitely far away, the problem becomes the HS-droplet problem. The initial domain is a drop of a given shape which expands via inflow of liquid in some interior point. The problem is formulated in the usual way, without pressure drop across the interface. Using a simple geometric argument, the known equation of motion for the interface is derived; in his notation:

$$f'(\zeta, t) + \frac{\partial f^\star}{\partial t} + (\zeta^2 f'(\zeta, t))^\star \frac{\partial f}{\partial t} = \frac{Q}{\pi} \frac{1}{\zeta}, \qquad (3.62)$$

where the right hand side comes from the point source at the origin $\sim \frac{Q}{2\pi} \ln(z)$. Define the complex moments of a closed domain D:

$$C_N = \int \int_D z^N dx dy \qquad (3.63)$$

and notice that the 0th moment is the area of D and $\frac{C_1}{C_0}$ the center of mass. Differentiating equation (3.63) and using equation (3.62) equation (3.64) follows immediately:

$$\frac{dC_N}{dt} = \frac{Q}{2\pi i} \int_{\Gamma'} \frac{f^N}{\zeta} d\zeta, \qquad (3.64)$$

where Γ' denotes the unit circle. This means that all but one of the moments are conserved in time; only the area is increasing at a given rate. The moments are directly related to the Schwarz function; this approach can be impractical. If the initial domain is given by a polynomial of degree N, $C_k = 0, k > N$ which means that those moments remain zero: polynomials are solutions and the problem reduces to solving a system of N algebraic equations (since the area is changing).

Injection gives rise to a smoother boundary than suction, which is logical since in the latter case the less viscous fluid is driving.

Summary of the paper of Entov et al. [43]

0: Instead of a potential with a single pole as studied in [42], they study multipoles using the complex moments.

I: Let $F(z)$ be the complex potential; a pole of order n and strength M at z_0 is defined as follows:

$$F(z) = -\frac{M}{2\pi}(z - z_0)^{-n} + \phi(z), \qquad (3.65)$$

where $\phi(z)$ is analytic at z_0. This expression is obtained by superposition of sources and sinks of strength $\frac{1}{2}M\epsilon^{-n}$ around z_0 at distance ϵ around z_0 and taking $\epsilon \to 0$; this implies that the $n = 1$ case is called a dipole and $n = 2$ a quadrupole. Both droplets (source in bounded domain) and bubbles (source at infinity and bounded complement) can be described. The unregularized HS-equations completely specify the evolution of an intial domain D_0 under action of a multipole.

II: Evolution of domain with pole of order n: C_n varies linearly, the other moments are constant.(bubble is the same with appropriate definition of the C_n.

III: Richardson's results is recalled; polynomials of degree N are solutions iff the $C_k = 0, k > N$

IV: Exact solutions for the droplet; multipole of order n, polynomial of degree n+1, which breaks down in finite time, after $t^\star$, due to cusp formation; this property holds for all initial domains, since addition of more modes makes it worse, shorter lifetime. The same holds in the bubble case.

VI: Surface tension included to study equilibrium shapes; the complex potential $F(z)$ has as boundary condition $T\kappa$; the analytic continuation of this function has only one singularity inside D, which turns out to be sufficient to reconstruct D. The Schwarz function is a curve $\Gamma\mathbb{C}$ such that there exists an analytic $g(z)$ in the neighbourhood of Γ and

$$g(z) = z^\star, \quad z \in \Gamma. \qquad (3.66)$$

Important properties of the Schwarz function are listed in [56]. It is convenient in this case, since the normal and the curvature can be expressed easily in g. The complex potential is given in terms of $g(z)$:

$$F(z) = \pm\frac{iTg''(z)}{2(g(z))^{3/2}} \qquad (3.67)$$

and this means that the quotient on the right hand side has just one singularity inside D. This turns out to be sufficient to derive an equation for g. The droplet and the bubble are treated seperately. Using the information about the singularities, an expression for the mapping function is derived; a one parameter family of solutions in terms of M and T. If the surface is large enough, one or two solutions can exist. Although no stability analysis is performed, they conjecture that the solution is stable if one exists and stable/unstable if two solutions exist.

Summary of the paper of Nie and Tian [44]

I: This paper studies time-dependent solutions with surface tension; in [43] they found requirements for stationary solutions; order multipole greater than one, sufficiently large surface tension and center of fluid at the multipole.

II: Setup droplet problem with a multipole at the origin in the presence of surface tension. Equivalence complex moments and PDE problem is shown in presence of surface tension. Even in the presence of surface tension, the first moment can be calculated analytically and increases linearly in time in the dipole case. This means that it either extends to infinity or develops cusps as time goes to infinity. For multipoles of higher order, the center of mass is time-independent; all stationary solutions of [43] had a coinciding center of mass and source, which means that those can only be attained when the two coincide initially. Without surface tension, a polynomial ansatz can be inserted and integrated (for comparison reasons).

III+IV: Numerical method and numerical solutions. Dipole develops cusps without T, but cusp is regularized by surface tension and reaches dipole instead. This critical time can be estimated and agrees nicely with the theoretical argument. Larger surface tension, less pointed. Different initial condition used; cusps still regularized away.

Quadrupole gives the same results, cusps without surface tension and former cusps are fingers reaching the quadrupole. If surface tension is increased, they manage to obtain one of the stationary shapes predicted by [43]. If they move the position, the former cusp reaches the pole again and no stationary shape exists.

Multipole of order 3 gives the same results; if surface tension is large enough, a stationary shape can be reached.

The complex moments of the streamer

In the unregularized case, the streamer is completely equivalent to a bubble with a dipole at infinity. This means that, apart from the first moment, all moments are conserved. Instead of solving N ODE's, one could solve N algebraic equations instead to trace the interface. This is, however, numerically equally complicated, so I decided to stick to the ODE-formulation. The question is, whether analytic progress could be made with the Schwarz function for the regularized case. Although this worked particularly well in [43], it may be a bit more complicated due to the different boundary condition. This may be a direction for future analytic research, though.

Chapter 4

Solutions of the unregularized problem

The framework developed in the previous chapter is applied to the unregularized problem. It is possible to derive an explicit expression for the complex potential. I use a power series expansion

$$f_t(\omega) = \sum_{k=-1}^{\infty} a_k(t)\omega^k \qquad (4.1)$$

for the mapping and derive an (infinite) set of coupled ODE's for the coefficients of the expansion. If the initial condition truncates after some power N, the coefficient $a_k(t) = 0, k > N \quad \forall t > 0$, which means that any solution of the ODE can be characterized by N, the number of modes in the initial condition. Analytic solutions are derived for the two trivial cases $(N = 0, 1)$, I prove two theorems for the first nontrivial case $(N = 2)$. Finally, numerical solutions are given for larger values of N. Cusp formation in finite time seems to be inevitable.

The analysis and the results of this chapter have been published in Phys. Rev. E [47].

4.1 Calculation of the potential

In chapter 3 the general form of the mapping function and the complex potential were derived. Let me recall the explicit expressions:

$$f_t(\omega) = \frac{a_{-1}(t)}{\omega} + \quad \text{an analytic function of } \omega \qquad (4.2)$$

and

$$\hat{\Phi}(\omega, t) = \frac{E_0 a_{-1}(t)}{\omega} + g(\omega, t), \qquad (4.3)$$

where $g(\omega, t)$ is a time dependent analytic function of ω. In the unregularized problem, the streamer is equipotential and I gauge its potential to zero. This leads to:

$$\phi(x, y) = \phi_0 = 0 \tag{4.4}$$

on the streamer. This gives us

$$\text{Re } \hat{\Phi}(\omega, t) = 0, \quad \text{if} \quad |\omega| = 1. \tag{4.5}$$

I have to solve a Dirichlet problem for $g(\omega, t)$; $g(\omega, t)$ is analytic inside the unit disc and has to satify

$$0 = \text{Re } g(\omega = e^{i\alpha}, t) + E_0 a_{-1}(t) \cos \alpha \tag{4.6}$$

on the unit disc where $\omega = e^{i\alpha}$. It is easy to verify that the function

$$g(\omega, t) = -E_0 a_{-1}(t)\omega. \tag{4.7}$$

has the desired properties. Insertion of (4.7) yields an expression for the complex potential:

$$\hat{\Phi}(\omega) = E_0 a_{-1}(t) \left(-\omega + \frac{1}{\omega} \right). \tag{4.8}$$

One could also use Fourier analysis to solve the problem. Writing

$$g(\omega) = b_0 + 2 \sum_{n=1}^{\infty} b_n \omega^n, \tag{4.9}$$

yields

$$\text{Re } g(e^{i\alpha}) = b_0 + \sum_{n=1}^{\infty} b_n e^{in\alpha} + b_n^{\star} e^{-in\alpha}. \tag{4.10}$$

In this case, I obtain

$$b_0 = 0, \tag{4.11}$$

$$b_1 = \frac{-E_0 a_{-1}(t)}{2}, \tag{4.12}$$

$$b_n = 0, \quad n \geq 2. \tag{4.13}$$

Using equations (4.11)-(4.13) I obtain again the expression for the complex potential

$$\hat{\Phi}(\omega) = E_0 a_{-1}(t) \left(-\omega + \frac{1}{\omega} \right), \tag{4.14}$$

which is the same expression as the one derived in equation (4.8).

4.2   Derivation of a coupled set of ODE's

In Chapter 3, I derived the general form of the mapping function $f_t(\omega)$:

$$f_t(\omega) = \frac{a_{-1}}{\omega} + \text{analytic terms.} \qquad (4.15)$$

Any analytic function can be written as a convergent Taylor series,

$$f_t(\omega) = \frac{a_{-1}}{\omega} + \sum_{k=0}^{\infty} a_k \omega^k. \qquad (4.16)$$

I study interfaces which are mirror symmetric about the x-axis, i.e. $x \to x$ and $y \to -y$ if $\alpha \to -\alpha$, where the unit disc is parametrized by α: $\omega = e^{i\alpha}$. This is equivalent to imposing that all a_k are real. Use the explicit expression for $\hat{\Phi}(\omega)$ derived in section 4.1

$$\hat{\Phi}(\omega) = E_0 a_{-1} \left(-\omega + \frac{1}{\omega} \right) \qquad (4.17)$$

and the equation of motion for the mapping function, equation (3.48), derived in chapter 3:

$$\text{Re} \left(i\partial_\alpha f^\star \partial_t f \right) = \text{Re}(-i\partial_\alpha \hat{\Phi}(\alpha)). \qquad (4.18)$$

Substitution of the explicit expression for $\hat{\Phi}$ gives us the right hand side of the equation:

$$\text{Re}(-i\partial_\alpha \hat{\Phi}(\alpha)) = -i\partial_\alpha \left(-2iE_0 a_{-1} \sin \alpha \right) = -2E_0 a_{-1} \cos \alpha. \qquad (4.19)$$

Substitution of the equation for the mapping function (4.16) on the left hand side of the equation 4.18 gives us:

$$\text{Re} \left(i\partial_\alpha f^\star \partial_t f \right) = \text{Re} \left(\sum_{k,k'=-1}^{\infty} k a_k e^{-ik\alpha} \dot{a}_{k'} e^{ik'\alpha} \right) \qquad (4.20)$$

$$= \sum_{k,k'=-1}^{\infty} k a_k \dot{a}_{k'} \cos((k-k')\alpha). \qquad (4.21)$$

Equations (4.18)-(4.20) yield the desired equation:

$$\sum_{k,k'=-1}^{\infty} k a_k \dot{a}_{k'} \cos((k-k')\alpha) = -2E_0 a_{-1} \cos \alpha. \qquad (4.22)$$

This equation is an identical reformulation of the moving boundary problem. Ordering coefficients of $\cos k\alpha$ leads to an infinite countable number of ODE's.

4.2.1   Discussion of the equations

It is useful to prove the following theorem:

Theorem 8 *If there exists an N such that the initial condition $f_0(\omega)$ can be written in the form*

$$f_0(\omega) = \sum_{k=-1}^{N} a_k(0)\omega^k, \tag{4.23}$$

then the solutions $f_t(\omega)$ of the unregularized problem can be written in this form for $t > 0$:

$$f_t(\omega) = \sum_{k=-1}^{N} a_k(t)\omega^k. \tag{4.24}$$

Theorem 8 implies that the unregularized dynamics won't generate higher modes than those present in the initial condition. This means that a solution of the problem can be characterized by the cut-off N.

Proof of theorem 8:

Assume $N > 1$; the cases $N = 0$ and $N = 1$ will be treated separately, since one can solve the equations analytically in this case. The theorem holds in those cases as well, see section 4.3.1 and 4.3.2. Take an arbitrary integer M; I want to show that

$$a_k(t) = 0, \quad k = N+1,\ \ldots, N+M \quad \forall t > 0, \tag{4.25}$$

if the initial condition can be written as (4.23). For the highest mode, I can solve the equation directly, since the coefficient of $\cos((N+M+1)\alpha)$ in equation (4.22) gives

$$(N+M)a_{N+M}\dot{a}_{-1} - a_{-1}\dot{a}_{N+M} = 0, \tag{4.26}$$

which means

$$a_{N+M}(t) = a_{N+M}(0)\frac{a_{-1}(t)^{N+M}}{a_{-1}(0)^{N+M}} \tag{4.27}$$

and we see directly that all modes stay zero if they were zero initially, since we can work our way downward. This proves the theorem.

I would like to rewrite the equations (4.22) in matrix form; the first row of the matrix corresponds to the equation for $\cos 0\alpha = 1$, the second row to the equation for $\cos \alpha$ of equation (4.22) and so on. This allows us to solve them numerically rather easily, if the number of modes in the initial condition is limited by some number N. If this is the case, equation (4.22) reduces to $N+2$ ODE's for the modes a_k which can be written as follows: We have

$$(\mathbf{M}_1\{a_k\} + \mathbf{M}_2\{a_k\})\partial_t \mathbf{a} = \mathbf{r}, \tag{4.28}$$

where

$$
\mathbf{r} = \begin{pmatrix} 0 \\ -2E_0 a_{-1} \\ 0 \\ \vdots \\ 0 \end{pmatrix}, \tag{4.29}
$$

$$
\mathbf{a} = \begin{pmatrix} a_{-1} \\ a_0 \\ a_1 \\ \vdots \\ a_N \end{pmatrix}. \tag{4.30}
$$

The matrices are defined as follows:

$$
\mathbf{M}_1 = \begin{pmatrix} -a_{-1} & 0 & a_1 & \ldots & N a_N \\ 0 & -a_{-1} & 0 & \ldots & (N-1)a_{N-1} \\ 0 & 0 & -a_{-1} & \ldots & (N-2)a_{N-2} \\ \vdots & \vdots & \vdots & \ddots & \vdots \\ 0 & 0 & 0 & \ldots & -a_{-1} \end{pmatrix} \tag{4.31}
$$

and

$$
\mathbf{M}_2 = \begin{pmatrix} -a_{-1} & 0 & a_1 & \ldots & N a_N \\ 0 & a_1 & \ldots & N a_N & 0 \\ a_1 & \ldots & N a_N & 0 & 0 \\ \vdots & \vdots & \vdots & \vdots & \vdots \\ N a_N & 0 & 0 & \ldots & 0 \end{pmatrix} \tag{4.32}
$$

The solutions of the ODE's will be discussed in the next section.

4.3   Solutions of the ODE's

Theorem 8 shows that the number of modes is conserved in time. This means that N can be used as a classification of our solutions, where N is the number of modes in the initial condition. Let us take a look at the easiest cases first.

4.3.1   The circle: $N = 0$

If the initial condition is given by

$$
f_0(\omega) = \frac{a_{-1}(0)}{\omega}, \tag{4.33}
$$

we can solve the ODE's analytically. Substitution of $N = 0$ in equation (4.28) yields:

$$\left(\begin{pmatrix} -a_{-1} & 0 \\ 0 & -a_{-1} \end{pmatrix} + \begin{pmatrix} -a_{-1} & 0 \\ 0 & 0 \end{pmatrix} \right) \partial_t \begin{pmatrix} a_{-1} \\ a_0 \end{pmatrix} = \begin{pmatrix} 0 \\ -2E_0 a_{-1}(t) \end{pmatrix} \quad (4.34)$$

The first equation is solved as

$$a_{-1}\dot{a}_{-1} = 0 \Rightarrow a_{-1}(t) = a_{-1}(0), \quad (4.35)$$

(since $a_{-1} \in \mathbb{R}^+$ and thus nonzero) and the second equation as

$$-a_{-1}\dot{a}_0 = -2E_0 a_{-1} \Rightarrow a_0 = 2E_0 t. \quad (4.36)$$

This means that we have a uniformly translating circle with constant radius $a_{-1}(0)$ and speed $2E_0$, as

$$\begin{aligned} f_t(e^{i\alpha}) &= a_{-1}(t)e^{-i\alpha} + a_0(t) \Rightarrow & (4.37) \\ x(t) &= a_{-1}(0)\cos\alpha + 2E_0 t, \quad y(t) = -a_{-1}(0)\sin\alpha. & (4.38) \end{aligned}$$

4.3.2   The ellipse: $N = 1$

In this case I have

$$\begin{aligned} f_t(e^{i\alpha}) &= a_{-1}(t)e^{-i\alpha} + a_0(t) + a_1(t)e^{i\alpha} \Rightarrow & (4.39) \\ x(t) &= (a_{-1}(t) + a_1(t))\cos\alpha + a_0(t), & (4.40) \\ y(t) &= -(a_{-1}(t) - a_1(t))\sin\alpha, & (4.41) \end{aligned}$$

which is an ellipse with axes $a_{-1} \pm a_1$.

We can solve the equations again analytically; substitute $N = 1$ in equation (4.28):

$$\left(\begin{pmatrix} -a_{-1} & 0 & a_1 \\ 0 & -a_{-1} & 0 \\ 0 & 0 & a_{-1} \end{pmatrix} + \begin{pmatrix} -a_{-1} & 0 & a_1 \\ 0 & a_1 & 0 \\ a_1 & 0 & 0 \end{pmatrix} \right) \partial_t \begin{pmatrix} a_{-1} \\ a_0 \\ a_1 \end{pmatrix} = \quad (4.42)$$

$$\begin{pmatrix} 0 \\ -2E_0 a_{-1}(t) \\ 0 \end{pmatrix}. \quad (4.43)$$

Start with the last equation to obtain

$$a_1\dot{a}_{-1} - a_{-1}\dot{a}_1 = 0 \Rightarrow a_1(t) = \frac{a_1(0)}{a_{-1}(0)}a_{-1}(t). \quad (4.44)$$

and substitute the expression for $a_1(t)$ in the first equation:

$$a_1\dot{a}_1 - a_{-1}\dot{a}_{-1} = 0 \Rightarrow \dot{a}_{-1}\left(\left(\frac{a_1(0)}{a_{-1}(0)}\right)^2 - 1 \right) = 0. \quad (4.45)$$

We have $a_1(0) \pm a_{-1}(0) \neq 0$, since those quantities are the axes of the ellipse. Therefore we have $\dot{a}_{-1} = 0 \Rightarrow \dot{a}_1 = 0$: we have a translating ellipse, whose axes both are time independent. The velocity can be derived from the second equation:

$$\dot{a}_0(a_1(0) - a_{-1}(0)) = -2E_0 a_{-1}(0) \Rightarrow \dot{a}_0 = \frac{2E_0 a_{-1}(0)}{a_{-1}(0) - a_1(0)}. \qquad (4.46)$$

Notice that we find the circle back if we set $a_1(0) = 0$.

4.3.3   The first nontrivial case: $N = 2$

Although I am unable to solve the equations analytically, I am able to prove two theorems.
I am mainly interested in shapes with broader head than tail, since those shapes resemble the numerical solutions in [13]. This means that I have to impose $a_2(0) < 0$. Furthermore I assume a positive tip velocity and prove

Theorem 9 *If $a_2(0) < 0$ and if the velocity in the tip of the streamer stays positive, the curvature in the tip of the streamer will decrease in time.*

Theorem 9 implies that the streamer can make a transition from a convex to a concave shape and branches. Since the overall streamer velocity is positive due to the form of the potential, a negative tip velocity would also give rise to a flatter streamer; the tip is overtaken by the sides.
However, in chapter 6 I will prove the following theorem:

Theorem 10 *A non-conformality point will hit the unit disc in finite time.*

This means that a cusp is formed; we can not trace the time development of the interface further.
Proof of theorem 9:
The general expression for the curvature of a curve parametrized by f is given by equation (4.47)

$$\kappa(\alpha, t) = -\text{Im} \frac{\partial_\alpha^2 f}{|\partial_\alpha f| \partial_\alpha f}. \qquad (4.47)$$

Inserting ansatz (4.16) with $N = 2$ in equation (4.47) for the tip of the shape $\alpha = 0$ yields:

$$\kappa(0, t) = \frac{a_{-1}(t) + a_1(t) + 4a_2(t)}{(a_{-1}(t) - a_1(t) - 2a_2(t))^2} \qquad (4.48)$$

Differentiate the equation:

$$\dot{\kappa}(0, t) = \frac{n(t)}{(a_{-1}(t) - a_1(t) - 2a_2(t))^3}, \qquad (4.49)$$

where the numerator $n(t)$ is given by the following expression

$$
\begin{aligned}
n(t) = &(\dot{a}_{-1}(t)a_{-1}(t) + 3\dot{a}_{-1}(t)a_1(t) + 10\dot{a}_{-1}(t)a_2(t) - 3\dot{a}_1(t)a_{-1}(t) \\
&-\dot{a}_1(t)a_1(t) - 6\dot{a}_1(t)a_2(t) - 8\dot{a}_2(t)a_{-1}(t) - 8\dot{a}_2(t)a_2(t)).
\end{aligned} \tag{4.50}
$$

The equations of (4.28) are:

$$
2a_2\dot{a}_2 + a_1\dot{a}_1 - a_{-1}\dot{a}_{-1} = 0, \tag{4.51}
$$

$$
2a_2\dot{a}_1 + a_1\dot{a}_2 + a_1\dot{a}_0 - a_{-1}\dot{a}_0 = -2E_0a_{-1} \tag{4.52}
$$

$$
2a_2\dot{a}_0 + a_1\dot{a}_{-1} - a_{-1}\dot{a}_1 = 0, \tag{4.53}
$$

$$
2a_2\dot{a}_{-1} - a_{-1}\dot{a}_2 = 0. \tag{4.54}
$$

Substitute the following expressions that follow from (4.52), (4.54) and (4.54)

$$
-8a_2\dot{a}_2 + a_{-1}\dot{a}_{-1} - a_1\dot{a}_1 = -6a_2\dot{a}_2, \tag{4.55}
$$

$$
3a_1\dot{a}_{-1} - 3a_{-1}\dot{a}_1 = -6a_2\dot{a}_0, \tag{4.56}
$$

$$
10\dot{a}_{-1}a_2 - 8\dot{a}_2a_{-1} = -6\dot{a}_{-1}a_2, \tag{4.57}
$$

in the numerator $n(t)$ to obtain:

$$
\dot{\kappa}(0) \sim 6a_2(\dot{a}_{-1} + \dot{a}_0 + \dot{a}_1 + \dot{a}_2). \tag{4.58}
$$

I will prove now that the denominator of $\dot{\kappa}(0)$ is initially positive; this means that it stays positive. Otherwise, $\partial_\alpha f(0) = 0$ and the curvature would tend to infinity. The area A is given by (see Chapter 3 about the complex/Richardsons moments)

$$
A(0) = a_{-1}^2(0) - a_1^2(0) - 2a_2^2(0) > 0 \Rightarrow a_{-1}(0) > a_1(0). \tag{4.59}
$$

Since $a_2(0) < 0$, I obtain:

$$
a_{-1}(0) - a_1(0) - 2a_2(0) > 0 \tag{4.60}
$$

This means that the sign of the derivative of the curvature is determined by the numerator, given is equation (4.58). Since we have

$$
a_2 = a_2(0)\frac{a_{-1}^2(t)}{a_{-1}^2(0)}, \tag{4.61}
$$

we see that $a_2 < 0 \quad \forall t > 0$, since we assumed $a_2(0) < 0$. The part between brackets $(\dot{a}_{-1} + \dot{a}_0 + \dot{a}_1 + \dot{a}_2)$ is the velocity of the interface at the tip: $\partial_t f(\alpha = 0)$. Therefore the curvature at the tip decreases according to (4.58). This is completes the proof.

4.3.4   The general case: arbitrary N

In this case it is impossible to solve the equations analytically; the ODE's need to be solved numerically. The numerical implementation of equation (4.28) is done using a standard fortran algorithm from the Numerical Recipes [58], which solves an N-dimensional system of ODE's.
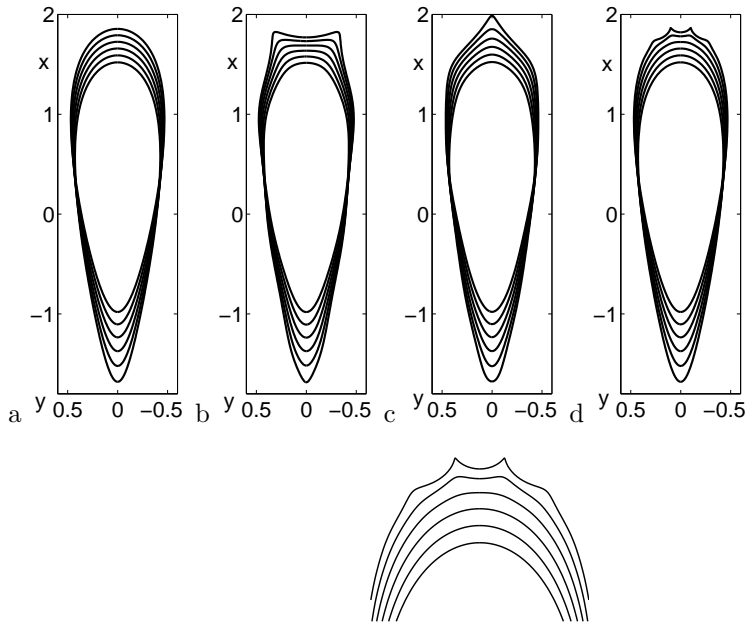
Figure 4.1: Upper panel: evolution of the interface in equal time steps up to time $t = 0.1/E_0$ with initial condition
a) $z_0(\alpha, 0) = e^{-i\alpha} + 0.6 \cdot e^{i\alpha} - 0.08 \cdot e^{2i\alpha}$,
b) $z(\alpha, 0) = z_0(\alpha, 0) - 5 \cdot 10^{-3} \cdot e^{8i\alpha}$
c) $z(\alpha, 0) = z_0(\alpha, 0) + 3 \cdot 10^{-3} \cdot e^{8i\alpha}$
d) $z(\alpha, 0) = z_0(\alpha, 0) - 4.5 \cdot 10^{-7} \cdot e^{30i\alpha}$,
and lower panel: zoom into the unstable head of Fig. d.

Figure 4.1 shows four runs of the program; the initial conditions for all four runs are almost the same; they only differ in a small perturbation of a high mode. After some evolution the interfaces depend a lot on this initial condition, though. Furthermore, we see the emergence of cusps at the interface: points with infinite curvature. If I continue the simulation, I get self-intersections at the interface. This means, that it makes no sense to continue the simulation after a cusp is reached. Physically, we see those cusps since a regularization mechanism for the short length scales is missing. This corresponds mathematically to the loss of conformality of the mapping function at a point on the boundary. When performing those simulations, I usually keep track of the minimum of the $|\partial_\alpha f|$; at a certain time, this minimum decreases rapidly towards zero and a cusp at the

interface is formed, ending the simulation. From the simulations in figure 4.1 we clearly see, that the cusp formation is a generic property of the unregularized problem.

I will investigate in later chapters whether a regularization can be found that prevents cusps; in figure 4.2 we studied a more elongated streamer; the back part is not shown. This figure shows, that the streamer head is able to become concave, even if it is initially convex.
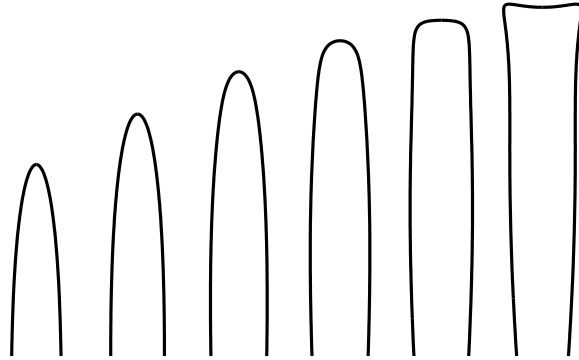
Figure 4.2: Evolution of the tip of an elongated "streamer" in equal time steps up to time $t = 0.1/E_0$; initial condition $z(\alpha, 0) = e^{-i\alpha} + 0.9 \cdot e^{i\alpha} - 0.03 \cdot e^{2i\alpha} - 1.2 \cdot 10^{-5} \cdot e^{12i\alpha}$.

The conclusion of this chapter is that the unregularized problem shows promising features, the transition from convex to concave of the streamer head. It is still lacking a physical ingredient: a mechanism which regularizes the short length scales. This mechanism will be the subject of the next chapter.

Chapter 5

Derivation and implementation of a new boundary condition

The purpose of this chapter is the derivation of a streamer specific condition on the moving boundary. Regularization can be hoped for, but has not been fully tested up to now. This boundary condition reads

$$\phi = \epsilon(\nabla\phi)_n, \tag{5.1}$$

where ϵ introduces a new lengthscale. Previously, the problem was scale invariant, since the electrodes where placed at infinity. The size of the boundary layer with respect to the size of the streamer is introduced via the boundary condition (5.1). It is still possible to derive analytic solutions; the uniformly translating circle is a solution of the regularized problem. For more general initial conditions, the complex potential can not be calculated analytically. I use a mode expansion of $\hat{\Phi}$ in terms of the mapping function to calculate the potential numerically. In order to solve the full PDE problem, the analyticity of the $f_t(\omega)$ needs to be preserved. An expansion in ω is used for f as well to analyze the full nonlinear problem. The previous chapter motivated truncated series, but the following chapters will show that this is not appropriate.

5.1 Derivation of the boundary condition

In Chapter 8 planar solutions of the streamer equations (2.9)-(2.11) will be discussed. Those can be derived by inserting the comoving coordinate ξ in the equations

$$\sigma(\mathbf{r}, t) = \sigma(\xi = z - vt), \quad \text{similarly for } \rho \text{ and } \mathbf{E}. \tag{5.2}$$

We are looking for fronts, connecting the ionized state behind the streamer to the non-ionized state in front of the streamer:

$$\rho = \sigma, \quad \mathbf{E} = 0 \quad \text{as} \quad \xi \to -\infty \tag{5.3}$$

and

$$\rho = \sigma = 0, \quad \mathbf{E} \to -E_0 \hat{\xi} \quad \text{as} \quad \xi \to \infty. \tag{5.4}$$

Those solutions can be calculated analytically [9], [12]. A shock front is obtained for $D = 0$. The coordinate ξ is chosen such that the position of the jump is exactly at $\xi = 0$. A picture of the planar solutions is given in figure 5.1.
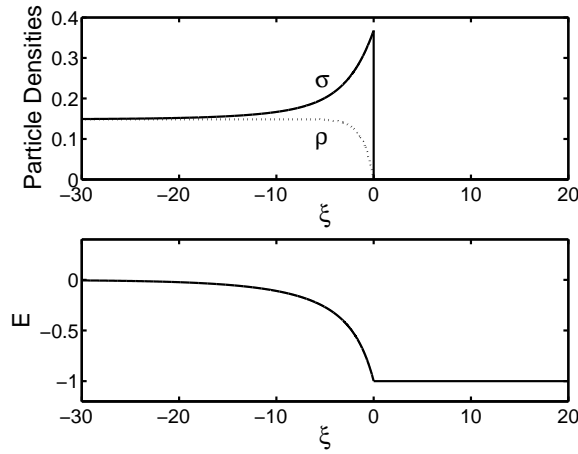
Figure 5.1: The planar front in a field $E_0 = 1$ from [12].

It is possible to calculate the jump of the potential across the interface in the planar case (almost) analytically, since the expression for the electrical field is given. Let ξ be the comoving coordinate and calculate the jump in the potential:

$$-\int_{-\infty}^{0} E d\xi = \phi(0) - \phi(-\infty). \tag{5.5}$$

We have, for $\xi < 0$

$$\xi_2 - \xi_1 = \int_{E(\xi_1)}^{E(\xi_2)} \frac{v + x}{\rho[x]} \frac{dx}{x}, \tag{5.6}$$

where $v = E_0 > 0$ and

$$\rho[x] = \int_{|x|}^{E_0} \alpha(x) dx, \tag{5.7}$$

$$\alpha(x) = e^{-1/x}. \tag{5.8}$$

Far ahead of the front, we have a constant electrical field $\mathbf{E} = -E_0\hat{\xi}$. Substitution of $\xi_1 = 0$ and renaming $\xi_2 = \xi$ in equation (5.6) yields

$$\xi = \int_{-E_0}^{E(\xi)} \frac{v+x}{\rho[x]}\frac{dx}{x}. \tag{5.9}$$

Partial integration of equation (5.5) gives us

$$\phi(0) - \phi(-\infty) = -\int_{-\infty}^{0} E d\xi = (\xi E) + \int_{0}^{-E_0} \xi dE = \int_{0}^{-E_0} \xi dE, \tag{5.10}$$

since either the electrical field E or ξ vanishes at the boundaries of the integration. Substitute equation (5.9) in equation (5.10) to obtain

$$\phi(0) - \phi(-\infty) = \int_{0}^{-E_0} dE \int_{-E_0}^{E} \frac{v+x}{\rho[x]}\frac{dx}{x}. \tag{5.11}$$

It is possible to change the order of integration in the following way:

$$\int_{E=0}^{E=-E_0} dE \int_{x=-E_0}^{x=E} f(x)dx = \int_{x=-E_0}^{x=0} dx \int_{E=0}^{E=x} f(x)dE = \int_{x=-E_0}^{x=0} dx\, x f(x) \tag{5.12}$$

Rewriting equation 5.11 in this way gives us

$$\phi(0) - \phi(-\infty) = \int_{-E_0}^{0} dx \frac{v+x}{\rho[x]}. \tag{5.13}$$

Lemma 1

$$\frac{\phi(0) - \phi(-\infty)}{E_0} \to 1 \tag{5.14}$$

if E_0 large enough.

Lemma 1 implies that the jump in the potential is given by the local electric field, provided the field is large enough. What 'large enough' means can be seen from the direct numerical integration of equation (5.13) for different values of E_0.

Proof of Lemma 1:

The idea of the proof is to give upper and lower bounds on the integral and to show that both bounds tend to E_0 if E_0 tends to infinity. Substitute $y = -x$ and $v = E_0$ in equation (5.13):

$$\phi(0) - \phi(-\infty) = \int_{0}^{E_0} dy \frac{E_0 - y}{\rho[y]}. \tag{5.15}$$

One of the estimates on the jump in the potential is easy:

$$\rho[y] = \int_{y}^{E_0} e^{-1/x}\, dx < \int_{y}^{E_0} e^{-1/E_0}\, dx = e^{-1/E_0}(E_0 - y) \tag{5.16}$$

and

$$\phi(0) - \phi(-\infty) > E_0 e^{1/E_0} > E_0 \qquad (5.17)$$

The other bound is more complicated. Choose $0 < \epsilon \ll 1$ arbitrary and define $x^\star > 0$

$$1 - e^{1/x^\star} = \epsilon. \qquad (5.18)$$

Notice that the function $\alpha(x) = e^{-1/x}$ is monotone, $\alpha(0) = 0$ and $\alpha(\infty) = 1$, which means that $x^\star$ is well defined and unique. This definition allows me to estimate $\rho[x]$ for $x > x^\star$:

$$\rho[x] = \int_x^{E_0} e^{-1/x} > (E_0 - x)(1 - \epsilon), \qquad (5.19)$$

since the function is monotone.
Similar estimates for $0 < x < x^\star$:

$$\rho[x] = \int_x^{E_0} e^{-1/x} = \int_x^{x^\star} e^{-1/x} + \int_{x^\star}^{E_0} e^{-1/x} > (1 - \epsilon)(E_0 - x^\star), \qquad (5.20)$$

since the first integral is positive. This implies

$$\phi(0) - \phi(-\infty) = \int_0^{x^\star} \frac{E_0 - x}{\rho[x]} + \int_{x^\star}^{E_0} \frac{E_0 - x}{\rho[x]} <$$

$$\frac{x^\star}{(1 - \epsilon)(E_0 - x^\star)}\left(E_0 - \frac{1}{2}x^\star\right) + \frac{1}{1 - \epsilon}(E_0 - x^\star) =$$

$$\frac{E_0}{1 - \epsilon} + \frac{\frac{1}{2}(x^\star)^2}{E_0 - x^\star} < \frac{E_0}{1 - \epsilon} + \frac{1}{2x^\star}, \qquad (5.21)$$

provided I choose E_0 large enough, $E_0 > (x^\star)^3 + x^\star$. Since ϵ was arbitray, we see that $\phi(0) - \phi(\infty)$ tends to E_0 from both sides taking $\epsilon \to 0$. This completes the proof.
Numerical integration of equation (5.13) gives us $\phi(0) - \phi(\infty)$ for different values of E_0.
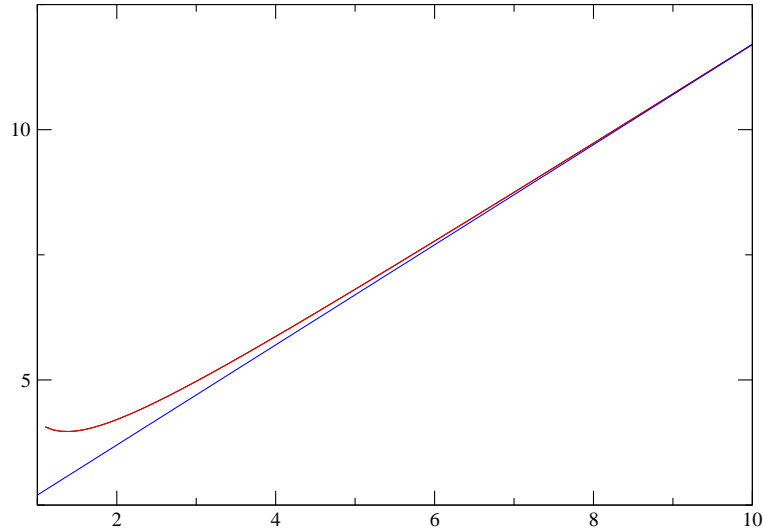
Figure 5.2: $\phi(0)-\phi(\infty)$ as a function of E_0; the numerical calculation of equation (5.11) is given by the upper curve and approaches the straight line for large E_0

From figure (5.2) we clearly see that $\phi(0) - \phi(-\infty)$ grows approximately linearly if $E_0 > 3$.

The electric field in front of the jump is the constant negative far field in the planar case:

$$\mathbf{E} = -E_0 \hat{z}. \tag{5.22}$$

We have according to the results of this section

$$\phi(0) - \phi(-\infty) = -E_0 + \text{constant}, \tag{5.23}$$

and combining this yields at the front

$$\phi = (\nabla \phi)|_n. \tag{5.24}$$

We choose $\phi(-\infty)$ to get rid of the constant, since we are only interested in the jump of the potential across the interface. Furthermore the normal coincides with $\hat{z} = \hat{\xi}$ in the planar case. $\phi/(\nabla \phi)|_n$ has the dimension of length; instead of keeping in mind, that I need to set the overall size of the streamer with respect to this length, I prefer to set the size of the streamer to unity and to introduce ϵ and set,

$$\phi = \epsilon(\nabla \phi)|_n. \tag{5.25}$$

to denote the width of the layer with respect to the size of the streamer.

5.2   Implementation of the boundary condition

The implementation of the new boundary condition is investigated in this section. Use equation (3.47)

$$(\nabla\phi)|_n = \frac{\mathrm{Re}\left(i\partial_\alpha\hat{\Phi}(e^{i\alpha})\right)}{|\partial_\alpha f|} \tag{5.26}$$

to rewrite equation (5.25):

$$\mathrm{Re}(\hat{\Phi}(e^{i\alpha})) = \epsilon\frac{\mathrm{Re}(i\partial_\alpha\hat{\Phi}(e^{i\alpha}))}{|\partial_\alpha f|}. \tag{5.27}$$

We see, that we need the information about the mapping function via $|\partial_\alpha f|$ to calculate the potential. Only if this derivative is trivial, which happens to be the case for the circle, I am able to calculate solutions of the full PDE's analytically. This will be done in Section 5.3.

Otherwise I have to use a numerical method. We still use the formulation of chapter 3 which implies that $\hat{\Phi}(\omega)$ has the following form:

$$\hat{\Phi}(\omega) = \frac{E_0 a_{-1}}{\omega} + \text{analytic terms} \tag{5.28}$$

which can be written without loss of generality

$$\hat{\Phi}(\omega) = \frac{E_0 a_{-1}}{\omega} + \sum_{k=0}^{\infty}\alpha_k\omega^k, \tag{5.29}$$

where the α_k are complex time dependent constants. Due to the left-right symmetry imposed by the mapping function, one would expect the same symmetry for the potential. This is indeed the case: I will rigorously show this in lemma 2.

I want to calculate the α_k numerically, so I will have to use a cut-off:

$$\hat{\Phi}(\omega) = \frac{E_0 a_{-1}}{\omega} + \sum_{k=0}^{N}\alpha_k\omega^k. \tag{5.30}$$

The subsequent calculation was done in two ways; in Section 5.4 I calculate the coefficients α_k for some given mapping function f; an equation of the form

$$\mathbf{M}[|\partial_\alpha f|]\alpha = \mathbf{b}[|\partial_\alpha f|] \tag{5.31}$$

is derived, where the vector α contains the α_k. The matrix $\mathbf{M}$ and the vector $\mathbf{b}$ are given in terms of $|\partial_\alpha f|$. I can go one step further though; since we use the Ansatz

$$f_t(\omega) = \sum_{k=-1}^{\infty} a_k(t)\omega^k \tag{5.32}$$

on f, we have

$$|\partial_\alpha f| = \frac{b_0}{2} + \sum_{k=1}^{\infty} b_k \cos(k\alpha). \qquad (5.33)$$

I use this equation for $|\partial_\alpha f|$ in Section 5.5 to derive an equation of the following form

$$\mathbf{M}[b_k]\alpha = \mathbf{b}[b_k]. \qquad (5.34)$$

This is, however, inefficient; it requires a lot of analysis and has no advantages for the numerics.
I still like to prove in the following lemma that the α_k are real.

Lemma 2 *If $|\partial_\alpha f|$ is given by the Ansatz (5.33) and if $\hat{\Phi}(\omega)$ is given by (5.30), $\alpha_k \in \mathbb{R} \quad \forall k > -1$, provided the determinant of the matrix $\mathbf{M_1} - \mathbf{M_2}$, defined below, is nonzero.*

Proof of Lemma 2:
If $b_k = 0 \quad \forall k > 0$ we have a circle. In this case we can solve the problem analytically, see section 5.3.
Substitution of the *Ansätze* 5.33 and 5.30 in equation 5.27 yields the following equations for the α_k:

$$\left(\sum_{k=-1}^{N} \alpha_{k,r} \cos(k\alpha) - \alpha_{k,i} \sin(k\alpha) \right) \left(\frac{b_0}{2} + \sum_{k=1}^{M} b_k \cos(k\alpha) \right) = \qquad (5.35)$$

$$-\epsilon \left(\sum_{k=-1}^{N} k\alpha_{k,r} \cos(k\alpha) - k\alpha_{k,i} \sin(k\alpha) \right), \qquad (5.36)$$

where we wrote

$$\alpha_k = \alpha_{k,r} + i\alpha_{k,i}. \qquad (5.37)$$

Compare the odd terms on both sides (notice that we calculated $\alpha_{-1,i} = 0$ already explicitly and that $\alpha_{0,i} = 0$ since it only appears in the left hand side):

$$\left(\sum_{k=1}^{N} \alpha_{k,i} \sin(k\alpha) \right) \left(\frac{b_0}{2} + \sum_{k=1}^{M} b_k \cos(k\alpha) \right) = -\epsilon \sum_{k=1}^{N} k\alpha_{k,i} \sin(k\alpha). \qquad (5.38)$$

We need to compare $\sin(m\alpha)$ on both sides by calculating

$$\frac{1}{\pi} \int_0^{2\pi} d\alpha \sin m\alpha f(\alpha), \qquad (5.39)$$

where the left and right hand side of equation (5.38) need to be substituted for $f(\alpha)$. It is convenient to rewrite the equations in matrix form, where the

first component corresponds to the equation for $m = 1$ and the last equation to $m = N$. I will derive an equation of the following form

$$\mathbf{M}_1\mathbf{a} = -\epsilon\mathbf{M}_2\mathbf{a}, \tag{5.40}$$

where

$$\mathbf{a} = \begin{pmatrix} \alpha_{1,i} \\ \alpha_{2,i} \\ \vdots \\ \alpha_{N,i} \end{pmatrix}. \tag{5.41}$$

After rewriting equation (5.38) we only have to keep track of the determinant of the matrix $\mathbf{M}_1 - \mathbf{M}_2$. Rewriting the right hand side of equation (5.38) is easy:

$$\mathbf{M}_2 = \begin{pmatrix} 1 & 0 & \dots & 0 \\ 0 & 2 & \dots & 0 \\ \vdots & \vdots & \ddots & \vdots \\ 0 & 0 & \dots & N \end{pmatrix} \tag{5.42}$$

The contributions of the left hand side are a bit more difficult. Use

$$\sin(l\alpha)\cos(k\alpha) = \frac{1}{2}(\sin((l+k)\alpha) - \sin((l-k)\alpha)). \tag{5.43}$$

The integration in equation (5.39) will give three different contributions: for $l + k = m, l - k = m$ and $k - l = m$. The left hand side consists of those three contributions:

$$\frac{1}{\pi}\int_0^{2\pi}\sum_{k,l=1}^{N}\sin(l\alpha)\cos(k\alpha)\sin(m\alpha)\alpha_{l,i}b_k = \frac{1}{2}(\mathbf{M}_{1,a} + \mathbf{M}_{1,b} + \mathbf{M}_{1,c})\mathbf{a}, \tag{5.44}$$

where the matrices are given below:

$$\mathbf{M}_{1,a} = \begin{pmatrix} \frac{b_0}{2} & 0 & \dots & 0 \\ b_1 & \frac{b_0}{2} & \dots & 0 \\ \vdots & \vdots & \ddots & \vdots \\ b_{N-1} & b_{N-2} & \dots & \frac{b_0}{2} \end{pmatrix}, \tag{5.45}$$

$$\mathbf{M}_{1,b} = \begin{pmatrix} b_2 & b_3 & \dots & b_{N+1} \\ b_3 & b_4 & \dots & b_{N+2} \\ \vdots & \vdots & \ddots & \vdots \\ b_{N+1} & b_{N+2} & \dots & b_{2N} \end{pmatrix}, \tag{5.46}$$

and

$$\mathbf{M}_{1,c} = \begin{pmatrix} \frac{b_0}{2} & b_1 & \dots & b_{N-1} \\ 0 & \frac{b_0}{2} & \dots & b_{N-2} \\ \vdots & \vdots & \ddots & \vdots \\ 0 & 0 & 0 & \frac{b_0}{2} \end{pmatrix}. \tag{5.47}$$

We see that $\mathbf{a} = 0$ solves the equation; since I assumed the determinant of $\mathbf{M}_1 - \mathbf{M}_2$ to be nonzero. This proves the theorem.

Notice that this determinant depends strongly on the mapping function at each time. For any physical solution, this assumption will probably not be restricitive. The real part of the α_k will be calculated in Section 5.5; in this case, the matrix equation is inhomogeneous, due to the term present because of the far field E_0, which implies that this equation will have a non trivial solution.

5.3   Analytical solution: the circle

In this section we will show that the circle is a uniform translating solution in the regularized case, more precisely formulated in Theorem 11:

Theorem 11 *If the initial condition of the regularized problem is a circle, then the solution will stay a circle.*

Proof of theorem 11: We will prove that the time derivatives of all a_k are zero initially, execpt a_{-1}, thus proving that they remain zero, which implies that the circle is a uniformly translating solution. Initially we have:

$$f_0(\omega) = \frac{1}{\omega}, \tag{5.48}$$

and

$$|\partial_\alpha f| = 1, \tag{5.49}$$

Since the size of the streamer was set to unity, $a_{-1}(0) = 1$. I am able to calculate the α_k analytically at $t = 0$:

$$\mathrm{Re}(\hat{\Phi}(e^{i\alpha})) = E_0 \cos\alpha + \sum_{k=0}^{\infty} \alpha_k(0) \cos(k\alpha) \tag{5.50}$$

and

$$\mathrm{Re}(i\partial_\alpha \hat{\Phi}(e^{i\alpha}) = E_0 \cos\alpha - \sum_{k=0}^{\infty} k\alpha_k(0) \cos(k\alpha) \tag{5.51}$$

and using the boundary condition (5.27) we see that

$$E_0(1-\epsilon)\cos(\alpha) = -\sum_{k=0}^{\infty}(1+k\epsilon)\alpha_k(0)\cos(k\alpha) \tag{5.52}$$

which means that

$$\alpha_1(0) = -E_0\frac{1-\epsilon}{1+\epsilon}, \ \alpha_k(0) = 0 \quad for \quad k \neq 1 \tag{5.53}$$

This means that driving force in the equation of motion (3.48) is given by

$$\operatorname{Re}(-i\partial_\alpha \hat{\Phi}(e^{i\alpha})) = \cos\alpha(-E_0 + \alpha_1). \tag{5.54}$$

Insertion of the explicit expression for α_1 of equation (5.53) into equation (5.54) gives us $\operatorname{Re}(-i\partial_\alpha \hat{\Phi}(e^{i\alpha}))$:

$$\operatorname{Re}(-i\partial_\alpha \hat{\Phi}(e^{i\alpha})) = -2E_0 \cos\alpha \frac{1}{1+\epsilon}. \tag{5.55}$$

Notice that the dynamics of the regularized equation is very similar to the dynamics of the unregularized problem, where we had

$$\operatorname{Re}(-i\partial_\alpha \hat{\Phi}(e^{i\alpha})) = -2E_0 \cos\alpha. \tag{5.56}$$

We can use the same argument as in this case: since the time derivatives of all the higher modes are initially zero, they will stay zero and the explicit solution is:

$$a_{-1}(t) = a_{-1}(0) = 1, \ a_0(t) = \frac{2E_0 t}{1+\epsilon}, \ a_k(t) = 0 \text{ for } k > 0 \tag{5.57}$$

This means that we have a uniformly translating circle. This proves the theorem.

5.4   Towards a numerical scheme: calculation of the potential 1

For a general initial condition, I need a numerical scheme to solve the problem. This means that I will have to calculate the potential Φ when the mapping function is given. I will rewrite the boundary condition

$$\operatorname{Re}\hat{\Phi} = \epsilon \frac{\operatorname{Re}(i\partial_\alpha \Phi)}{|\partial_\alpha f|} \tag{5.58}$$

with the ansatz

$$\hat{\Phi}(\omega) = E_0 a_{-1} \left(\frac{1}{\omega} + \sum_{k=0}^{\infty} \alpha_k \omega^k \right) \tag{5.59}$$

in the following form:

$$\mathbf{M}\alpha = \mathbf{b}, \tag{5.60}$$

where the matrix $\mathbf{M}$ and the vector $\mathbf{b}$ depend on $|\partial_\alpha f|$ and

$$\alpha = \begin{pmatrix} \alpha_0 \\ \alpha_1 \\ \vdots \\ \alpha_N \end{pmatrix} \tag{5.61}$$

In Section 5.5 I use a mode expansion for the absolute value as well. This approach offers no numerical advantages, but was used to obtain the numerical results in the last section. Using the next section instead would be preferable in the future.

5.4.1   Derivation of the equation for the potential

We would like to determine the coefficients α_k using the boundary condition given in equation (5.58). Although this means that we have to determine an infinite number of coefficients, we expect that the α_k become very small if $k > N$, where N is chosen sufficiently large such that their impact on the dynamics is negligible.

Substitution of equation (5.59) in equation (5.58) yields

$$\sum_{k=-1}^{\infty} |\partial_\alpha f| \alpha_k \cos(k\alpha) = -\epsilon \sum_{k=-1}^{\infty} k\alpha_k \cos(k\alpha), \qquad (5.62)$$

where $\alpha_{-1} = 1$. Insert this in equation (5.62) to obtain:

$$-\epsilon \sum_{k=1}^{\infty} k\alpha_k \cos(k\alpha) = -\epsilon \cos \alpha + |\partial_\alpha f| \left(\cos \alpha + \sum_{k=0}^{\infty} \alpha_k \cos(k\alpha) \right). \qquad (5.63)$$

Use

$$-\epsilon m \alpha_m = \frac{-\epsilon}{\pi} \int_0^{2\pi} \cos(m\alpha) \sum_{k=1}^{\infty} k\alpha_k \cos(k\alpha) d\alpha \qquad (5.64)$$

and combine the equations (5.63) and (5.64) to obtain

$$\epsilon m \alpha_m = \epsilon \delta_{m1} - \frac{1}{\pi} \int_0^{2\pi} \cos(m\alpha) |\partial_\alpha f| \left(\cos(\alpha) + \sum_{k=0}^{\infty} \alpha_k \cos(k\alpha) \right) d\alpha, \quad (5.65)$$

where I used

$$\frac{1}{\pi} \int_0^{2\pi} \cos(\alpha) \cos(m\alpha) d\alpha = \delta_{m1} \qquad (5.66)$$

Remark Notice that equation (5.65) also holds for $m = 0$.

It is convenient to rewrite equation (5.65) in matrix form; the first equation corresponds to $m = 0$ and so on.

$$\epsilon \mathbf{A} \alpha = \epsilon \begin{pmatrix} 0 \\ 1 \\ 0 \\ \vdots \\ 0 \end{pmatrix} + \mathbf{b}_1 + \mathbf{M}_1 \alpha, \qquad (5.67)$$

where

$$\mathbf{A} = \begin{pmatrix} 0 & 0 & 0 & \dots & 0 \\ 0 & 1 & 0 & \dots & 0 \\ 0 & 0 & 2 & \dots & 0 \\ \vdots & \vdots & \vdots & \ddots & \vdots \\ 0 & 0 & 0 & 0 & N \end{pmatrix}, \qquad (5.68)$$

$$\mathbf{M}_1 = - \begin{pmatrix} m_{0,0} & m_{0,1} & m_{0,2} & \cdots & m_{0,N} \\ m_{1,0} & m_{1,1} & m_{1,2} & \cdots & m_{1,N} \\ m_{2,0} & m_{2,1} & m_{2,2} & \cdots & m_{2,N} \\ \vdots & \vdots & \vdots & \vdots & \vdots \\ m_{N,0} & m_{N,1} & m_{N,2} & \cdots & m_{N,N} \end{pmatrix}, \tag{5.69}$$

$$\mathbf{b}_1 = - \begin{pmatrix} m_{0,1} \\ m_{1,1} \\ m_{2,1} \\ \vdots \\ m_{N,1} \end{pmatrix}, \tag{5.70}$$

where $m_{i,j}$ is defined as follows:

$$m_{i,j} = \frac{1}{\pi} \int_0^{2\pi} \cos(i\alpha) \cos(j\alpha) |\partial_\alpha f| d\alpha. \tag{5.71}$$

We see, that this gives us the desired form of the equation, since

$$\mathbf{M}\alpha = (\epsilon\mathbf{A} - \mathbf{M})\alpha = \epsilon \begin{pmatrix} 0 \\ 1 \\ 0 \\ \vdots \\ 0 \end{pmatrix} + \mathbf{b}_1 = \mathbf{b}. \tag{5.72}$$

I will show that those results are still consistent with known results, which is always a good check for errors. In the circular case, f is independent of α and $|\partial_\alpha f| = 1$

$$m_{i,j} = \delta_{ij} + \delta_{00}. \tag{5.73}$$

Use the expression from equation (5.73) to simplify equation (5.67):

$$\epsilon\mathbf{A}\alpha = (\epsilon - 1) \begin{pmatrix} 0 \\ 1 \\ 0 \\ \vdots \\ 0 \end{pmatrix} - \mathbf{I}\alpha, \tag{5.74}$$

where $\mathbf{I}$ is the a diagonal matrix

$$\mathbf{I} = \begin{pmatrix} 2 & 0 & \cdots & 0 \\ 0 & 1 & \cdots & 0 \\ \vdots & \vdots & \ddots & \vdots \\ 0 & 0 & \cdots & 1 \end{pmatrix}. \tag{5.75}$$

We see immediately that

$$\alpha_1 = -\frac{1-\epsilon}{1+\epsilon}, \ \alpha_k = 0 \text{ if } k \neq 1, \tag{5.76}$$

as expected.

If $\epsilon \to 0$ (the unregularized case), we can neglect the left hand side and the first term on the right hand side of equation (5.67). This means that equation (5.67) reduces to equation (5.77):

$$\mathbf{M}_1 \alpha = -\mathbf{b}_1. \tag{5.77}$$

Notice that the first row of the matrix M is the same as the vector $\mathbf{b}$. We can solve equation (5.77) directly:

$$\alpha = \begin{pmatrix} 0 \\ -1 \\ 0 \\ \vdots \\ 0 \end{pmatrix} \tag{5.78}$$

and we see that we obtain

$$\hat{\Phi}(\omega) = E_0 a_{-1} \left(\frac{1}{\omega} - \omega \right), \tag{5.79}$$

which is exactly the expression we obtained in the unregularized case. Finally we see that for large ϵ (which would physically correspond to switching of the electrical field) both $\mathbf{M}$ and $\mathbf{b}$ can be neglected, which means

$$\alpha = \begin{pmatrix} 0 \\ 1 \\ 0 \\ \vdots \\ 0 \end{pmatrix}, \tag{5.80}$$

and this means that

$$\text{Re}(\omega \partial_\omega \hat{\Phi}(\omega)) = a_{-1} E_0 \text{Re}(2i \sin(\alpha)) = 0. \tag{5.81}$$

There is no driving force left and the streamer gets stuck.

Equation (5.67) reproduces all desired limits correctly.

5.5 Towards a numerical scheme: calculation of the potential 2

In this section, I will proceed the analysis one step further, using

$$|\partial_\alpha f| = \frac{b_0}{2} + \sum_{k=1}^{N} b_k \cos(k\alpha), \quad \hat{\Phi}(\omega) = \frac{E_0}{\omega} + \sum_{k=0}^{N} \alpha_k \omega^k. \tag{5.82}$$

At this point, I do not need to impose any cut-off on the mapping function itself; I only limit the number of terms I calculate in the expansion of its derivative. Equation 5.27 defines the coefficients α_k implicitly:

$$|\partial_\alpha f|\mathrm{Re}(\hat{\Phi}(e^{i\alpha})) = \epsilon \mathrm{Re}(i\partial_\alpha \Phi(e^{i\alpha})). \tag{5.83}$$

Insertion of equation (5.82) in equation 5.83 yields

$$\left(\frac{1}{2}b_0 + \sum_{k'=1}^{N} b_{k'} \cos(k'\alpha)\right)\left((E_0 a_{-1} + \alpha_1)\cos(\alpha) + \alpha_0 + \sum_{k=2}^{N} \alpha_k \cos(k\alpha)\right)$$
$$= \epsilon\left((E_0 a_{-1} - \alpha_1)\cos(\alpha) - \sum_{k=2}^{N} k\alpha_k \cos(k\alpha)\right). \tag{5.84}$$

Comparing the terms $\cos(\alpha)$ until $\cos((N+1)\alpha)$ will give us $N+1$ linear equations for $\alpha_0, \ldots, \alpha_N$. I would like to rewrite these equations in the following form:

$$\mathbf{M}[b_k]\alpha = \mathbf{b}, \tag{5.85}$$

where

$$\alpha = \begin{pmatrix} \alpha_0 \\ \alpha_1 \\ \vdots \\ \alpha_N \end{pmatrix} \tag{5.86}$$

contains the α_k and the matrix $\mathbf{M}$ and the vector $\mathbf{b}$ are given in terms of the b_k. We obtain those equation by mulitplying both sides of equation 5.84 with $\cos(m\alpha)$ and integrating;

$$eq_m = \frac{1}{\pi}\int_0^{2\pi} g(\alpha)\cos(m\alpha), \quad m = 1,\ldots N+1, \tag{5.87}$$

where

$$g(\alpha) = |\partial_\alpha f|\mathrm{Re}(\hat{\Phi}(e^{i\alpha})) - \epsilon \mathrm{Re}(i\partial_\alpha \hat{\Phi}(e^{i\alpha})). \tag{5.88}$$

Evaluating the contribtions of $\epsilon \mathrm{Re}(i\partial_\alpha \hat{\Phi}(e^{i\alpha}))$ is easy (I will call this integral rhs for further reference):

$$rhs = \frac{1}{\pi}\int_0^{2\pi}\cos(m\alpha)\epsilon \mathrm{Re}(i\partial_\alpha \hat{\Phi}(e^{i\alpha}))d\alpha = \epsilon\begin{pmatrix} 0 \\ E_0 a_{-1} - \alpha_1 \\ -2\alpha_2 \\ \vdots \\ -N\alpha_N \end{pmatrix}. \tag{5.89}$$

The contributions of $|\partial_\alpha f|\text{Re}(\hat{\Phi}(e^{i\alpha}))$ are more involved, since some of them involve integrations over multiple cosines. I will evaluate the integral in parts:

$$\frac{1}{\pi}\int_0^{2\pi}\cos(m\alpha)|\partial_\alpha f|\text{Re}(\hat{\Phi}(e^{i\alpha}))d\alpha =$$
$$lhs_1 + lhs_2 + lhs_3 + lhs_{4,m=0} + lhs_{4,a} + lhs_{4,b} + lhs_{4,c} \tag{5.90}$$

Terms containing a b_0:

$$lhs_1 = \begin{pmatrix} \alpha_0 b_0 \\ \frac{1}{2}b_0(E_0 a_{-1} + \alpha_1) \\ \frac{1}{2}b_0 \alpha_2 \\ \vdots \\ \frac{1}{2}b_0 \alpha_N \end{pmatrix} \tag{5.91}$$

Terms containing α_0:

$$lhs_2 = \alpha_0 \begin{pmatrix} 0 \\ b_1 \\ \vdots \\ b_N \end{pmatrix}. \tag{5.92}$$

Terms of the form $\cos\alpha\cos k\alpha\cos m\alpha$ yield different contributions:

$$lhs_3 = \frac{1}{2}(E_0 a_{-1} + \alpha_1)\left(\begin{pmatrix} 2b_1 \\ b_2 \\ \vdots \\ b_N \\ 0 \end{pmatrix} + \begin{pmatrix} 0 \\ 0 \\ b_1 \\ \vdots \\ b_{N-1} \end{pmatrix}\right). \tag{5.93}$$

This leaves us with terms of the following form:

$$\int_0^{2\pi} d\alpha \sum_{k=1}^{N} b_k \cos(k\alpha) \sum_{k'=2}^{N} \alpha_{k'}\cos(k'\alpha)\cos(m\alpha) \neq 0 \quad \text{if} \quad k \pm k' = \pm m. \tag{5.94}$$

Let us look first of all at the case where $m = 0$; in this case we get:

$$\frac{1}{\pi}\int_0^{2\pi} d\alpha \sum_{k=1}^{N} b_k \cos(k\alpha) \sum_{k'=2}^{N} \alpha_{k'}\cos(k'\alpha) \sum_{k=2}^{N} b_k \alpha_k. \tag{5.95}$$

Rewrite equation 5.95 and the other equations in a matrix form:

$$lhs_{4,m=0} = \pi \begin{pmatrix} 0 & 0 & b_2 & \dots & b_N \\ 0 & 0 & 0 & \dots & 0 \\ 0 & 0 & 0 & \dots & 0 \\ 0 & 0 & 0 & \dots & 0 \\ 0 & 0 & 0 & \dots & 0 \end{pmatrix} \begin{pmatrix} \alpha_0 \\ \alpha_1 \\ \alpha_2 \\ \vdots \\ \alpha_N \end{pmatrix} \tag{5.96}$$

We have four possibilities, but since k, k' and m are positive, $k + k' = -m$ gives no contribution. Let us start with lhs_{4a}, where we consider $k - k' = -m$; this means $k' = m + k$ and we have for $m = 1$:

$$b_1\alpha_2 + b_2\alpha_3 + .. + b_{N-1}\alpha_N, \tag{5.97}$$

for $m = 2$:

$$b_1\alpha_3 + .., \tag{5.98}$$

this last contribution comes from $m = N - 1$ and gives $b_1\alpha_N$. These results can be summarized in a matrix:

$$lhs_{4a} = \begin{pmatrix} 0 & 0 & 0 & \ldots & 0 \\ 0 & 0 & b_1 & \ldots & b_{N-1} \\ 0 & 0 & 0 & \ddots & \vdots \\ 0 & 0 & 0 & 0 & b_1 \\ 0 & 0 & 0 & 0 & 0 \end{pmatrix} \begin{pmatrix} \alpha_0 \\ \alpha_1 \\ \alpha_2 \\ \vdots \\ \alpha_N \end{pmatrix}. \tag{5.99}$$

We continue with lhs_{4b} where we investigate the case where $k - k' = m$; this means $k' = k - m$ and we get get the following terms; $m = 1$:

$$b_3\alpha_2 + b_4\alpha_3 + .. + b_N\alpha_{N-1}, \tag{5.100}$$

for $m = 2$

$$b_4\alpha_2 + b_5\alpha_3 + .. + b_N\alpha_{N-2} \tag{5.101}$$

and for $m = N - 2$ we have $b_N\alpha_2$. This can be summarized in a matrix:

$$lhs_{4b} = \begin{pmatrix} 0 & 0 & 0 & 0 & 0 & 0 \\ 0 & 0 & b_3 & \ldots & b_N & 0 \\ 0 & 0 & \vdots & \ddots & 0 & 0 \\ 0 & 0 & b_N & 0 & 0 & 0 \\ 0 & 0 & 0 & 0 & 0 & 0 \\ 0 & 0 & 0 & 0 & 0 & 0 \end{pmatrix} \begin{pmatrix} \alpha_0 \\ \alpha_1 \\ \alpha_2 \\ \vdots \\ \alpha_N \end{pmatrix}. \tag{5.102}$$

Finally we investigate the case where $k + k' = m$. We will call this case lhs_{4c}. If $m = 3$, we have $b_1\alpha_2$, if $m = 4$, we have $b_1 + \alpha_3 + b_2\alpha_2$ and so on until $m = N$ where we have

$$b_{N-2}\alpha_2 + .. + b_1\alpha_{N-1}. \tag{5.103}$$

Summarizing this in a matrix yields:

$$lhs_{4c} = \begin{pmatrix} 0 & 0 & 0 & \ldots & 0 & 0 \\ 0 & 0 & 0 & \ldots & 0 & 0 \\ 0 & 0 & 0 & \ldots & 0 & 0 \\ 0 & 0 & b_1 & 0 & 0 & 0 \\ 0 & 0 & \vdots & \ddots & 0 & 0 \\ 0 & 0 & b_{N-2} & \ldots & b_1 & 0 \end{pmatrix} \begin{pmatrix} \alpha_0 \\ \alpha_1 \\ \alpha_2 \\ \vdots \\ \alpha_N \end{pmatrix}. \tag{5.104}$$

I am now ready to rewrite equation 5.84 in the desired form:

$$\mathbf{M}[b_k]\alpha = \mathbf{b}, \tag{5.105}$$

where the matrix $\mathbf{M}$ and the vector $\mathbf{b}$ depend on the b_k. Rewriting the equation with rhs and all parts of the equations with lhs in the approprate form yields the following equations:

$$rhs = \begin{pmatrix} 0 \\ E_0 a_{-1} \\ 0 \\ \vdots \\ 0 \end{pmatrix} - \mathbf{M}_0 \alpha \tag{5.106}$$

where M_0 is defined as follows:

$$\mathbf{M}_0 = \begin{pmatrix} 0 & 0 & 0 & \dots & 0 \\ 0 & 1 & 0 & \dots & 0 \\ 0 & 0 & 2 & \dots & 0 \\ 0 & 0 & 0 & \ddots & 0 \\ 0 & 0 & 0 & 0 & N \end{pmatrix} \tag{5.107}$$

Adding the last term for the equation of lhs_3, $\frac{1}{2}$ of the first term of lhs_2 and the first term of equation $lhs_1 - \frac{1}{2}\alpha_0 b_0$ to the matrix of equation lhs_{4c} gives us term M_3:

$$\mathbf{M}_3 \alpha = \frac{1}{2} \begin{pmatrix} b_0 & 0 & 0 & \dots & 0 \\ b_1 & b_0 & 0 & \dots & 0 \\ \vdots & \dots & \ddots & 0 & 0 \\ b_{N-1} & \dots & b_1 & b_0 & 0 \\ b_N & b_{N-1} & \dots & b_1 & b_0 \end{pmatrix} \alpha. \tag{5.108}$$

Adding the first term of $lhs_3 - \frac{b_1 \alpha_1}{2}$, the other half of the first term of equation lhs_2, a half of equation $lhs_{4,m=0}$ and $\frac{1}{2}\alpha_0 b_0$ (remaining from the previous equation) to the matrix of equation lhs_{4b} gives us term M_2:

$$\mathbf{M}_2 \alpha = \frac{1}{2} \begin{pmatrix} b_0 & b_1 & b_2 & \dots & b_N \\ b_1 & b_2 & \dots & b_N & 0 \\ \vdots & \vdots & \ddots & 0 & 0 \\ b_{N-1} & b_N & 0 & \dots & 0 \\ b_N & 0 & 0 & \dots & 0 \end{pmatrix} \alpha. \tag{5.109}$$

Collecting the remaining terms, $b_1\alpha_1$, the other half of $lhs_{4,m=0}$ and the matrix from lhs_{4a} we obtain an equation for M_1:

$$\mathbf{M}_1\alpha = \begin{pmatrix} 0 & b_1 & b_2 & \ldots & b_N \\ 0 & 0 & b_1 & \ldots & b_{N-1} \\ 0 & 0 & 0 & \ddots & \vdots \\ 0 & 0 & 0 & 0 & b_1 \\ 0 & 0 & 0 & 0 & 0 \end{pmatrix}\alpha \tag{5.110}$$

I have taken care of all terms involving α and I can collect all the contribtions in the matrix $\mathbf{M}$:

$$\mathbf{M} = \mathbf{M}_0 + \mathbf{M}_1 + \mathbf{M}_2 + \mathbf{M}_3, \tag{5.111}$$

where M_0 is the term coming from the rhs in equation 5.106. Collecting the terms without α_k we obtain an expression for the vector $\mathbf{b}$:

$$\mathbf{b} = \frac{1}{2}E_0 a_{-1}\left(\begin{pmatrix} 0 \\ 2-b_0 \\ 0 \\ 0 \\ \vdots \\ 0 \end{pmatrix} - \begin{pmatrix} 2b_1 \\ b_2 \\ b_3 \\ \vdots \\ b_N \\ 0 \end{pmatrix} - \begin{pmatrix} 0 \\ 0 \\ b_1 \\ b_2 \\ \vdots \\ b_{N-1} \end{pmatrix}\right). \tag{5.112}$$

We notice that we have $N+1$ linear equations for the α_k if the b_k are known. In general it is impossible to give the b_k in terms of the a_k; we will have to compute them numerically. After the calculation of the b_k we can solve the linear equations for the α_k numerically. This gives us the regularized dynamics. The results of the numerical computations are given in the last section of this chapter.

5.6　　Numerical results

After the cumbersome calculation of the previous section, the numerical routine is surprisingly simple. The dynamical equation for the mapping function reads

$$\mathrm{Re}(i\partial_t f \partial_\alpha f^\star) = \mathrm{Re}(i\partial_\alpha \hat{\Phi}(e^{i\alpha})), \tag{5.113}$$

where $\hat{\Phi}$ can be calculated once the mapping function is given:

$$\hat{\Phi} = \frac{E_0 a_{-1}}{\omega} + \sum_{k=0}^{N} \alpha_k \omega^k, \tag{5.114}$$

and

$$\mathbf{M}[b_k]\alpha = \mathbf{b}. \tag{5.115}$$

The b_k are the coefficients of the Fourrier transform of the norm of the derivative of the mapping function f. I do not need to use a series expansion for f here, but I did anyhow to preserve analyticity. The first set of pictures is made with a fixed value of $\epsilon = 0.001$ and varying values of the cut-off in Figures 5.3 and 5.4:
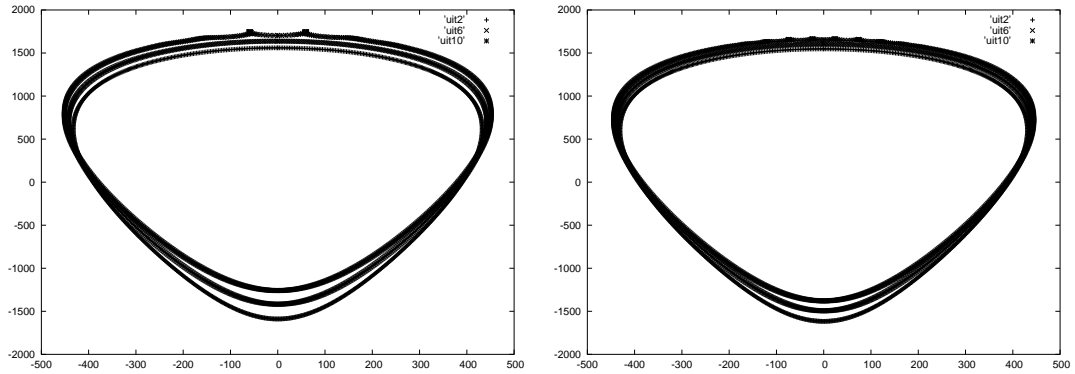
Figure 5.3: The interface with $\epsilon = 0.001$, $N = 50$ and $N = 100$.
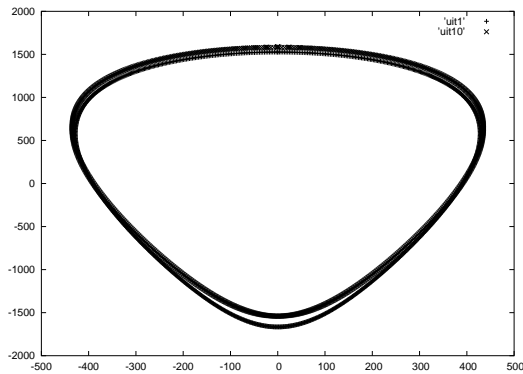
Figure 5.4: The interface with size $\epsilon = 0.001$, $N = 200$.

We see that cusps are formed and that the cusp formation depends on the cut-off N. This means that we have to get rid of this cut-off in order to get reliable results. For $\epsilon = 1$ and $N = 100$ we obtain the following set of pictures 5.5:
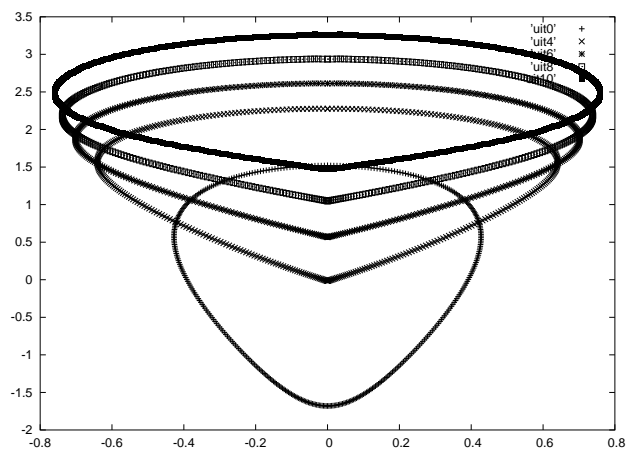
Figure 5.5: The interface with $\epsilon = 1$, $N = 100$

We see that cusps are still encountered, although later. I can include a lot more modes than previously. The obvious question is, whether e.g. the mode expansion for the mapping function causes the cusps or whether this is due to the lack of regularization from the boundary condition. This will be central question of the following two chapters: is this boundary condition able to regularize the problem.

Chapter 6

Behaviour non-conformality points

The emergence of a cusp is related to the motion of the nonconformality points in the complex plane. I study this motion in particular cases with and without regularization. If a zero of the derivative $\partial_\omega f$ hits the unit disc, a cusp will occur in the physical plane. (The curvature will blow up.) This ends the numerical integration of the ODE's. I checked this numerically by tracking the minimum of the absolute value of the derivative on the circle. In the unregularized problem, this cusp formation is probably unavoidable.

I will study the dynamics of these zeros, non-conformality points, in this case for the first nontrivial case, $N = 2$. The $N = 0, 1$ cases will be discussed as well, to get a feeling for the type of analysis. In the trivial cases, the zeros stay where they are and do not reach the unit disc, as expected. In the $N = 2$ case, the zeros are described by two parameters, r and R. The first one denotes two complex conjugate zeros in front of the streamer, the second one a real zero behind the streamer. It is possible to obtain a 2D-phase plane for (r, R) which shows that the solutions tend to $r = 1$. This means that the pair will hit the unit disc, thus ending the solution.

In section 6.3 the regularized case is analyzed in a similar way. Since higher modes will be generated in this case, it is impossible to calculate a phase plane. I can draw a 2D-phase plane, assuming that all terms for $N > 2$ are small; the ODE's will not follow the flow arbitrarily long, but they might do this for some time. The interesting part of this analysis is that arrows, which where originally directed in the direction of the $r = 1$ axis turn around, if the regularization is switched on. This gives hope that the mechanism may be able to regularize the problem.

6.1   The circle and the ellipse: uniformly translating for $\epsilon = 0$

In the unregularized case, the number of modes is conserved in the mapping function; this also means, that the number of zeros of the derivative is conserved. Those zeros are called the 'mother'-singularities of the function. One can easily check that the number of mother singularities equals $N + 1$. This means that the circle and the ellipse are relatively easy cases with one/two zeros. They will be treated in this section.

The mapping function for the circle is

$$f_t(\omega) = \frac{a_{-1}}{\omega} + a_0(t) \tag{6.1}$$

and it is immediately seen that the derivative

$$\partial_\omega f = \frac{-a_{-1}}{\omega^2} \tag{6.2}$$

is nonvanishing on the unit disc $|\omega| \leq 1$, since a_{-1} is the (constant) radius of the circle.

The ellipse is a bit more complicated:

$$f_t(\omega) = \frac{a_{-1}}{\omega} + a_0(t) + a_1(t)\omega, \tag{6.3}$$

$$\partial_\omega f = \frac{-a_{-1}}{\omega^2} + a_1(t), \tag{6.4}$$

which has zeros if

$$\omega^2 = \frac{a_{-1}(t)}{a_1(t)}. \tag{6.5}$$

But

$$\partial_t \frac{a_{-1}(t)}{a_1(t)} = \frac{\dot{a}_{-1}a_1 - \dot{a}_1 a_{-1}}{a_1^2} = 0, \tag{6.6}$$

since the numerator is one of the dynamical equations. This means that the zeros stay where they are and do not hit the unit disc. This can also be seen from the fact that the right hand side of equation (6.5) is real, which means that solutions only exist for $\omega^2 = \pm 1$, which would imply

$$a_1 \pm a_{-1} = 0, \tag{6.7}$$

but those are the axes of the ellipse. The first nontrivial case will be a bit harder.

6.2   The first nontrivial case for $\epsilon = 0$: $N = 2$

The general form of the mapping function in this case is:

$$f_t(\omega) = \frac{a_{-1}(t)}{\omega} + a_0(t) + a_1(t)\omega + a_2(t)\omega^2.$$

(6.8)

Direct calculation would involve roots of a third order equation, so I used a detour. I will use a convenient ansatz on $\partial_\omega f$ to find the zeros and to track whether they are real or not.

Let me rewrite the mapping function in the following form

$$\frac{r^3}{a_{-1}}\partial_\omega f = \frac{-r^3}{\omega^2} + e^{2i\alpha}\left(\frac{\omega - re^{i\alpha}}{e^{-i\alpha} - e^{i\alpha}}\right) + e^{-2i\alpha}\left(\frac{\omega - re^{-i\alpha}}{e^{i\alpha} - e^{-i\alpha}}\right).$$

(6.9)

Notice that this mapping has the following properties:

$$f \to \frac{a_{-1}}{\omega} \quad \text{if} \quad \omega \to 0,$$

(6.10)

$$\partial_\omega f = 0 \quad \text{if} \quad \omega = re^{\pm i\alpha}.$$

(6.11)

Although the ansatz (6.9) has almost all required properties, it is not the most general way to rewrite equation (6.8). The equation $\partial_\omega f = 0$ is a third order equation; we can either have three real roots or one real root and two complex conjugate roots since the a_k are real.
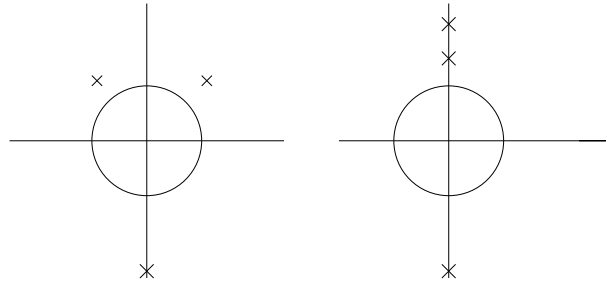
Figure 6.1: Two possibilities for the location of the non-conformality points

I have to extend the ansatz to the first case as well by rewriting f in a convenient form. Rewriting equation (6.9) yields

$$\partial_\omega f = \frac{-a_{-1}}{\omega^2} + \frac{a_{-1}(4\cos^2(\alpha) - 1)}{r^2} - \omega\frac{2a_{-1}\cos\alpha}{r^3}.$$

(6.12)

Integration of equation (6.12) yields the mapping function

$$f = \frac{a_{-1}}{\omega} + a_0 + a_1\omega + a_2\omega^2,$$

(6.13)

with

$$a_1 = \frac{a_{-1}(4\cos^2\alpha - 1)}{r^2}, \quad a_2 = \frac{-a_{-1}\cos\alpha}{r^3}. \tag{6.14}$$

It is convenient to define

$$S = \cos\alpha. \tag{6.15}$$

This allows us to rewrite equation 6.12 as follows:

$$\partial_\omega f = \frac{-a_{-1}}{\omega^2}\left(1 - \frac{\omega^2(4S^2 - 1)}{r^2} + \frac{2S\omega^3}{r^3}\right). \tag{6.16}$$

Use

$$(\omega - re^{i\alpha})(\omega - re^{-i\alpha}) = \omega^2 - 2\omega r\cos\alpha + r^2 \tag{6.17}$$

to rewrite equation (6.16)

$$\partial_\omega f = \frac{-a_{-1}}{\omega^2}(\omega^2 - 2\omega rS + r^2)(\omega + R)\frac{2S}{r^3}, \tag{6.18}$$

where R is the third, real, zero. Comparing equations (6.16) and (6.18) shows that they are equivalent if we set

$$R = \frac{r}{2S}. \tag{6.19}$$

If we take a closer look at equation (6.16) we see that this ansatz already incorporates the case with three real zeros. Apart from the zero at $\frac{-r}{2S}$ I have

$$|S| < 1 \quad , \qquad \omega_\pm = re^{\pm i\alpha} \tag{6.20}$$

$$|S| > 1 \quad , \qquad \omega_\pm = rS\left(1 \pm \sqrt{1 - \frac{1}{S^2}}\right) \tag{6.21}$$

$$|S| = 1 \quad , \qquad \omega = rS \quad \text{double zero.} \tag{6.22}$$

This means that the parameters r and S determine the position of the zeros. Let $a_2(0) < 0$, which means that it remains smaller than zero: $2a_2\dot{a}_{-1} - a_{-1}\dot{a}_2 = 0$ and the number of modes is conserved. Since

$$a_2 = -a_{-1}\frac{S}{r^3} \tag{6.23}$$

according to equation (6.14), we have $S \neq 0$ and $rS > 0$. Due to our initial interpretation of r we set both $r > 0$ and $S > 0$. This means that $R = \frac{r}{2S}$ approaches the interface from behind. Notice that we can rewrite the four dynamical equations for the a_k in terms of r, R and a_0 and a_{-1}. I want to prove, that a zero of the derivative only reaches the interface in the case $r = 1$ or $R = 1$; this means that I need to exclude the case $S > 1$, since one of the two real roots could be smaller than one, while $r > 1$. I will prove that this is impossible in the following Lemma:

Lemma 3 *If $S > 1$ and $R > 1, |\omega_\pm| > 1$.*

This means that we will have to look for two complex conjugate non-conformality points in front of the streamer; a real point is impossible, since the point in the back would be 'earlier'.

Proof of Lemma 3:

Use the following inequalities:

$$R = \frac{r}{2S} > 1 > 1 - \frac{1}{2rS}, \qquad (6.24)$$

which implies

$$\frac{r^2 + 1}{2rS} > 1, \quad \text{and squaring} \quad (r^2 + 1)^2 > 4r^2 S^2. \qquad (6.25)$$

Division by $S^4 r^4$ gives us

$$\frac{1}{S^4} + \frac{1}{r^4 S^4} - \frac{4}{r^2 S^2} + \frac{2}{r^2 S^4} > 0. \qquad (6.26)$$

Add on both sides $4(1 - \frac{1}{S^2})$: this gives us $(2 - \frac{1}{S^2} - \frac{1}{r^2 S^2})^2$ on the left hand side of equation (6.26). Since $|S| > 1$ (we are looking at the real roots), $4(1 - \frac{1}{S^2}) > 0$ and we can take the square roots of both sides of the equation to obtain:

$$2\sqrt{1 - \frac{1}{S^2}} < 2 - \frac{1}{S^2} - \frac{1}{r^2} S^2. \qquad (6.27)$$

Since both the left hand side and the right hand side are positive $r, S > 1$, we also have -left hand side<right hand side and we can write

$$\pm 2\sqrt{1 - \frac{1}{S^2}} < 2 - \frac{1}{S^2} - \frac{1}{r^2} S^2 \qquad (6.28)$$

and

$$\pm 2\sqrt{1 - \frac{1}{S^2}} > -2 + \frac{1}{S^2} + \frac{1}{r^2} S^2. \qquad (6.29)$$

Multiplying by $r^2 S^2$ and rearrangement of terms yields:

$$r^2 S^2 \left(1 + 1 - \frac{1}{S^2} \pm 2\sqrt{1 - \frac{1}{S^2}}\right) = r^2 S^2 \left(1 \pm \sqrt{1 - \frac{1}{S^2}}\right)^2 > 1. \qquad (6.30)$$

I finally obtain

$$\omega_\pm^2 > 1, \qquad (6.31)$$

which implies $|\omega_\pm| > 1$. This proves the lemma.

In equation (6.14), a_1 and a_2 are expressed in terms of r and S, use equation

(6.19) to express them in terms of r and R:

$$a_1 = a_{-1}\left(\frac{1}{R^2} - \frac{1}{r^2}\right), \quad a_2 = -\frac{a_{-1}}{2Rr^2}. \tag{6.32}$$

Use the equations (4.28) which are explicitly given in (4.51). The first equation gives

$$2a_2\dot{a}_{-1} - a_{-1}\dot{a}_2 = 0, \tag{6.33}$$

which implies

$$a_2(t) = a_2(0)a_{-1}(t)^2. \tag{6.34}$$

This yields

$$a_{-1} = \frac{-1}{2a_2(0)Rr^2}. \tag{6.35}$$

Substitute the expressions for a_1 and a_2 given by equation (6.32) in the equations (6.36) and (6.37):

$$2a_2\dot{a}_0 + a_1\dot{a}_{-1} - a_{-1}\dot{a}_1 = 0 \tag{6.36}$$

$$2a_2\dot{a}_2 + a_1\dot{a}_1 - a_{-1}\dot{a}_{-1} = 0 \tag{6.37}$$

to obtain equations in terms of r, R, a_{-1} and their derivatives. We can eliminate a_{-1} using equation (6.35). This yields the following equations for r and R:

$$\dot{a}_0 r^3 R^3 a_2(0) + \dot{R}r^3 - \dot{r}R^3 = 0, \tag{6.38}$$

$$-2\dot{r}R^3 - \dot{R}rR^2 - 2\dot{r}r^4R - 3\dot{R}r^5 + 6\dot{r}r^2R^3 + 4\dot{R}R^2r^3$$
$$-4\dot{r}R^5 - \dot{R}R^4r + 2\dot{r}r^4R^5 + \dot{R}R^4r^5 = 0. \tag{6.39}$$

We can use equation (6.38) to eliminate $\dot{r}$ from equation (6.39), this will be equation (6.40). We can also use it to eliminate $\dot{R}$ this will be equation (6.41):

$$f(r, R)\dot{R} + g(r, R)\dot{a}_0 = 0 \tag{6.40}$$

$$-f(r, R)\dot{r} + h(r, R)\dot{a}_0 = 0, \tag{6.41}$$

where

$$f(r, R) = -2r^2R^2 - R^4 - 2r^6 + 3r^4R^2 - R^6 + 2r^6R^4 + r^4R^6 \tag{6.42}$$

$$g(r, R) = -2a_2(0)r^2R^3(R^2 + r^4 - 3r^2R^2 + 2R^4 - r^4R^4) \tag{6.43}$$

and

$$h(r, R) = -a_2(0)r^3R^2(R^2 + 3r^4 - 4r^2R^2 + R^4 - r^4R^4). \tag{6.44}$$

It is convenient to prove the following Lemma first:

Lemma 4 *If $r > 1$ and $R > 1$, $f(r, R) > 0$.*

Proof of Lemma 4:
Let us assume first that $r > R$, this means $r^4 > R^2$, since they are both greater than one. Now we can estimate all terms of equation (6.42):

$$3r^4 R^2 - 2r^2 R^2 - R^4 = 2R^2 r^2(r^2 - 1) + R^2(r^4 - R^2) > 0, \qquad (6.45)$$

since $r > 1$ and $r^4 > R^2$ and

$$-2r^6 + 2r^6 R^4 - R^6 + r^4 R^6 = 2r^6(R^4 - 1) + R^6(r^4 - 1) > 0, \qquad (6.46)$$

since $R > 1, r > 1$.
This proves the Lemma in this case. Now we assume the other case, $R > r$, which implies $R^4 > r^2$. We have some different estimates for equation (6.42):

$$-2R^2 r^2 + 2r^4 R^2 = 2r^2 R^2(r^2 - 1) > 0, \qquad (6.47)$$

since $r > 1$,

$$-r^6 + r^4 R^2 = r^4(R^2 - r^2) > 0, \qquad (6.48)$$

since $R > r$,

$$2r^6 R^4 - R^4 - r^6 = r^6(R^4 - 1) + R^4(r^6 - 1) > 0, \qquad (6.49)$$

since $r > 1$ and $R > 1$,

$$r^4 R^6 - R^6 = R^6(r^4 - 1) > 0, \qquad (6.50)$$

since $r > 1$. This proves the Lemma in this case. If $r = R$, we have

$$f(r, R) = 3r^6(r^4 - 1) > 0, \qquad (6.51)$$

since $r > 1$.
This proves the Lemma.
Since $f(r, R) > 0$ and $\dot{a}_0 > 0$ (proof given in Lemma 6 at the end of this section) , we see that the dynamics of r and R is determined by the sign of $g(r, R)$ and $h(r, R)$. Since $a_2(0) < 0$, we see that:

$$\dot{r} < 0 \quad \text{if} \quad R^2 + 3r^4 - 4r^2 R^2 + R^4 - r^4 R^4 < 0 \qquad (6.52)$$

and

$$\dot{R} < 0 \quad \text{if} \quad R^2 + r^4 - 3r^2 R^2 + 2R^4 - r^4 R^4 > 0. \qquad (6.53)$$

The curves where $\dot{r} = 0$ and $\dot{R} = 0$ are shown in Figures 6.2 and 6.3.
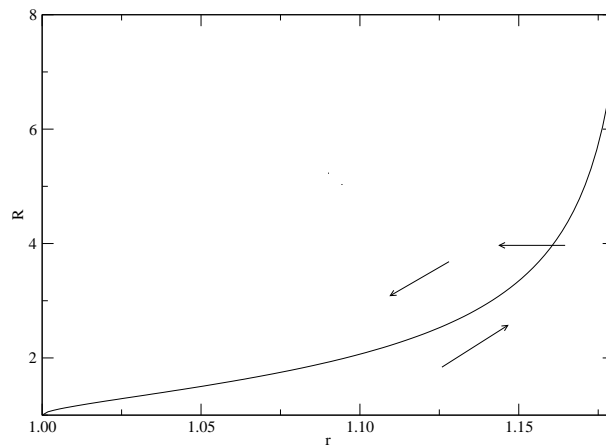
Figure 6.2: The curve $g(r, R) = 0$ where $\dot{R} = 0$
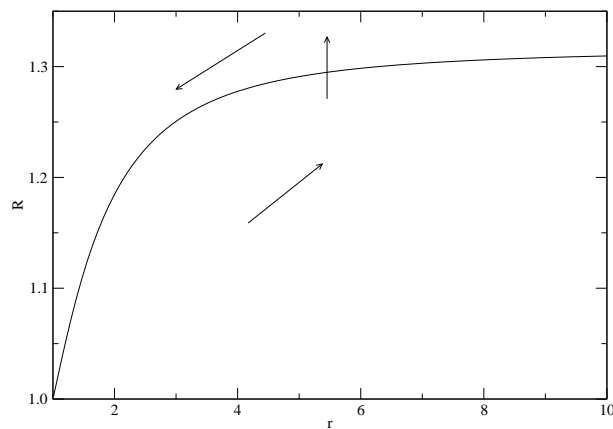
Figure 6.3: The curve $h(r, R) = 0$ where $\dot{r} = 0$
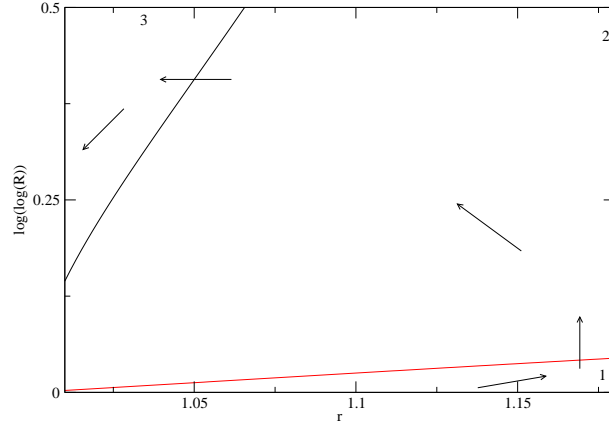
Figure 6.4: The complete phase plane composed of the previous two figures. The logarithms are taken to fit both curves into one figure.

A picture of the full phase plane is given in Figure 6.4; $\log(\log(R))$ is plotted on the y-axis instead of R to fit both curves in one picture. We see that any solution will eventually end up in region 3, which it can not leave, which means that it will finally reach the axis where $r = 1$; this means that a non-conformality point hits the unit disc and the solution ceases to exist. This is true for any initial condition (which is initially conformal).

Lemma 5 *A necessary condition for a conformal initial condition is given by*

$$a_{-1}(0)^2 - a_1(0)^2 - 4a_2(0)^2 > 0. \tag{6.54}$$

Remark Although this isn't a 'sharp' bound, it gives a good estimate for admissible initial conditions.

Proof of Lemma 5:

Substitute the expressions for a_1 and a_2 from equation (6.32) in equation (6.54) to obtain:

$$
\begin{aligned}
c(r, R) &= a_{-1}(0)^2 \left(-1 + \left(\frac{1}{R^2} - \frac{1}{r^2} \right)^2 + \frac{1}{R^4 r^4} \right) \\
&= a_{-1}(0)^2 \frac{-R^4 r^4 + r^4 + R^4 - 2R^2 r^2 + R^2}{R^4 r^4}.
\end{aligned} \tag{6.55}
$$

We have to show that $c(r, R) < 0$ if $R > 1$ and $r > 1$. If $R^2 > r^2$, we have

$$
\begin{aligned}
&-R^4 r^4 + r^4 + R^4 - 2R^2 r^2 + R^2 \\
&= R^4 (1 - r^4) + r^2 (r^2 - R^2) + R^2 (-r^2 + 1) < 0, \tag{6.56}
\end{aligned}
$$

since all terms are negative. If $r^2 > R^2$, we have

$$-R^4 r^4 + r^4 + R^4 - 2R^2 r^2 + R^2$$
$$= r^4(1 - R^4) + R^2(-r^2 + R^2) + R^2(-r^2 + 1) < 0, \qquad (6.57)$$

since all terms are negative. If $R = r$, we have

$$-R^4 r^4 + r^4 + R^4 - 2R^2 r^2 + R^2 = r^2(1 - r^6) < 0. \qquad (6.58)$$

This proves the Lemma.
We still had to prove a small Lemma containing the velocity, $\dot{a}_0(t)$:

Lemma 6 *If $r, R > 1$, $\dot{a}_0(t) > 0$.*

Proof of Lemma 6:
Use the last equation

$$2a_2 \dot{a}_1 + a_1 \dot{a}_0 + a_1 \dot{a}_2 - a_{-1} \dot{a}_0 = -2E_0 a_{-1} \qquad (6.59)$$

combined with equations (6.36) and (6.37) to obtain an equation for $\dot{a}_0(t)$:

$$\dot{a}_0(t) = 2E_0 \frac{g_1(r, R)}{f_1(r, R)}, \qquad (6.60)$$

where

$$f_1(r, R) = (R^2 - 1)(r^2 - 1)$$
$$(r^4(R^4 - 1) + r^4 R^4 + r^6(R^4 - 1) + r^2 R^4 + R^2 + 3r^4 R^2 + 3r^2 R^2) > 0, \quad (6.61)$$

and

$$g_1(r, R) = R^4 r^2(-r^4 + R^4 r^4 + 2r^2 R^2 - R^2 - R^4). \qquad (6.62)$$

If $r^2 > R^2$, we have

$$g_1(r, R) = r^2 R^2 - R^4 + r^2 R^2 - R^2 + R^4 r^4 - r^4$$
$$= R^2(r^2 - R^2) + R^2(r^2 - 1) + r^4(R^4 - 1) > 0. \qquad (6.63)$$

If $R^2 > r^2$, we have

$$g_1(r, R) = r^2 R^2 - r^4 + r^2 R^2 - R^2 + R^4 r^4 - R^4$$
$$= r^2(R^2 - r^2) + R^2(r^2 - 1) + R^4(r^4 - 1) > 0. \qquad (6.64)$$

This means that $\dot{a}_0(t) > 0$, which proves the lemma.
The conclusion is that $r \to 1$, independent of the initial condition. A non-conformality point will hit the unit disc in finite time (the velocity is strictly positive).

6.3 The short time evolution for $\epsilon > 0$

In Chapter 5, I derived a boundary condition for the streamer. Since implementation of this boundary condition and integration of the full problem is a difficult numerical problem, we ask ourselves first whether this boundary condition is able to regularize the easiest problem. We also like to get a feeling for the values of the regularization parameter which regularize this problem. We would like to see whether the boundary condition (5.25) is able to suppress cusps in the easiest case. The first nontrivial case is the case where $N = 2$; this is the case which will be studied. In section 6.2 we reformulated the dynamics of the a_k in terms of the variables a_{-1}, a_0, R and r. The latter variables all have a clear interpretation: size, position and location of the singularities in front of and behind the streamer. We were able to derive a picture of the phase plane, which showed that all flow went to the $r = 1$-axis, implying that a non-conformality point would hit the unit disc in finite time, creating a cusp, independently of the initial condition. In the following sections, our goal is the derivation of a phase plane in the regularized case. Since the regularization mechanism leads to the emergence of higher modes, a $2D$ phase space will never suffice to describe the full problem. New zeros of the derivative will appear; those are called 'daughter'-singularities. But we can try to answer the following question: suppose we start close to a cusp, with an initial condition defined by r, R and a_{-1}, are there any values for the regularization parameter ϵ such that the solution initially moves away from the cusp? If there exists such a regime, we can hope that at least the zeros of the derivative, present in the initial condition are regularized by this boundary condition. Those zeros are called 'mother'-singularities. Higher modes will be created in the time evolution, thus causing 'daughter'-singularities: new zeros of the derivative in different regions from the ω-space. We are unable to trace the daughter singularities; we will investigate the mother singularities in the following sections.

6.4 Tracing the 'mother'-singularities

In this section we will formulate the problem. Since we would like to look at the cusps of the regularized problem, we will combine the results of chapter 5, the derivation of the regularized dynamics of the a_k, with the results of section 6.2, the dynamics of the non-conformality points. We will start close to a cusp, without higher modes, to study the short time behaviour. This translates into the following Ansatz on $f_t(\omega)$:

$$f_t(\omega) = \sum_{k=-1}^{\infty} a_k \omega^k. \tag{6.65}$$

We substitute

$$a_1 = a_{-1} \left(\frac{1}{R^2} - \frac{1}{r^2} \right), \quad a_2 = -\frac{a_{-1}}{2Rr^2} \tag{6.66}$$

$$a_k(0) = 0, \quad \dot{a}_k(0) \neq 0, \text{ for } k > 2. \tag{6.67}$$

We will discuss the consequences of this ansatz for both sides of the dynamical equation (6.68) first:

$$\sum_{k,k'=-1}^{\infty} k a_k \dot{a}_{k'} \cos(k - k')\alpha = \text{Re}(-i\partial_\alpha \hat{\Phi}(e^{i\alpha})). \tag{6.68}$$

We will investigate the temporal flow of r and R for small t, therefore it is sufficient to evaluate both sides for $t = 0$. The right hand side depends on $\hat{\Phi}$, which depends on the absolute value of the spatial derivative of f. Using equation (6.65) and setting $a_{-1}(0) = 1$ (information about the size of the streamer is transferred to the regularization parameter ϵ), we see that the right hand side depends on the choices of r, R and ϵ:

$$\text{Re}(-i\partial_\alpha \hat{\Phi}(e^{i\alpha})) = F(r, R) \quad \text{at } t = 0. \tag{6.69}$$

We see that insertion of ansatz (6.67) simplifies equation (6.68) a lot; in fact, it 'decouples' the higher modes from the lower ones. Since only $-a_{-1}, a_1$ and $2a_2$ are nonzero we have

$$\sum_{k,k'=-1}^{\infty} k a_k \dot{a}_{k'} \cos(k - k')\alpha = \sum_{k=-1}^{\infty} (-a_{-1}\dot{a}_k \cos(k + 1)\alpha +$$
$$a_1 \dot{a}_k \cos(k - 1)\alpha + 2a_2 \dot{a}_k \cos(k - 2)\alpha). \tag{6.70}$$

I need to evaluate this expression numerically, which means that I need to introduce a cut-off N: $\dot{a}_k = 0$ if $k > N$. Closer examination of equation (6.70) reveals that the quantities $\dot{a}_3(0)..\dot{a}_N(0)$ are determined by the last $N - 3$ equations; the equations $\cos 4\alpha, \ldots, \cos(N+1)\alpha$. The only coupling to the lower modes is via the values of $\dot{a}_3, \ldots, \dot{a}_5$. This is an important observation, since this means that we can split in problem in three parts:

- determine $\text{Re}(-i\partial_\alpha \hat{\Phi})$ as a function of r and R

- calculate $\dot{a}_3..\dot{a}_5$ solving the last $N - 3$ equations

- solve the first four equations which give us $\dot{r}$ and $\dot{R}$

In Section 6.5 I will show that the phase space does not change if N is doubled; this means that our results are not sensitive anymore for changes in N. This is a very important result.

6.5   Numerical results

For different, fixed values of ϵ, we are interested in $\dot{r}$ for varying R close to $r = 1$; previously all flow was directed toward the $r = 1$ axis, which caused the cusp. In the pictures, we will show the curve $\dot{r} = 0$. To the left of this curve, $\dot{r} < 0$.

This means that we have two regimes: if r is small, but not too small, $\dot{r} > 0$ for certain values of R and ϵ. This means that we have a regime of shapes which can be regularized.
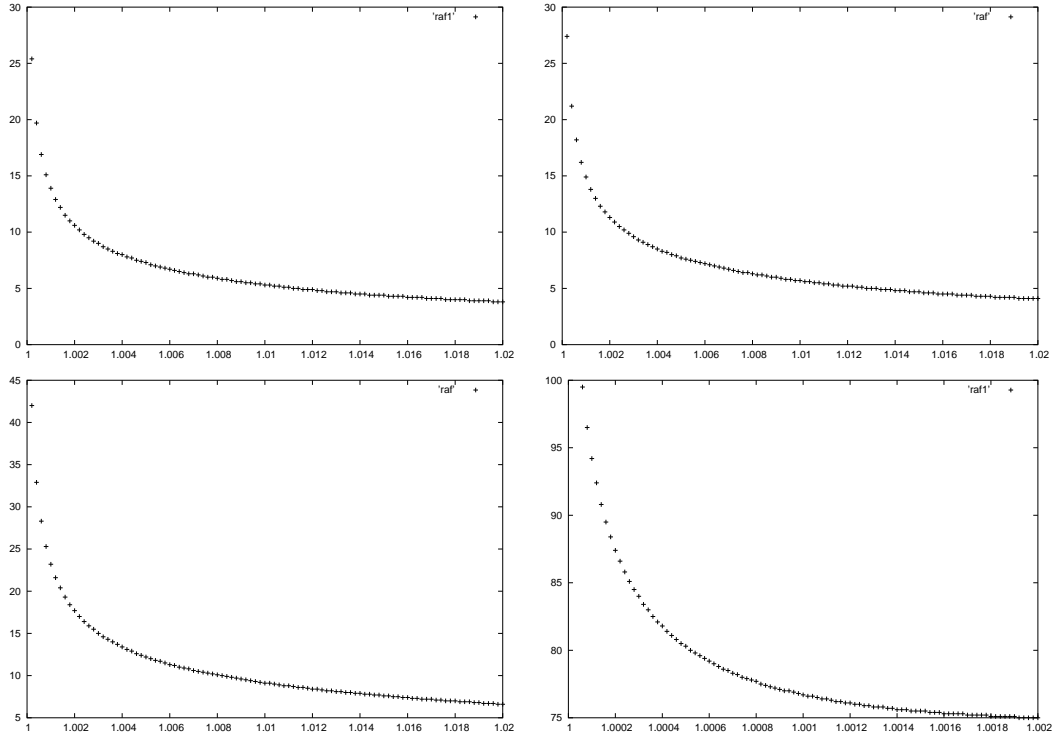
Figure 6.5: The line where $\dot{r} = 0$ for different values of ϵ : $\epsilon = 100, 10, 1, 0.1$

We investigated the dependence of the curves on the value of N as well. In the pictures below we plotted $\dot{r} = 0$ and $\dot{R} = 0$ for fixed $\epsilon = 7$ and two different values of N : $N = 36$ and $N = 144$:
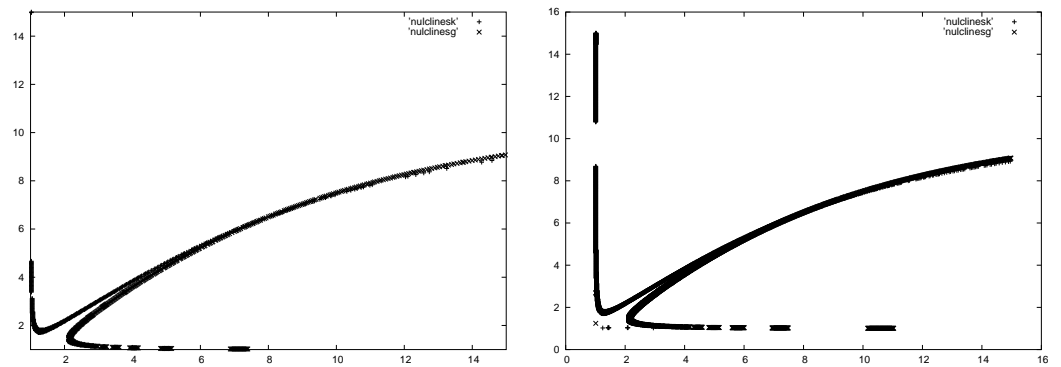
Figure 6.6: The nulclines where $\dot{r} = 0$ (lower curve) and $\dot{R} = 0$ (upper curve). The only difference between the two curves is $N : N = 36$ or $N = 144$; we see that the phase space is independent of N.

In the following set of pictures we show the shape of the interface at the points 1-4 in Figure 6.7.
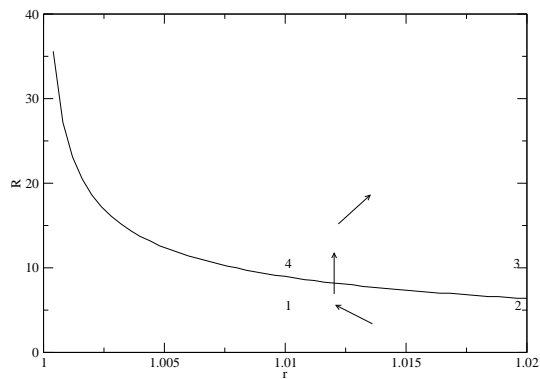
Figure 6.7: Interfaces can flow to more stable regions in the regularized case.
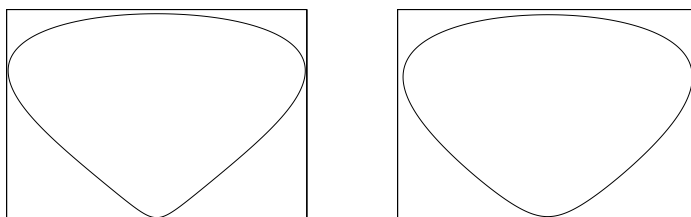
Figure 6.8: $r = 5$ and $R = 1.01, 1.02$ (points 1 and 2)
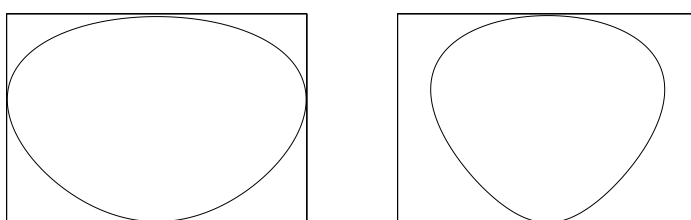
Figure 6.9: $r = 10$ and $R = 1.02, 1.01$ (points 3 and 4)

We have shown in this chapter that the interface will develop cusps in the unregularized case. In the regularized case, we see that flow to more stable regions is possible. This means that our boundary condition may indeed regularize the problem.

Chapter 7

Linear stability analysis of the circle

In Chapter 4 I derived explicit analytic solutions for the unregularized case: circles and ellipses; in Chapter 6 we saw that circles remain solutions in the regularized case. The stability of those solutions will be the topic of the present chapter. I will investigate the linear stability for the unregularized case ($\epsilon = 0$) in Section 7.1 and the stability for the regularized problem in Section 7.2, by writing

$$f_t(\omega) = f_0 + \delta\beta, \tag{7.1}$$

where f_0 is the circle and δ small.
If I use a mode expansion for β, $\beta = \sum_{k=0}^{\infty} a_k \omega^k$ and truncate the series, the linear stability analysis yields an equation of the form

$$\partial_t \mathbf{a} = \mathbf{M}\mathbf{a}. \tag{7.2}$$

The eigenvalues of the matrix $\mathbf{M}$ would determine the stability, but they turn out to be all zero. Clearly, the mode expansion is not the right idea in this case. In Section 7.1.2 a PDE for the perturbation is derived instead of the series approximation. This PDE can be solved analytically and we see that the circle is unstable.
The regularized case is investigated along the same lines in section 7.2. A mode expansion in this case yields purely imaginary eigenvalues. Instead of the mode expansion, we derive a PDE for the perturbation in section 7.3. It is possible to derive analytic solutions for this PDE if $\epsilon = 1$. Those solutions show, that perturbations may be amplified initially, but are always convected away to the back of the streamer. This means that the circle is a stable solution. We know on the other hand, that planar fronts are unstable; this means that the mechanism regularizes in regions where the curvature is large enough. This means that all shapes might be finally regularized.

I would like to point out, that this is exactly the same scenario as in the regularized viscous fingering, where this feature was observed both experimentally and numerically (see Chapter 3). But here we can show this fully analytically for an arbitrary initial perturbation.

For $\epsilon \neq 1$ we have no analytic solutions; we will have to solve the problem numerically, e.g. by a mode expansion. The analytic solutions in the $\epsilon = 1$ case also offer the opportunity to check the validity of the numerical solutions; I can check how many modes are needed to describe the correct solution and how long this solutions holds. In order to do so, I use a transformation of the unit disc

$$u = \frac{\omega + T}{\omega T + 1}, \ T = \tanh\frac{t}{2} \tag{7.3}$$

and I rewrite the PDE for the perturbation in terms of u. I can preserve the analyticity of β numerically by an expansion in either u or ω; the coefficients are given in terms of each other. The former is more convenient numerically, the equations are solved in terms of an expansion in u; the coeficients of the expansion in ω can be calculated and compared to the analytical expressions. These match perfectly, which means that the expansion is valid, at least in the regime I tested.

7.1 The unregularized case: perturbing the circle

The mapping function f_0

$$f_0 = \frac{R}{\omega} + 2E_0 t \tag{7.4}$$

describes a uniformly translating circle with radius R and velocity $v = 2E_0$. We perturb this solution with f_1:

$$f_1 = \sum_{k=-1}^{\infty} a_k \omega^k \tag{7.5}$$

and set

$$f = f_0 + \delta f_1, \tag{7.6}$$

where δ is a small parameter. The dynamical equation is

$$\mathrm{Re}\,(i\partial_\alpha f^\star \partial_t f) = -2E_0\cos(\alpha)(R + \delta a_{-1}). \tag{7.7}$$

Expanding in 0th order in δ yields

$$-Rv\cos(\alpha) = -2E_0 R\cos(\alpha) \tag{7.8}$$

which reproduces the solution (7.4). In first order we obtain

$$\sum_{k=-1}^{\infty} k a_k v \cos(k\alpha) + \sum_{k=-1}^{\infty} -R\dot{a}_k \cos(k+1)\alpha = -v a_{-1} \cos(\alpha) \qquad (7.9)$$

Let me first try to use an eigenvalue approach to study the stability.

7.1.1 The perturbation in matrix form

Using a truncation of the series (7.5) by a large order N brings equation (7.9) in matrix form

$$v\mathbf{U}_1\mathbf{a} - R\partial_t\mathbf{a} = \begin{pmatrix} 0 \\ -va_{-1} \\ 0 \\ \vdots \\ 0 \end{pmatrix} \qquad (7.10)$$

where

$$\mathbf{a} = \begin{pmatrix} a_{-1} \\ a_0 \\ a_1 \\ \vdots \\ a_N \end{pmatrix}, \qquad (7.11)$$

$\mathbf{U}_1$ is given by

$$\mathbf{U}_1 = \begin{pmatrix} 0 & 0 & 0 & 0 & \dots & 0 \\ -1 & 0 & 1 & 0 & \dots & 0 \\ 0 & 0 & 0 & 2 & \dots & 0 \\ \vdots & \vdots & \vdots & \vdots & \ddots & \vdots \\ 0 & 0 & 0 & 0 & \dots & N \\ 0 & 0 & 0 & 0 & \dots & 0 \end{pmatrix}. \qquad (7.12)$$

Notice that the vector $(0, -va_{-1}, 0, \dots, 0)^T$ is cancelled by the $(2,1)$ matrix element of $\mathbf{U}_1$; equation (7.9) reduces to

$$\partial_t\mathbf{a} = \frac{v}{R}\mathbf{U}_2\mathbf{a}, \qquad (7.13)$$

where

$$\mathbf{U}_2 = \begin{pmatrix} 0 & 0 & 0 & 0 & \dots & 0 \\ 0 & 0 & 1 & 0 & \dots & 0 \\ 0 & 0 & 0 & 2 & \dots & 0 \\ \vdots & \vdots & \vdots & \vdots & \ddots & \vdots \\ 0 & 0 & 0 & 0 & \dots & N \\ 0 & 0 & 0 & 0 & \dots & 0 \end{pmatrix}. \qquad (7.14)$$

Notice first of all that $\partial_t a_{-1} = 0$, which means that the perturbed radius is constant and can be absorbed in the unperturbed radius: choose $a_{-1}(0) = 0$. The same holds for a_0 and the expansion for the perturbation can be written as

$$f_1(0) = \sum_{k=1}^{N} a_k(t)\omega^k \tag{7.15}$$

Insert

$$f_1(\omega, t) = e^{\lambda t} f_\lambda(\omega) \tag{7.16}$$

in equation (7.13) and determine the eigenvalues λ to study the stability; this means that we need to evaluate the eigenvalues of the matrix $\mathbf{U}_2$: this easy, since it is an upper triangular matrix, the eigenvalues are the numbers on the diagonal which happen to be all zero.

We can also derive the temporal evolution of the polynomial initial condition (7.15),

$$f_1(t) = \sum_{k=1}^{N} a_k(0) \left(\omega + \frac{v}{R}t\right)^k . \tag{7.17}$$

We see a non-trivial temporal behaviour, which seems to contradict the previous result about the eigenvalues. But eigenvalues can not be derived, since they require $N \to \infty$. We will get rid of the cut-off N in the next section and construct solutions for a general perturbation.

7.1.2   A PDE for the perturbation

Use again

$$f_t(\omega) = f_0 + \delta\beta(\omega, t) \tag{7.18}$$

and evaluate the first order in δ (set again $a_{-1}(t) = 0$: this means that $\beta(\omega, t)$ is an analytic function of ω):

$$0 = \mathrm{Re}\,(i\partial_\alpha f^\star \partial_t f) = \mathrm{Re}\,(i\partial_\alpha f_0^\star \partial_t \beta) + \mathrm{Re}\,(i\partial_\alpha \beta \partial_t f_0) =$$
$$\mathrm{Re}(-Re^{i\alpha}\partial_t\beta + vi\partial_\alpha\beta^\star) \tag{7.19}$$

and use $\mathrm{Re}(iz^\star) = \mathrm{Re}(-iz)$ to obtain

$$\mathrm{Re}\,(R\omega\partial_t\beta - v\omega\partial_\omega\beta) = 0. \tag{7.20}$$

Set $R = 1$, absorb v in a redefinition of time and note

$$\mathrm{Re}(\omega g) = 0 \quad \text{and g analytic} \Rightarrow g = 0 \tag{7.21}$$

to derive

$$\partial_t\beta - \partial_\omega\beta = 0. \tag{7.22}$$

This equation can be solved analytically:

$$\beta(\omega, t) = \beta(\omega + t, 0) \tag{7.23}$$

for an initial condition $\beta(\omega, 0)$. This is the generalization of equation (7.17). Notice

- a perturbation of the radius of the circle and the perturbation of the position are time independent; the first can be absorbed in the unperturbed problem and the second set to zero.

- the eigenvalue approach of the truncated series misses all interesting dynamics of the problem, because there are no terms exponential in time.

In this case, the eigenvalues give little information about the stability of the problem; I need to derive the PDE for the perturbation to investigate the problem; all $\lambda \in \mathbb{C}$ turn out to be eigenvalues. Notice that the derivative of the perturbation will blow up, if the time becomes large enough, thus causing a cusp. This means, that the solution ceases to exist after some time, which is consistent with the results of chapter 6.

7.2 The regularized case: the circle

In chapter 5 an analytic solution of the regularized problem was found: a uniformly translating circle described by f_0:

$$f_0 = \frac{1}{\omega} + vt, \tag{7.24}$$

$$v = 2E_0 \frac{1}{1 + \epsilon} \tag{7.25}$$

is the velocity of the circle. The potential is given by

$$\Phi_0 = E_0 \left(\frac{1}{\omega} - \frac{1 - \epsilon}{1 + \epsilon} \omega \right). \tag{7.26}$$

I would like to investigate the stability of the circle in this section. Add a small perturbation to this solution and expand the mapping function f:

$$f = f_0 + \delta f_1, \tag{7.27}$$

where

$$f_1 = \sum_{k=-1}^{\infty} a_k(t) \omega^k. \tag{7.28}$$

This means that the potential will be perturbed as well:

$$\hat{\Phi} = \Phi_0 (1 + \delta a_{-1}) + \delta \Phi_1, \tag{7.29}$$

where Φ_1 is an analytic function of ω; I will use an expansion here as well:

$$\Phi_1 = \sum_{k=0}^{\infty} \alpha_k \omega^k. \tag{7.30}$$

I will have to expand both the boundary condition

$$\mathrm{Re}\Phi = \epsilon \frac{\mathrm{Re}(i\partial_\alpha \Phi)}{|\partial_\alpha f|} \tag{7.31}$$

and the dynamical equation

$$\mathrm{Re}\left(i\partial_\alpha f^\star \partial_t f\right) = \mathrm{Re}(-i\partial_\alpha \Phi) \tag{7.32}$$

up to linear order in δ. The hardest part is the expansion of the potential which will be treated in the next section.

7.2.1   The calculation of the potential

The boundary condition reads

$$\mathrm{Re}(\Phi_0(1 + \delta a_{-1}) + \delta\Phi_1)|\partial_\alpha f| = \epsilon \mathrm{Re}\left(i\partial_\alpha \Phi_0(1 + \delta a_{-1})\right) + \epsilon \mathrm{Re}(i\delta\partial_\alpha \Phi_1) \tag{7.33}$$

Expand the derivative of the mapping function:

$$f = \frac{1}{\omega} + vt + \delta \sum_{k=-1}^{\infty} a_k \omega^k, \tag{7.34}$$

$$|\partial_\alpha f| = 1 - \delta \sum_{k=-1}^{\infty} k a_k \cos(k+1)\alpha \tag{7.35}$$

and insert this is the boundary condition to obtain

$$\mathrm{Re}\left(\Phi_0(1 + \delta a_{-1})\right) = \mathrm{Re}\left(i\partial_\alpha \Phi_0(1 + \delta a_{-1})\right), \tag{7.36}$$

which gives the 0th order equation for Φ_0:

$$\Phi_0 = E_0 \left(\frac{1}{\omega} - \frac{1-\epsilon}{1+\epsilon}\omega \right) \tag{7.37}$$

The first order in δ yields

$$-\mathrm{Re}\Phi_0 \sum_{k=-1}^{\infty} k a_k \cos(k+1)\alpha + \sum_{k=0}^{\infty} \alpha_k \cos k\alpha = -\epsilon \sum_{k=0}^{\infty} k\alpha_k \cos k\alpha \tag{7.38}$$

and using the expression for Φ_0 I derive

$$\frac{2\epsilon E_0}{1+\epsilon} \cos\alpha \sum_{k=-1}^{\infty} k a_k \cos(k+1)\alpha = \sum_{k=0}^{\infty} (1 + \epsilon k) \cos k\alpha \tag{7.39}$$

I would like to rewrite equation (7.39) in matrix form, where the first component corresponds to the equation for $\cos 0 \, \alpha$, the second to $\cos \alpha$ and so on. Introduce the vectors $\mathbf{a}$ and α

$$\mathbf{a} = \begin{pmatrix} a_{-1} \\ a_0 \\ a_1 \\ \vdots \\ a_{N-1} \end{pmatrix}, \quad \alpha = \begin{pmatrix} \alpha_{-1} \\ \alpha_0 \\ \alpha_1 \\ \vdots \\ \alpha_{N-1} \end{pmatrix}. \tag{7.40}$$

The calculation of the right hand side is straightforward:

$$\sum_{k=0}^{N} (1 + \epsilon k) \cos k\alpha = \mathbf{D}_3 \alpha, \tag{7.41}$$

where

$$\mathbf{D}_3 = \begin{pmatrix} 1 & 0 & \dots & 0 \\ 0 & 1+\epsilon & \dots & 0 \\ \vdots & \vdots & \ddots & \vdots \\ 0 & \dots & 0 & 1+N\epsilon \end{pmatrix}. \tag{7.42}$$

Use $\cos a \cos b = \frac{1}{2}(\cos(a+b) + \cos(a-b))$ to rewrite the left hand side:

$$\frac{2\epsilon E_0}{1+\epsilon} \cos \alpha \sum_{k=-1}^{\infty} k a_k \cos(k+1)\alpha =$$

$$\frac{\epsilon E_0}{1+\epsilon} \left(\sum_{k=1}^{\infty} k a_k (\cos \alpha + (\cos(k+2)\alpha) - 2a_{-1} \cos \alpha \right) \tag{7.43}$$

which is in vector form

$$E_0 \frac{\epsilon}{1+\epsilon} \begin{pmatrix} 0 \\ -2a_{-1} + a_1 \\ 2a_2 \\ 3a_3 + a_1 \\ 4a_4 + 2a_2 \\ \vdots \\ (N-1)a_{N-1} + (N-3)a_{N-3} \\ (N-2)a_{N-2} \end{pmatrix}. \tag{7.44}$$

and in matrix form:

$$E_0 \frac{\epsilon}{1+\epsilon} \mathbf{T}_1 \mathbf{T}_2 \mathbf{a}, \tag{7.45}$$

where $\mathbf{T}_2$ only put the right factor in front of the a_k:

$$
\mathbf{T}_2 = \begin{pmatrix}
-1 & 0 & 0 & \ldots & 0 \\
0 & 0 & 0 & \ldots & 0 \\
\vdots & \vdots & \ddots & \vdots & \vdots \\
0 & \ldots & 0 & N-2 & 0 \\
0 & \ldots & 0 & 0 & N-1
\end{pmatrix}
\tag{7.46}
$$

and $\mathbf{T}_1$ 'mixes' the terms correctly:

$$
\mathbf{T}_1 = \begin{pmatrix}
0 & 1 & 0 & 0 & 0 & \ldots & 0 \\
2 & 0 & 1 & 0 & 0 & \ldots & 0 \\
0 & 1 & 0 & 1 & 0 & \ldots & 0 \\
\vdots & \vdots & \ddots & \vdots & \ddots & \vdots & \vdots \\
0 & \ldots & 0 & 1 & 0 & 1 & 0 \\
0 & \ldots & 0 & 0 & 1 & 0 & 1 \\
0 & \ldots & 0 & 0 & 0 & 1 & 0
\end{pmatrix}.
\tag{7.47}
$$

Combining equations (7.41) and (7.45) yields the desired expression of the α_k in terms of the a_k:

$$
\alpha = \frac{E_0 \epsilon}{\epsilon + 1} \mathbf{D}_3^{-1} \mathbf{T}_1 \mathbf{T}_2 \mathbf{a}.
\tag{7.48}
$$

We are now ready to calculate the right hand side of the dynamical equations $\mathrm{Re}(-i\partial_\alpha \Phi)$, since we have the perturbed potential Φ_1:

$$
\mathrm{Re}(-i\partial_\alpha \Phi) = -2E_0 \frac{1}{1+\epsilon} \cos\alpha(1 + \delta a_{-1}) + \delta \sum_{k=0}^{N} k\alpha_k \cos(k\alpha),
\tag{7.49}
$$

which yields at order δ in matrix form

$$
\mathrm{Re}(-i\partial_\alpha \Phi) = \frac{-2E_0}{1+\epsilon} \begin{pmatrix} 0 \\ a_{-1} \\ 0 \\ \vdots \\ 0 \end{pmatrix} + \frac{E_0 \epsilon}{1+\epsilon} \mathbf{D}_2 \mathbf{D}_3^{-1} \mathbf{T}_1 \mathbf{T}_2 \mathbf{a}.
\tag{7.50}
$$

The expansion of the left hand side of the dynamical equation $\mathrm{Re}(i\partial_\alpha f^\star \partial_t f)$ is similar to the unregularized case:

$$
\mathrm{Re}(i\partial_\alpha f^\star \partial_t f) = v\mathrm{Re}(i\partial_\alpha f_1^\star) - \mathrm{Re}(e^{i\alpha}\partial_t f_1) =
$$
$$
-va_{-1}\cos\alpha + v\sum_{k=0}^{\infty} ka_k \cos k\alpha - \sum_{k=-1}^{\infty} \dot{a}_k \cos(k+1)\alpha
\tag{7.51}
$$

which is in matrix notation

$$\text{Re}(i\partial_\alpha f^\star \partial_t f) = \frac{-2E_0}{1+\epsilon} \begin{pmatrix} 0 \\ a_{-1} \\ 0 \\ \vdots \\ 0 \end{pmatrix} + \frac{2E_0}{1+\epsilon} \mathbf{D}_1 \mathbf{a} - \partial_t \mathbf{a}, \qquad (7.52)$$

where

$$\mathbf{D}_1 = 2 \begin{pmatrix} 0 & 0 & 0 & 0 & \dots & 0 \\ 0 & 0 & 1 & 0 & \dots & 0 \\ 0 & 0 & 0 & 2 & \dots & 0 \\ \vdots & \vdots & \vdots & \vdots & \ddots & \vdots \\ 0 & \dots & 0 & 0 & 0 & N-1 \\ 0 & \dots & 0 & 0 & 0 & 0 \end{pmatrix} \qquad (7.53)$$

Again two terms at the place (2,1) cancel eachother and we end up with:

$$\partial_t \mathbf{a} = \frac{E_0}{1+\epsilon} \left(\mathbf{D}_1 - \epsilon \mathbf{D}_2 \mathbf{D}_3^{-1} \mathbf{T}_1 \mathbf{T}_2 \right) \mathbf{a} \qquad (7.54)$$

which implies that the matrix $\mathbf{M}_{tot}$ is defined in equation (7.54):

$$\partial_t \mathbf{a} = \mathbf{M}_{tot} \mathbf{a} \qquad (7.55)$$

Define the factors r_k for convenience to derive a compact expression for the matrix $\mathbf{M}_{tot}$:

$$r_k = \frac{\epsilon k}{1+\epsilon k}. \qquad (7.56)$$

(Notice $0 < r_k < 1$). This gives us

$$\mathbf{M}_{tot} = \begin{pmatrix} 0 & 0 & 0 & 0 & 0 & 0 & \dots \\ 2r_1 & 0 & (2-r_1) & 0 & 0 & 0 & \dots \\ 0 & 0 & 0 & 2(2-r_2) & 0 & 0 & \dots \\ 0 & 0 & -r_3 & 0 & 3(2-r_3) & 0 & \dots \\ 0 & 0 & 0 & -2r_4 & 0 & 4(2-r_4) & \dots \\ 0 & 0 & 0 & 0 & -3r_5 & 0 & \dots \\ \vdots & \vdots & \vdots & \vdots & \vdots & \vdots & \ddots \end{pmatrix} . \ (7.57)$$

The eigenvalues of $\mathbf{M}_{tot}$ determine the stability of the circle. In the next section we will show that they are purely imaginary.

7.2.2   The eigenvalues

We need to calculate the zeros of the determinant of $\mathbf{M}_{tot} - \lambda\mathbf{I}$; expanding to
the first row and column consecutively yields an equation of the following form:

$$\lambda^2\det\begin{pmatrix} -\lambda & a_{n-1} & 0 & 0 & \ldots & 0 \\ -b_{n-1} & -\lambda & a_{n-2} & 0 & \ldots & 0 \\ \vdots & \ddots & \ddots & \ddots & \vdots & \vdots \\ 0 & \ldots & -b_3 & -\lambda & a_2 & 0 \\ 0 & \ldots & 0 & -b_2 & -\lambda & a_1 \\ 0 & \ldots & 0 & 0 & -b_1 & -\lambda \end{pmatrix} = 0, \qquad (7.58)$$

where

$$a_k = (n-k+1)(2-r_{n-k+1}), \ b_k = (n-k+2)r_{n-k+2}, \ k = 1,\ldots,n-1 \qquad (7.59)$$

the precise form of the a_k and b_k is not important, while the fact that they are
positive is important. Denote the determinant in equation (7.58) by M_n: We
see

$$M_n = -\lambda M_{n-1} - a_{n-1}b_{n-1}M_{n-2} \qquad (7.60)$$

and

$$M_2 = \lambda^2 + a_1 b_1, \ M_3 = -\lambda(\lambda^2 + a_1 b_1) - \lambda a_2 b_2. \qquad (7.61)$$

Let us define the skew(anti)symmetric matrix $\mathbf{S}_n$ as follows:

$$\mathbf{S}_n = \begin{pmatrix} 0 & A_{n-1} & 0 & 0 & \ldots & 0 \\ -A_{N-1} & 0 & A_{N-2} & 0 & \ldots & 0 \\ \vdots & \ddots & \ddots & \ddots & \vdots & \vdots \\ 0 & \ldots & -A_3 & 0 & A_2 & 0 \\ 0 & \ldots & 0 & -A_2 & 0 & A_1 \\ 0 & \ldots & 0 & 0 & -A_1 & 0 \end{pmatrix}, \qquad (7.62)$$

where $A_k = \sqrt{a_k b_k}, k = 1..n-1$. Calculating the eigenvalues of S_n, we see

$$\det(\mathbf{S}_n - \lambda\mathbf{I}) = M_n, \qquad (7.63)$$

because it satisfies the same recursion relation and since equation (7.58) holds
for $N = 2$ and $N = 3$. This means that we can study the eigenvalues of $\mathbf{S}_n$
instead of the eigenvalues of $\mathbf{M}_{tot}$ since these eigenvalues are equal. But

$$\mathbf{S} \quad \text{skew symmetric} \Rightarrow i\mathbf{S} \quad \text{Hermitian}, \qquad (7.64)$$

which means that the eigenvalues of $i\mathbf{S}$ are real and the eigenvalues of $\mathbf{S}$ purely
imaginary. We conclude that the eigenvalues of $\mathbf{M}_{tot}$ are purely imaginary as
well.

7.2.3 Conclusion

If we have a general initial condition, one expects to see a superposition of oscillating eigenmodes. If we use a very small cut-off, say $N = 2$, we see those oscillations in the modes, since there are only two complex conjugate eigenvalues, so one period. Using a higher cut-off, we could see an oscillation with a period with is the least common multiple (lcm) of the individual periods; since those periods become very large, this lcm becomes even larger and we are unable to observe this numerically. The question arises how accurate the stability is described by this mode expansion. In the section about the unregularized case, we saw that the eigenvalue approach was not the right one, when applied to a truncated series. In section 7.3 we will get rid of the mode expansion and derive a PDE for the perturbation in order to analyze the stability.

7.3 The stability analysis in terms of a PDE for $\epsilon > 0$

In this section we will reformulate the linear stability problem of the circle in terms of a PDE. Instead of a mode expansion for the perturbation, we will set:

$$f_t(\omega) = \frac{1}{\omega} + vt + \delta\beta(\omega, t), \tag{7.65}$$

where δ is a small parameter. In section 7.4 we will derive a PDE for $\beta(\omega, t)$, in section 7.5 we will derive analytic solutions of the PDE for $\epsilon = 1$. We notice that a certain transformation of the unit disc

$$u(\omega, T(t)) = \frac{\omega + T(t)}{\omega T(t) + 1}, \quad T(t) = \tanh\left(\frac{vt}{2}\right) \tag{7.66}$$

plays a very important role in this case. Precomposing $f_t(\omega)$ with this mapping transforms the PDE; in section 7.6 we insert an expansion in the transformed PDE:

$$\tilde{\beta}(u, t) = \sum_{k=0}^{N} b_k(t) u^k \tag{7.67}$$

and derive a set of $N + 1$ coupled ODE's for the $b_k(t)$. We solve those ODE's and show that the results do not depend on the cut-off N. This leads to some conclusions given in section 7.7.

7.4 Derivation

Perturb the uniformly translating circle

$$f_t(\omega) = \frac{1}{\omega} + t + \delta\beta(\omega, t) \tag{7.68}$$

and the potential

$$\hat{\Phi}(\omega) = E_0 \left(\frac{1}{\omega} - \frac{1 - \epsilon}{1 + \epsilon} \omega \right) + \delta\phi_1(\omega), \tag{7.69}$$

where δ is a small parameter and β and ϕ_1 are analytic. (I absorbed the velocity in t, by setting $\tau = vt$ and renaming $\tau \to t$). Inserting (7.68) and (7.69) in the dynamical equation for the mapping

$$\text{Re}(i\partial_\alpha f^\star \partial_t f) = \text{Re}(-i\partial_\alpha \hat{\Phi}) \tag{7.70}$$

yields (first order in δ):

$$\text{Re}(e^{i\alpha}\partial_t\beta + i\partial_\alpha\beta) = \text{Re}(i\partial_\alpha\phi_1). \tag{7.71}$$

(Use: $\text{Re}(-iz) = \text{Re}(iz^\star)$).

Substitute $\omega = e^{i\alpha}$ in equation (7.71) and notice that we obtain an equation of the following form:

$$\text{Re}(\omega g) = 0 \quad \text{on } \omega = e^{i\alpha} \text{ and g analytical}. \tag{7.72}$$

This implies that $g = 0$, so the real parts can be cancelled in equation (7.71) and we obtain:

$$\omega\partial_t\beta - v\omega\partial_\omega\beta + \omega\partial_\omega\phi_1 = 0. \tag{7.73}$$

Rewriting and rearranging the boundary condition

$$\text{Re}\left(\hat{\Phi}\right) = \epsilon\text{Re}\left(\frac{i\partial_\alpha\hat{\Phi}}{|\partial_\alpha f|}\right) \tag{7.74}$$

yields

$$\text{Re}(\phi_1 + \phi_0\text{Re}(ie^{i\alpha}\partial_\alpha\beta)) = \epsilon\text{Re}(i\partial_\alpha\phi_1), \tag{7.75}$$

since

$$\partial_\alpha f = -ie^{-i\alpha} + \delta\partial_\alpha\beta \Rightarrow |\partial_\alpha f| = 1 + \delta\text{Re}(i\partial_\alpha\beta). \tag{7.76}$$

Insert

$$\text{Re}(\phi_0) = \epsilon\cos(\alpha) \tag{7.77}$$

to obtain

$$\epsilon\cos(\alpha)\text{Re}(ie^{i\alpha}\partial_\alpha\beta) = \text{Re}(\epsilon i\partial_\alpha\phi_1 - \phi_1). \tag{7.78}$$

Substitute the expression for $\partial_\omega\phi_1$ from equation (7.73) and $\omega = e^{i\alpha}$ in equation (7.78) to obtain an expression for the real part of ϕ_1 in terms of β:

$$\text{Re}(\phi_1) = \epsilon\text{Re}\left(\frac{1}{2}(\omega^2 - 1)\omega\partial_\omega\beta + \omega\partial_t\beta\right). \tag{7.79}$$

This is possible, since we can define equation (7.79) for all $|\omega| \leq 1$; the expressions are analytic in ω, their real part is given on the boundary, which means that we can extend their definition to the whole unit disc. We can not cancel the real parts in equation (7.79), since we can pick up an imaginary constant, $C(t)$. However, the fact that β and ϕ have to stay analytic dictates this choice. We need to have

$$\phi_1 = \epsilon \left(\frac{1}{2}(\omega^2 - 1)\omega \partial_\omega \beta + \omega \partial_t \beta \right), \tag{7.80}$$

where

$$\phi_1(\omega = 0, t) = 0 \quad \forall t \tag{7.81}$$

in order to preserve the analyticity of ϕ_1. In the following section we will show why we need to impose this condition.

7.4.1 Imposing $\phi_1(\omega = 0, t) = 0$

Combine equations (7.80) and (7.73) to eliminate $\partial_t \beta$. This leaves us with an expression for ϕ_1 in terms of β:

$$\phi_1 + \epsilon \omega \partial_\omega \phi_1 = \frac{1}{2}\epsilon(\omega^3 + \omega)\beta. \tag{7.82}$$

We see, that we can always add a solution of the form

$$\phi_1 = \frac{f(t)}{\omega^\epsilon} + \tilde{\phi}_1. \tag{7.83}$$

to equation (7.82). This is undesirable, since ϕ_1 loses its analyticity. We have to prevent this explicitly setting

$$\phi_1(\omega = 0, t) = 0 \quad \forall t \Rightarrow f(t) = 0 \quad \forall t \tag{7.84}$$

in order to preserve analyticity.
If $\epsilon = 1$ we can show explicitly what happens if $\phi_1(\omega = 0, t) \neq 0$. In this case we have:

$$i\phi_1 = -\partial_\alpha \phi_1 + \frac{1}{2}(e^{2i\alpha} + 1)\partial_\alpha \beta, \tag{7.85}$$

$$ie^{i\alpha}\partial_t \beta = \partial_\alpha \beta - \partial_\alpha \phi_1 \tag{7.86}$$

Substitution of

$$\beta = \tilde{\beta} + f(t)e^{-2i\alpha}, \quad \phi_1 = \tilde{\phi} + g(t)e^{-2i\alpha} + h(t)e^{-i\alpha} \tag{7.87}$$

and comparison of terms with $e^{-i\alpha}$ and $e^{-2i\alpha}$ yields

$$f(t) = g(t), \qquad \dot{f}(t) = -h(t), \qquad f(t) = \phi_1(\omega = 0, t). \tag{7.88}$$

and equations (7.85) and (7.86) with $\tilde{\beta}$ and $\tilde{\phi}$ instead of β and ϕ_1. This means that the wrong choice of the boundary condition yields terms $\sim e^{-2i\alpha}$ in β and ϕ_1. Imposing $\phi_1(\omega = 0, t) = 0$ allows us to get rid of those terms. The physical reason to get rid of those terms is that they would contribute to the electrical field at infinity.

This is observed in the following section as well, where we have to choose a proper boundary condition in order to get rid of those non-analyticities.

7.4.2   Derivation of the operator L_ϵ

Differentiate equation (7.80) to obtain an expression for $\partial_\omega \phi_1$:

$$\partial_\omega \phi_1 = \epsilon \left(\frac{1}{2}(3\omega^2 - 1)\partial_\omega \beta + \frac{1}{2}(\omega^3 - \omega)\partial_\omega^2 \beta + \partial_t \beta + \omega\partial_\omega\partial_t \beta \right) \qquad (7.89)$$

and substitue the expression for $\partial_\omega \phi_1$ from equation (7.73) in equation (7.89) to eliminate ϕ_1:

$$-\partial_t \beta + \partial_\omega \beta = \epsilon \left(\frac{1}{2}(3\omega^2 - 1)\partial_\omega \beta + \frac{1}{2}(\omega^3 - \omega)\partial_\omega^2 \beta + \partial_t \beta + \omega\partial_\omega\partial_t \beta \right) \quad (7.90)$$

which can be rewritten as

$$L_\epsilon \beta = 0, \qquad (7.91)$$

where L_ϵ is defined as follows:

$$L_\epsilon = -\epsilon(1 - \omega^2)\omega\partial_\omega^2 - (2 + \epsilon - 3\epsilon\omega^2)\partial_\omega + 2\epsilon\omega\partial_\omega\partial_t + 2(1 + \epsilon)\partial_t. \qquad (7.92)$$

It turns out that we can calculate explicit solutions of equation (7.91) for $\epsilon = 1$. For $\epsilon \neq 1$ I will need to write a numerical code; this needs evaluation of the equation on the boundary, as will be explained in Section 7.5.2. The analytic solutions for $\epsilon = 1$ will be discussed in the next section.

7.5   Solutions for $\epsilon = 1$

We can rewrite the operator L_ϵ as a product:

$$L_1 = (2\partial_t - (1 - \omega^2)\partial_\omega)(2 + \omega\partial_\omega) \qquad (7.93)$$

which means that we can introduce the function

$$g(\omega, t) = (2 + \omega\partial_\omega)\beta(\omega, t) \qquad (7.94)$$

that obeys the equation

$$(2\partial_t - (1 - \omega^2)\partial_\omega)g(\omega, t) = 0 \qquad (7.95)$$

which can be solved directly; g has to be a function of u only, where

$$u(\omega, t) = \frac{\omega + T}{\omega T + 1},$$ (7.96)

and

$$T = \tanh\left(\frac{t}{2}\right).$$ (7.97)

Notice that $t = 0$ corresponds to $T = 0$; at $t = 0$, we have $u = \omega$. This means that $g(\omega, t)$ can be obtained directly from the initial condition $\beta(\omega, 0)$. Define

$$G(\omega) = g(\omega, 0) = (2 + \omega\partial_\omega)\beta(\omega, 0).$$ (7.98)

The general solution $g(\omega, t)$ reads

$$g(\omega, t) = G\left(\frac{\omega + T}{\omega T + 1}\right)$$ (7.99)

and $\beta(\omega, t)$ can be calculated:

$$\beta(\omega, t) = \int_0^\omega \frac{x\,dx}{\omega^2}G\left(\frac{x + T}{xT + 1}\right).$$ (7.100)

A particular example for a given initial condition will be given in Section 7.5.1. We can derive the asymptotic behaviour of the analytical solution, since we can expand about $T = 1$. Expanding T yields

$$T = \tanh\frac{t}{2} = 1 - 2e^{-t} + O(e^{-2t})$$ (7.101)

and use this to expand $u(\omega, T) = \frac{\omega + T}{\omega T + 1}$:

$$u(\omega, T) = 1 - 2\frac{1 - \omega}{1 + \omega}e^{-t} + O(e^{-2t})$$ (7.102)

and the expansion of $G(u)$ reads

$$G(u) = G(1) - 2\frac{1 - \omega}{1 + \omega}e^{-t}G'(1) + O(e^{-2t}).$$ (7.103)

Insert this in equation (7.100) to obtain an expansion for $\beta(\omega, t)$:

$$\beta(\omega, t) = \frac{1}{2}G(1) + \frac{G'(1)}{\omega^2}\int_0^\omega dx\frac{x(1 - x)}{1 + x}dx\,e^{-t} + O(e^{-2t}).$$ (7.104)

Evaluating the integral yields the desired equation for $\beta(\omega, t)$:

$$\beta(\omega, t) = \frac{1}{2}G(1) + G'(1)\left(1 - \frac{4}{\omega} + \frac{4\log(1 + \omega)}{\omega^2}\right)e^{-t} + O(e^{-2t}).$$ (7.105)

This means, that only a shift is remaining of the original perturbation after a long time; the shape of the circle is not changed. We have universal relaxation for $t \to \infty$ independent of the precise form of $\beta(\omega, 0)$. The results of the stability analysis have been published in Phys. Rev. Lett. [48].

7.5.1   An explicit analytic solution

We know that g has to depend on ω and T via the variable u:

$$u = \frac{\omega + T}{\omega T + 1}. \tag{7.106}$$

This is a bilinear transformation; an automorphism of the unit disc. This means that analyticity of a function with respect to ω implies analyticity with respect to u and vice versa. This means that we can take any analytic function of u, but let us take

$$\tilde{g}(u) = \frac{1}{u - \Gamma}, \tag{7.107}$$

where $\Gamma = \gamma e^{i\alpha_0}, \gamma > 1$, which is an analytic function of $|u| \leq 1$ due to the constraint on γ. This gives us

$$g(\omega, t) = \frac{\omega T + 1}{\omega(1 - \Gamma T) + (T - \Gamma)} = \frac{1}{T - \Gamma} \frac{\omega T + 1}{\omega b + 1}, \tag{7.108}$$

where

$$b = \frac{1 - T\Gamma}{T - \Gamma}. \tag{7.109}$$

Use

$$\beta(\omega, t) = \frac{1}{\omega^2} \int_0^\omega x g(x) dx \tag{7.110}$$

to obtain

$$\beta(\omega, t) = \frac{1}{\omega^2} \frac{1}{T - \Gamma} \int_0^\omega \frac{x(xT + 1)}{xb + 1} dx. \tag{7.111}$$

Evaluating the integral gives us $\beta(\omega, t)$:

$$\beta(\omega, t) = \frac{1}{2} \frac{T}{b} + \frac{1}{\omega b}\left(1 - \frac{T}{b}\right) + \left(1 - \frac{T}{b}\right) \frac{-1}{b^2 \omega^2} \log(\omega b + 1). \tag{7.112}$$

Notice that $\beta(\omega, t)$ is analytic for $\omega = 0$, since the singularities cancel each other. **Sidestep** The expansion of the logarithm is possible, since $|b| < 1$:

$$|b|^2 = \frac{1 - 2T\gamma \cos(\alpha_0) + T^2\gamma^2}{T^2 + \gamma^2 - 2T\gamma \cos(\alpha_0)} < 1, \tag{7.113}$$

since

$$\gamma^2(1 - T^2) > (1 - T^2) \Rightarrow$$
$$T^2 + \gamma^2 - 2T\gamma \cos(\alpha_0) > 1 + T^2\gamma^2 - 2T\gamma \cos(\alpha_0), \tag{7.114}$$

which implies equation (7.113).

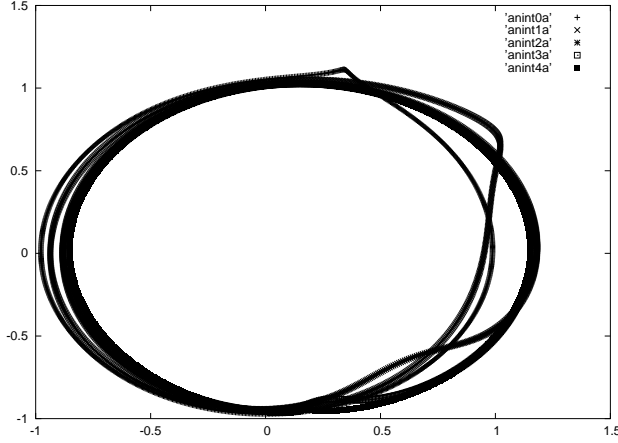The time evolution of this particular solution is shown in figure (7.1).

Figure 7.1: The particular solution of $\beta(\omega, t)$ with $\gamma = 1.1$ and $\alpha_0 = 0.3$. Consecutive timesteps are plotted on top on each other: the perturbation is convected away to the back of the circle.

We see that the cusp is convected away to the back of the streamer. This behaviour turns out to be generic for all solutions; solutions with

$$g(\omega, 0) \sim \omega^k \tag{7.115}$$

have been calculated and plotted as well. Those solutions show the same behaviour.

Analytic solutions have been derived for $\epsilon = 0, 1$. For different values, I have to rely on a numerical method. This will be the subject of the next section.

7.5.2   Towards a numerical scheme for general ϵ

I need to preserve the analyticity of β and ϕ. This means that I need to evaluate β for $\omega = e^{i\alpha}$. Use

$$\omega^2 \partial_\omega^2 = -\partial_\alpha^2 + i\partial_\alpha \tag{7.116}$$

to rewrite the operator L_ϵ on the boundary of the unit disc

$$\frac{1}{2}L_\epsilon = -i\epsilon \sin(\alpha)\partial_\alpha^2 + (-i\epsilon e^{i\alpha} + ie^{-i\alpha})\partial_\alpha + ((1+\epsilon) - i\epsilon\partial_\alpha)\partial_t. \tag{7.117}$$

Rearranging terms gives us a more convenient form of L_ϵ:

$$L_\epsilon \beta = (\sin(\alpha)\partial_\alpha + \partial_t)g(\alpha, t) + i(1 - \epsilon)\cos(\alpha)\partial_\alpha\beta, \tag{7.118}$$

where g is defined below:

$$g(\alpha, t) = (-i\epsilon\partial_\alpha + (1+\epsilon))\beta(\alpha, t). \tag{7.119}$$

This means that I can determine g from β and make a time step with equation (7.118):

$$(\sin\alpha\partial_\alpha + \partial_t)g(\alpha, t) = -i(1-\epsilon)\cos\alpha\partial_\alpha\beta \tag{7.120}$$

Retrieving β from equation (7.119) is the difficult part. Terms like $e^{-i(1+\epsilon)\alpha}$ could be generated. I derived a condition at $\omega = 0$ to prevent those non-analytic terms. This condition should be translated in an initial value for β, say at $\alpha = 0$. Let us take

$$\mu = \beta(\alpha = 0, t). \tag{7.121}$$

Solving the integral equation with this particular initial value yields a solution $\beta(\alpha, t; \mu)$. We need to find the value of μ such that

$$m(\mu) = \int_{\alpha=0}^{\alpha=2\pi} \beta(\alpha; \mu)e^{(1+\epsilon)i\alpha}d\alpha = 0 \tag{7.122}$$

We can try to solve this problem in principle using a shooting algoritm: we choose some μ_0 and determine $\beta_0(\alpha; \mu_0)$. This gives us the value $m(\mu_0)$. Minimizing (the abolute value of) $m(\mu)$ gives us the correct value of μ. This has to be done every timestep; we can use the right value of μ of the previous timestep to find the new one of course.
It is easier to impose the analyticity of β using an explicit mode expansion. This will be done in section 7.6.

7.6   Transformation

Due to the factorization of the linear operator, we were able to calculate the solution for $\epsilon = 1$ analytically. Now a different method is needed for $\epsilon \neq 0, 1$. In Section 7.4 it became clear that the variable u

$$u = \frac{\omega + T}{\omega T + 1} \tag{7.123}$$

plays a very important role in solving the $\epsilon = 1$ case analytically. We will study now whether it also helps for the $\epsilon \neq 1$ case. Observe that equation (7.123) is a so called bilinear transformation for $0 \leq T < 1$. Those transformations map the unit disc conformally onto itself. This means, that we can precompose the mapping $f_t(\omega)$ with $u(\omega, T(t))$:

$$f_t(\omega) = \tilde{f}(t, u(\omega, T(t))). \tag{7.124}$$

Instead of deriving an equation of motion for the mapping of the unit disc in ω space, we can rewrite the equation in terms of the new variable u and derive an equation of motion of the unit disc in u space. The purpose of this precomposition is the transfer of a lot of dynamical information in the mapping u. This is actually an Ansatz on the dynamics of the mapping. We will do this for the equations of the stability analysis of the circle first in section 7.6.1. As discussed before, it is difficult to maintain the analyticity of the mapping numerically. In section 7.6.2 we impose the analyticity using a mode expansion. In section 7.6.3 we show the numerical results of this expansion and in particular we will show that the results of this expansion do not depend on the cut-off.

7.6.1   Transformation of the equations

We define L_ϵ, $g(\omega, t)$, $u(\omega, T(t))$ and $T(t)$ as before:

$$L_\epsilon = -\epsilon(1 - \omega^2)\omega\partial_\omega^2 - (2 + \epsilon - 3\epsilon\omega^2)\partial_\omega + 2\epsilon\omega\partial_\omega\partial_t + 2(1 + \epsilon)\partial_t \quad (7.125)$$

$$g(\omega, t) = (\epsilon\omega\partial_\omega + (1 + \epsilon))\beta(\omega, t), \quad (7.126)$$

This means that we have to solve

$$(2\partial_t - (1 - \omega^2)\partial_\omega)g(\omega, t) = -(1 - \epsilon)(1 + \omega^2)\partial_\omega\beta(\omega, t) \quad (7.127)$$

Define

$$\tilde{\beta}(u, t) = \beta(\omega, t) \quad \text{and} \quad \tilde{g}(u, t) = g(\omega, t) \quad (7.128)$$

$$u(\omega, T(t)) = \frac{\omega + T(t)}{\omega T(t) + 1}, \; \omega(u, T(t)) = \frac{-u + T(t)}{u T(t) - 1}, \; T(t) = \tanh\left(\frac{t}{2}\right). \; (7.129)$$

and use $u = e^{i\phi}$ to parametrize the unit disk in u-space.
Rewrite in the new coordinate u:

$$\frac{du}{d\omega} = \frac{(1 - uT)^2}{1 - T^2} \Rightarrow \partial_\omega = \frac{(1 - uT)^2}{1 - T^2}\partial_u. \quad (7.130)$$

Thus

$$\frac{1}{2}(\omega^2 - 1)\partial_\omega = \frac{1}{2}(u^2 - 1)\partial_u \quad (7.131)$$

and

$$\partial_t = \partial_t|_u + \frac{du}{dt}\partial_u. \quad (7.132)$$

Since

$$\frac{du}{dt} = \frac{du}{dT}\frac{dT}{dt} = -\frac{u^2 - 1}{1 - T^2}\frac{1}{2}(1 - T^2) = -\frac{1}{2}(u^2 - 1) \quad (7.133)$$

we have

$$(2\partial_t - (1-\omega^2)\partial_\omega)g = (u^2-1)\partial_u\tilde{g} + 2\partial_t\tilde{g}|_u + \frac{du}{dt}\partial_u\tilde{g} = 2\partial_t\tilde{g}|_u. \quad (7.134)$$

This is what we expected since we basically chose u such that we would obtain such an easy result.

Rewrite the other parts of L_ϵ:

$$\frac{-1}{2}(\omega^2+1)\partial_\omega = -\frac{u^2 - 4uT + T^2 + u^2T^2 + 1}{2(1-T^2)}\partial_u \quad (7.135)$$

which gives in terms of ϕ:

$$\frac{-1}{2}(\omega^2+1)\partial_\omega = i\frac{\cos(\phi)(1+T^2)-2T}{1-T^2}\partial_\phi. \quad (7.136)$$

We also need $\omega\partial_\omega$:

$$\omega\partial_\omega = \frac{(uT-1)(-u+T)}{1-T^2}\partial_u = -i\frac{1+T^2-2T\cos(\phi)}{1-T^2}\partial_\phi. \quad (7.137)$$

This means that the equation (7.127) is rewritten as:

$$\partial_t\tilde{g}(u,t) = (1-\epsilon)\frac{\cos(\phi)(1+T^2)-2T}{1-T^2}\partial_\phi\tilde{\beta}(e^{i\phi},t) \quad (7.138)$$

and equation (7.126) is rewritten as

$$\tilde{g}(u,t) = \left((1+\epsilon) - i\epsilon\frac{1+T^2-2T\cos(\phi)}{1-T^2}\partial_\phi\right)\tilde{\beta}(e^{i\phi},t). \quad (7.139)$$

Notice that we can encounter numerical problems again if we want to integrate equation (7.139). The term in front of the derivative ∂_ϕ is positive, since

$$1 + T^2 - 2T\cos(\phi) \geq 1 + T^2 - 2T = (1-T)^2 > 0, \quad (7.140)$$

which means that we have to prevent the emergence of nonanalytic zero modes. We will do so using a mode expansion for $\tilde{\beta}$ and $\tilde{g}$, given in the next Section 7.6.2.

7.6.2   Expansion

The easiest way to preserve the analyticity of a funtion is an expansion:

$$\beta = \sum_{k=0}^{\infty} a_k(t)\omega^k. \quad (7.141)$$

Inserting this ansatz will in general yield an infinite number of coupled ODE's. If we want to solve those ODE's numerically, we have to introduce a cut-off N:

$$\beta = \sum_{k=0}^{N} a_k(t)\omega^k. \quad (7.142)$$

This is only a good approximation, if the solution is independent of the cut-off N. This is easily checked by doubling and halving N. Previously, we found that such a mode expansion didn't work; the solutions depended heavily on the choice of the cut off N. But now we hope that most of the dynamics of the problem is transferred in the coordinate u, so we set:

$$\tilde{\beta} = \sum_{k=0}^{N} b_k(t) u^k, \quad \tilde{g} = \sum_{k=0}^{N} g_k(t) u^k. \tag{7.143}$$

Let us use a vector notation again and introduce

$$\tilde{\mathbf{b}} = \begin{pmatrix} b_0(t) \\ b_1(t) \\ b_2(t) \\ \vdots \\ b_N(t) \end{pmatrix} \tag{7.144}$$

and $\mathbf{g}$ in the same way.
Substitution of the Ansatze of equation (7.143) in equation (7.139) using vector notation yields

$$\mathbf{g} = (1 + \epsilon)\tilde{\mathbf{b}} + \epsilon \frac{1 + T^2}{1 - T^2} \mathbf{M}_1 \tilde{\mathbf{b}} + \frac{-\epsilon T}{1 - T^2} \mathbf{M}_2 \tilde{\mathbf{b}}, \tag{7.145}$$

where $\mathbf{M}_1$ and $\mathbf{M}_2$ read:

$$\mathbf{M}_1 = \begin{pmatrix} 0 & 0 & 0 & 0 & \ldots & 0 \\ 0 & 1 & 0 & 0 & \ldots & 0 \\ 0 & 0 & 2 & 0 & \ldots & 0 \\ \vdots & \vdots & \vdots & \ddots & \vdots & \vdots \\ 0 & \ldots & 0 & 0 & N-1 & 0 \\ 0 & \ldots & 0 & 0 & 0 & N \end{pmatrix}, \ \mathbf{M}_2 = \begin{pmatrix} 0 & 1 & 0 & 0 & \ldots & 0 \\ 0 & 0 & 2 & 0 & \ldots & 0 \\ 0 & 1 & 0 & 3 & \ldots & 0 \\ \vdots & \vdots & \ddots & \vdots & \ldots & \vdots \\ 0 & \ldots & 0 & N-2 & 0 & N \\ 0 & \ldots & 0 & 0 & N-1 & 0 \end{pmatrix} \tag{7.146}$$

Substitution in equation (7.138) yields equation (7.147):

$$\partial_t \mathbf{g} = (1 - \epsilon) \left(\frac{-2T}{1 - T^2} \mathbf{M}_1 \tilde{\mathbf{b}} + \frac{1}{2} \frac{1 + T^2}{1 - T^2} \mathbf{M}_2 \tilde{\mathbf{b}} \right). \tag{7.147}$$

Differentiating equation (7.145) gives us another expression for $\partial_t \mathbf{g}$, so we can eliminate it from equation (7.147) in order to obtain an equation for $\partial_t \tilde{\mathbf{b}}$ in terms of $\tilde{\mathbf{b}}$ and T.
Notice that the matrices don't depend on t but that some of the prefactors do via T. Use again

$$\frac{dT}{dt} = \frac{1}{2}(1 - T^2) \tag{7.148}$$

and apply ∂_t to g from equation (7.145) to obtain

$$\partial_t \mathbf{g} = i(1+\epsilon)\partial_t \tilde{\mathbf{b}} + \epsilon i \frac{1+T^2}{1-T^2}\mathbf{M}_1 \partial_t \tilde{\mathbf{b}} + \epsilon i \frac{2T}{1-T^2}\mathbf{M}_1 \tilde{\mathbf{b}} +$$
$$\frac{-i\epsilon T}{1-T^2}\mathbf{M}_2 \partial_t \tilde{\mathbf{b}} + \frac{-i\epsilon}{2}\frac{1+T^2}{1-T^2}\mathbf{M}_2 \tilde{\mathbf{b}}. \qquad (7.149)$$

Equating (7.147) and (7.149) we can elimate $\partial_t g$ and derive an expression for $\partial_t \mathbf{b}$ in terms of $\mathbf{b}$. Notice that the terms linear in ϵ which are present in equation (7.147) are in (7.149) as well: they will cancel each other. This means that the equation for $\partial_t \tilde{\mathbf{b}}$ simplifies a lot:

$$\left((1+\epsilon) + \epsilon \frac{1+T^2}{1-T^2}\mathbf{M}_1 + \frac{-\epsilon T}{1-T^2}\mathbf{M}_2 \right) \partial_t \tilde{\mathbf{b}} =$$
$$\frac{-2T}{1-T^2}\mathbf{M}_1 \tilde{\mathbf{b}} + \frac{1}{2}\frac{1+T^2}{1-T^2}\mathbf{M}_2 \tilde{\mathbf{b}}. \qquad (7.150)$$

Equation (7.150) has the following form:

$$\mathbf{A}(T)\partial_t \tilde{\mathbf{b}} = \mathbf{B}(T)\tilde{\mathbf{b}}, \qquad (7.151)$$

where $\mathbf{A}(T)$ and $\mathbf{B}(T)$ depend on time only. It is not difficult to solve this equation numerically; this will be done in section 7.6.3.

7.6.3   Numerical Results

Solving equation (7.150) numerically introduces several numerical errors. First of all we have the discretization of time; this could be delicate, since changing the time also changes the coeffients in the ODE's (via T). Previously, we did not find any problems here and this still doesn't cause problems. The second source of errors can be the cut-off and the discretization of space (which is used to calculate the $b_k(0)$ from an arbitrary initial condition). We denote the number of modes with N and simply set the number of points equal to $10N$, meaning that the 'fastest' cosine is still described by 10 points. First we notice that

$$T = \tanh \frac{t}{2}. \qquad (7.152)$$

We would like to stay away from $T = 1$, so we let our simulations end when $T \approx 0.9$, which means $t \approx 3$. Use

$$\tanh x = 1 - 2e^{-2x} + \text{higher powers in } e^{-2kx} \qquad (7.153)$$

to estimate this real time. The numerical solution, with the initial condition of Section 7.5.1 of the analytic solution, is plotted in Figure 7.2. It 'looks' the same as the analytical solution, a more precise comparison will be made in Section 7.6.4.
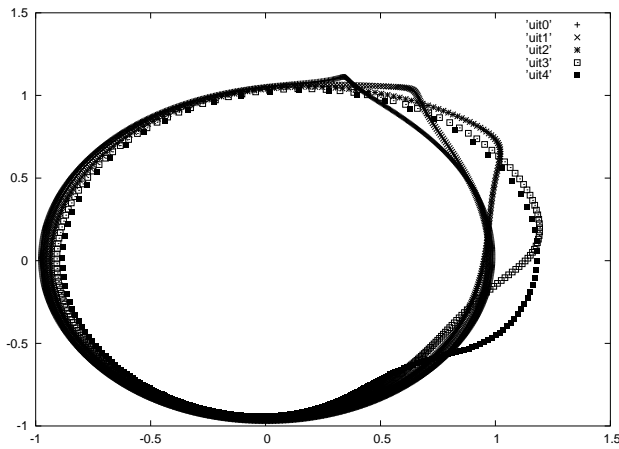
Figure 7.2: Time evolution of the interface for $\epsilon = 1$, 100 modes

I would like to study the effect of the cut off N. Simply plotting the shapes, containing all modes does not tell us much. I prefer to plot the spectrum; the number $k, k = 0, \ldots, N$ on the x-axis and the amplitude $b_k(T)$ for a certain $T > 0$ on the y-axis.
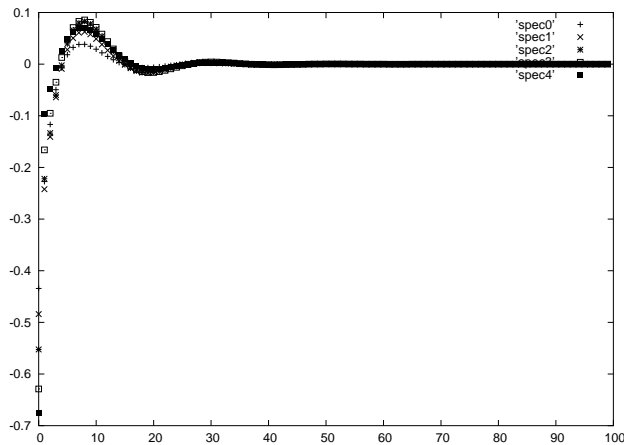

Figure 7.3: The spectrum: $b_k(T)$ as a function of k for $T = 0, 0.2, 0.4, 0.6, 0.8$, 100 modes

We see that the spectrum becomes essentially flat after approximately fourty modes; we conclude that the solution is independent of the cut off in this case.

7.6.4   Comparing analytical and numerical results

It is very important to compare the numerical results with mode expansion with the analytical results. I will compare the analytical result (7.112) with the numerics by inserting the proper initial condition and $\epsilon = 1$ into my numerical code. I calculate the coefficients $b_k(t)$

$$\tilde{\beta}(u, t) = \sum_{k=0}^{\infty} b_k(t) u^k, \tag{7.154}$$

which are in principal known from the analytic solution

$$\beta(\omega, t) = \sum_{k=0}^{\infty} a_k(t) \omega^k. \tag{7.155}$$

This allows me to see whether the mode expansion, which failed many times, works this time.

Applying brute force to write b_k in terms of a_k does not work. Use

$$k! b_k = \frac{d^k \tilde{\beta}}{du^k}(u = 0) = \left(\frac{d^k}{du^k} \right) \beta(\omega = -T). \tag{7.156}$$

Differentiating β with respect to u requires the chain rule and the product rule, which means that you pick up more terms for higher derivatives. The derivatives of ω to u are easy, since:

$$\omega = \frac{u - T}{-uT + 1} = \frac{-1}{T} + \frac{1 - T^2}{T} \frac{1}{1 - uT}, \tag{7.157}$$

we have

$$\frac{d^k \omega}{du^k}(u = 0) = \frac{1 - T^2}{T} \frac{k! T^k}{(1 - uT)^{k+1}}(u = 0) = k!(1 - T^2)T^{k-1}. \tag{7.158}$$

It turns out to be convenient to absorb the factors $k!$ in Ω_k

$$\Omega_k = \frac{1}{k!} \frac{d^k \omega}{du^k}(u = 0) = (1 - T^2)T^{k-1}. \tag{7.159}$$

Define in a similar way

$$A_k = \frac{1}{k!} \frac{d^k \beta}{d\omega^k}(\omega = -T) \tag{7.160}$$

and notice that $B_k = b_k$. We are now ready to derive expressions for the b_k in terms of the A_k and Ω_k. We have

$$B_0 = b_0 = \tilde{\beta}(0) = \beta(\omega = -T) = A_0, \tag{7.161}$$

$$B_1 = \frac{d\beta}{d\omega}(\omega = -T)\frac{d\omega}{du}(u = 0) = A_1 \Omega_1. \tag{7.162}$$

Now we get more terms:

$$2!B_2 = \frac{d^2\beta}{d\omega^2}(\omega = -T)\left(\frac{d\omega}{du}\right)^2(u=0) + \frac{d\beta}{d\omega}(\omega = -T)\frac{d^2\omega}{du^2}(u=0) \quad (7.163)$$

and we have

$$B_2 = A_2\Omega_1^2 + A_1\Omega_2 \tag{7.164}$$

In a similar way we derive the other coefficients:

$$B_3 = A_3\Omega_1^3 + 2A_2\Omega_1\Omega_2 + A_1\Omega_3 \tag{7.165}$$

$$\begin{aligned} B_4 = A_4\Omega_1^4 + 3A_3\Omega_1^2\Omega_2 + A_2(\Omega_2^2 \\ +\Omega_1\Omega_3) + A_1\Omega_4 \end{aligned} \quad ,$$

$$\begin{aligned} B_5 = A_5\Omega_1^5 + 4A_4\Omega_1^3\Omega_2 + 3A_3(\Omega_1\Omega_2^2 + \Omega_1^2\Omega_3)+ \\ 2A_2(\Omega_2\Omega_3 + \Omega_1\Omega_4) + A_1\Omega_5, \end{aligned} \tag{7.166}$$

$$\begin{aligned} B_6 = A_6\Omega_1^6 + 5A_5\Omega_1^4\Omega_2 + A_4(6\Omega_1^2\Omega_2^2 + 4\Omega_1^3\Omega_3) \\ +A_3(\Omega_2^3 + 3\Omega_1\Omega_2\Omega_3 + 3\Omega_1^2\Omega_4)+ \\ A_2(\Omega_3^2 + 2\Omega_2\Omega_4 + 2\Omega_1\Omega_5) + A_1\Omega_6. \end{aligned} \tag{7.167}$$

We need to calculate $\beta(\omega)$ and its derivatives which are given by the analytic expression

$$\beta(\omega) = \frac{1}{T-\Gamma}\left(\frac{1}{\omega b}\left(1 - \frac{T}{b}\right) + \frac{1}{2}\frac{T}{b} - \frac{1}{\omega^2 b^2}\left(1 - \frac{T}{b}\right)\log(1+\omega b)\right), \tag{7.168}$$

where

$$b = \frac{1 - T\Gamma}{T - \Gamma}, \qquad \Gamma = \gamma e^{i\alpha_0}. \tag{7.169}$$

We will choose $\gamma = 1.1$ and $\alpha_0 = 0.3$, derived in Section 7.5.1.
This is not a nice expression to differentiate and evaluate, fortunately we can go back one step in the derivation and notice:

$$(2 + \omega\partial_\omega)\beta = \frac{g}{i} = \frac{1}{T-\Gamma}\frac{\omega T + 1}{\omega b + 1}. \tag{7.170}$$

It is convenient to rewrite equation (7.170) in the following way:

$$(2 + \omega\partial_\omega)\beta = a_0(\Gamma, T) + a_1(\Gamma, T)\frac{1}{\omega b + 1}, \tag{7.171}$$

where

$$a_0(\Gamma, T) = \frac{T}{1 - \Gamma T} \quad \text{and} \quad a_1(\Gamma, T) = \frac{1 - T^2}{(1 - \Gamma T)(T - \Gamma)}. \tag{7.172}$$

Now we see that it is very easy to obtain all derivatives of β; differentiation of equation (7.171) gives the kth derivative in terms of a known function and the $(k-1)^{th}$ derivative:

$$\omega \frac{d^k\beta}{d\omega^k} = a_1(\Gamma, T)\frac{(k-1)!(-b)^{k-1}}{(\omega b+1)^k} - (k+1)\frac{d^{k-1}\beta}{d\omega^{k-1}} \qquad (7.173)$$

if $k > 1$. Evaluating at $\omega = -T$ and using the definition of A_k yields:

$$A_k = \frac{1}{-Tk}\left(a_1(\Gamma, T)\frac{(-b)^{k-1}}{(1-bT)^k} - (k+1)A_{k-1}\right). \qquad (7.174)$$

Notice that we need to be careful when evaluating this expression for small T; this corresponds to small ω, where the singularities in the analytic solution cancel each other. Since we are not interested in numerical problems due to an analytic feature of a certain solution, we will avoid this problem by starting the comparision at a small $T > 0$, say $T \approx t \approx 10^{-4}$. I will use the A_k, extracted from the analytical solution to calculate the B_k analytically and compare them to the B_k calculated in the numerical procedure. This comparison will be made in the next section.

7.6.5   Comparing numerics and analytical results: the pictures

In the figures below, we plot time $0 < t < 3$ on the x-axis, meaning $0 < T < 0.9$ and the real and imaginary parts of the first six b_k on the y-axis. Direct calculations of the analytical solution are compared with the numerical results with the same initial condition; both curves lie perfectly on top of eachother.
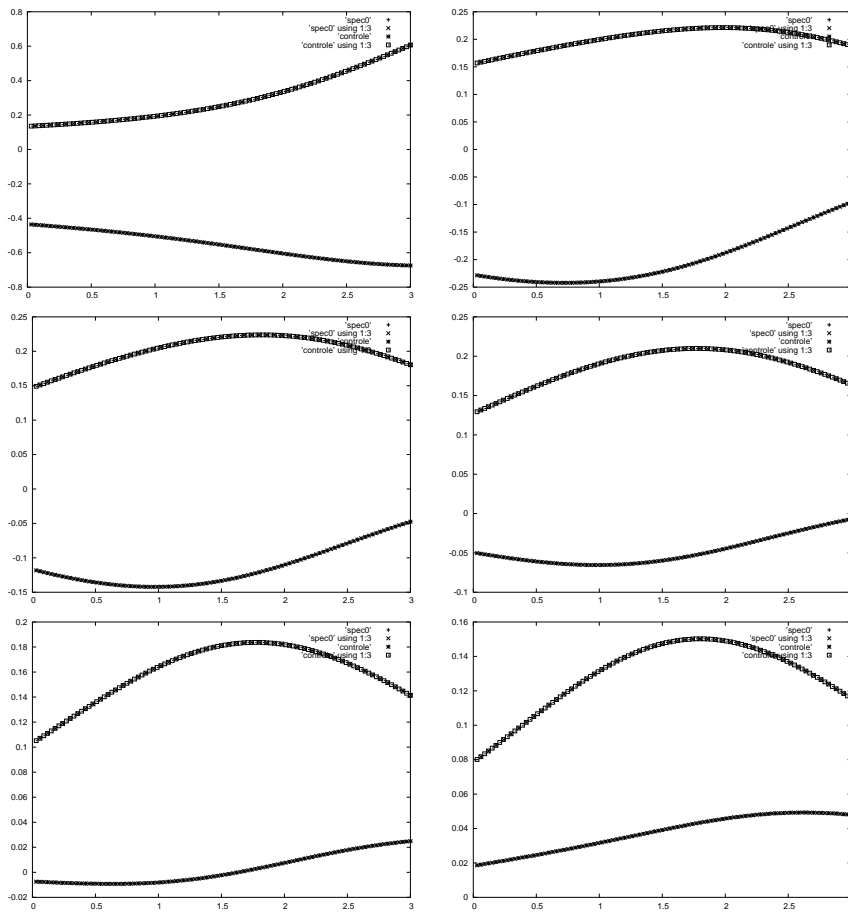
Figure 7.4: Comparison of the real and imaginary parts of $b_k, k = 0, \ldots 5$ as a function of time

Since the expressions for the higher b_k get lengthier, I decided to stop here, since the conclusion is obvious. There are no numerical problems for $\epsilon = 1$ with the mode expansion.

7.7   Conclusion

The circle is unstable for $\epsilon = 0$. A mode expansion gives both for $\epsilon = 0$ and $\epsilon > 0$ incorrect results; we derived a PDE for the perturbation instead and we were able to solve the PDE for $\epsilon = 1$. From those analytic solutions we see that the circle is linear convectively stable: perturbations may be amplified, but are convected away to the back were they disappear. This is the same scenario which was observed experimentally and numerically in viscous fingering. The

advantage of the analytical solution is that we can trace the dynamics up to $t \to \infty$ and identify a universal attractor of the long time dynamics.

It is desirable to have a reliable numerical for $\epsilon \neq 1$ when the PDE can not be solved analytically anymore. I used the analytic solutions for $\epsilon = 1$ to check the reliability of the mode expansion from the numerics. Since the numerical solutions matches perfectly with the analytical solution, I am confident that I will be able to use the code for $\epsilon \neq 1$ as well.

Chapter 8

Analysis of the planar front and a different regularization mechanism

This is chapter could have been the first chapter of my thesis, since the solutions which are analyzed are the 'easiest' nontrivial solutions of the PDE's. Solutions which are invariant in all but one of the spatial directions and invariant in time are studied, so called planar solutions, because also more complex solutions are, at least locally, planar. It is always possible to look for such solutions; substitution of

$$\xi = z - vt \tag{8.1}$$

in the PDE's yields a set of ODE's, which can be solved easier, either numerically or analytically. The existence and stability of those solutions was investigated in [9], [8]. Analytic expressions can be derived in the $D = 0$ case; the stability analysis can be performed analytically in the limits for small and large k [12]:

$$s(k) = \begin{cases} E_0 k & \text{for} \quad k \ll 1 \\ \frac{E_0}{2} e^{-1/E_0} & \text{for} \quad k \gg 1 \end{cases} \tag{8.2}$$

The points inbetween are obtained numerically using a shooting algorithm. Those results are presented in Section 8.1.

In Section 8.4 I will implement the dispersion relation as a new dynamical condition on the interface instead of the boundary condition on the potential from Chapter 5. This was our first effort to regularize the problem; it failed, but that may be due to some oversimplifications I made at that moment.

The planar solutions show some unphysical behaviour; they are unstable to transversal perturbations for all wavelengths. Once the diffusion is switched on in section 8.7 we still see unstable wavelengths, but only a band of wavelengths is unstable: the small wavelength instability is removed by the diffusion. In

contrast to (8.2) only the $k \ll 1$ asymptote can be derived analytically. The numerical solution of the eigenvalue problem and the numerical initial value problem both give the same dispersion curve.

8.1   Planar solutions with $D = 0$ and their stability

I will derive analytic expressions for the planar front in the first part of this section; those solutions are effectively one-dimensional, i.e. $E(\xi)$ etc., where $\xi = z - vt$ is a comoving coordinate. Furthermore the proper boundary conditions need to be imposed: zero net charge behind the front and no particles in front, a vanishing electric field behind the front and a constant field in front, which is just $-E_0$, the field far away. I will repeat the main steps of the analysis in [12] in section 8.1.1 and refer to this paper for more details.

The stability of the planar solutions is the subject of section 8.1.1; the linear stability analysis is performed in a standard way, using a transversal perturbation with wavevector k. The growth rate of such a perturbation is studied for any k, which yields a dispersion relation $s(k)$. This relation can be approximated analytically, but only for very small k

$$s(k) = E_0 k \tag{8.3}$$

and for large k:

$$s(k) = \frac{1}{2} E_0 e^{-1/E_0}. \tag{8.4}$$

This means that the solutions are unstable against large k perturbations; this unphysical behaviour is cured by including diffusion in Section 8.7.

8.1.1   Derivation of expressions for the planar front

The streamer equations were derived in Chapter 3:

$$\partial_t \sigma - \nabla \cdot (\sigma \mathbf{E}) = \sigma f(\mathbf{E}), \tag{8.5}$$
$$\partial_t \rho = \sigma f(\mathbf{E}), \tag{8.6}$$
$$\nabla \cdot \mathbf{E} = \rho - \sigma, \tag{8.7}$$

where

$$f(\mathbf{E}) = |\mathbf{E}| e^{-1/|\mathbf{E}|} \tag{8.8}$$

Use the ansatz

$$\xi = z - vt \tag{8.9}$$

and impose the conditions on the electric field and the particle densities

$$\mathbf{E} = \left\{ \begin{array}{ll} -E_0\hat{z} & z \to \infty \\ 0 & z \to -\infty \end{array} \right. \qquad \rho = \left\{ \begin{array}{ll} \sigma & z \to -\infty \\ \sigma = 0 & z \to \infty \end{array} \right.$$

to derive expressions for the uniformly translating front:

$$(v + E)\partial_\xi \sigma + (\rho - \sigma)\sigma + \sigma f(|E|) = 0 \tag{8.10}$$

$$v\partial_\xi \rho + \sigma f(|E|) = 0 \tag{8.11}$$

$$\rho - \sigma - \partial_\xi E = 0. \tag{8.12}$$

These equations were discussed in [9] and [12]; the velocity $v = E_0$, the far field, is the only solution fullfilling the requirement that the electron density vanishes beyond a certain point. This will be called the selected velocity. For any velocity, the equations (8.10)-(8.12) can be solved directly:

$$\sigma[E] = \frac{v}{v + E}\rho[E] \tag{8.13}$$

$$\rho[E] = \int_{|E|}^{E_0} e^{-1/x} \, dx \tag{8.14}$$

$$\xi_2 - \xi_1 = \int_{E(\xi_1)}^{E(\xi_2)} \frac{v + x}{\rho[x]} \frac{dx}{x} \tag{8.15}$$

$$\tag{8.16}$$

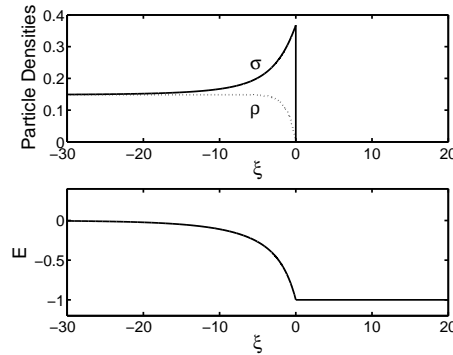The solutions for $v = E_0$ are plotted in Figure 8.1.1:

Figure 8.1: The densities and the electric field as a function of the comoving coordinate ξ. [12]

The front with $v = E_0$ exhibits a discontinuity at $\xi = 0$, which is removed by addition of diffusion. This would lead to pulled fronts, which means that even a small addition of diffusion changes the behaviour drastically. We stick here to the $D = 0$ case, but note that we have to take care around the point $\xi = 0$ in the linear stability analysis.

The stability of the planar solutions

To study the stability of the solutions, both the fields and the position of the front are perturbed by Δ_k:

$$\zeta = \xi - \Delta_k, \quad \sigma = \sigma_0(\zeta) + \sigma_1(\zeta)\Delta_k, \quad \Delta_k = \delta e^{ikx+st}. \tag{8.17}$$

This means that the jump in the electron density is located at $\zeta = 0$. Expanding the equation up to linear order in δ yields an equation of the following form:

$$\partial_t \mathbf{f}_1 = \mathbf{M}_{s,k}\mathbf{f}_1 - \mathbf{f}_2, \tag{8.18}$$

where the vector $\mathbf{f}_1$ contains the physcial fields like electron density, the matrix $\mathbf{M}$ and the vector $\mathbf{f}_2$ are given in terms of the 0th order solution and s and k. Conditions on the fields at $\zeta = \pm\infty$ fully specify the eigenvalues $s(k)$. Solutions can be found for general k using a shooting algorithm, the asymptotes for small and large values of k can be found analytically:

$$s(k) = \begin{cases} E_0 k & k \quad \text{small} \\ \frac{f(E_0)}{2} & k \quad \text{large} \end{cases} \tag{8.19}$$

The dispersion relation with its asymptotes is plotted in Figure 8.2 for $E_0 = 1$.
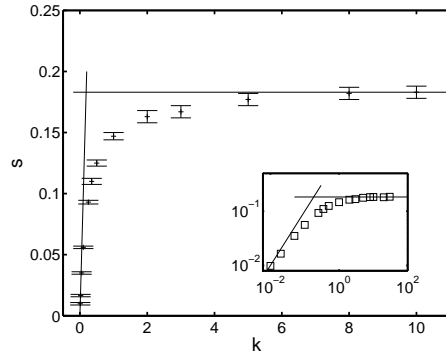

Figure 8.2: The dispersion relation $s(k)$ for $D = 0$ and $E_0 = 1$ with both asymptotes from [12]

8.2 Derivation of the dispersion relation with the new boundary condition

We will show in this section that an equation for $s(k)$ can be derived, when the boundary condition

$$\phi^+ - \phi^- = \epsilon(\nabla\phi^+)_n \tag{8.20}$$

derived in Chapter 5 is imposed as a boundary condition on the planar front. Use the explicit expression for ϕ^+

$$\phi^+ = E_0\xi + a\delta e^{-|k|\xi}\Delta_k + c.c. \tag{8.21}$$

to rewrite the boundary condition at front ($\xi = \zeta_0\Delta_k$):

$$\phi^+ - \phi^- = E_0\zeta_0\Delta_k + a\delta\Delta_k - \phi_- \tag{8.22}$$

and

$$\epsilon(\nabla\phi^+)_n = \epsilon(E_0 - |k|a\delta\Delta_k) \tag{8.23}$$

which implies (choose $\phi_- = -\epsilon E_0$)

$$E_0\zeta_0 + a = -\epsilon|k|a. \tag{8.24}$$

Turn the attention to the dynamic boundary condition

$$v_n = (\nabla\phi^+)_n \tag{8.25}$$

on the interface. Use

$$z = E_0 t + \delta\zeta_0\Delta_k \tag{8.26}$$

to calculate the velocity on the interface:

$$v_n = E_0 + s(k)\delta\zeta_0\Delta_k \tag{8.27}$$

and the previously obtained expression for $(\nabla\phi^+)_n$:

$$(\nabla\phi^+)_n = E_0 - |k|a\delta\Delta_k \tag{8.28}$$

to derive

$$s(k) = -\frac{a|k|}{\zeta_0}. \tag{8.29}$$

Combining equations (8.24) and (8.29) we obtain the dispersion relation $s(k)$:

$$s(k) = E_0\frac{|k|}{1 + \epsilon|k|}. \tag{8.30}$$

This agrees with the results of the previous section. The linear behaviour for small k is reproduced; for large k we have

$$s(k) \rightarrow \frac{E_0}{\epsilon} \text{ and } s(k) \rightarrow \frac{E_0\alpha(E_0)}{2}. \tag{8.31}$$

where $\frac{1}{\alpha(E_0)} \sim \epsilon$ is the characteristic lengthscale of the interface.

8.3   A different method to implement a regularization

It is also possible to implement the results of the linear stability analysis into a different regularization mechanism. There are different possibilities to regularize our problem, whether the outcome is the same is an open question. Both mechanisms implement the same dispersion relation; the dynamic boundary condition

$$v_n = (\nabla\phi)_n \tag{8.32}$$

led to the correct dispersion relation for a planar front, as we saw in Section 8.2. I will implement a different regularization mechanism in this Section. Let me introduce the same lengthscale as before, the width of the boundary layer, but I will use $k_0 \sim \frac{1}{\epsilon}$ in the following analysis, which means that the unregularized case corresponds to $k_0 \to \infty$.
Instead of taking the velocity proportional to the local field, I will use

$$(v(x))_n = \left(\int K(x - x')E(x')dx' \right)_n , \tag{8.33}$$

where the function $K(x-x')$ contains the parameter k_0, and basically determines how large the region of integration is. (We would retrieve the unregularized dynamical condition with a delta function for k). Furthermore, this function will be chosen such that the proper dispersion relation $s(k)$ is retrieved. This means that the same physics is implemented as in the regularization mechanism discussed in Chapter 5.
Intuitively one can see why this condition could regularize the problem as follows. Close to a sharp cusp in the interface, the electric field points (partly) in opposite directions on different sides of the cusp, since it is still normal to the equipotential boundary. This means that the velocity, which effectively takes the vector sum of the electric fields around a point, is decreased due to the cancellation of fields around the cusp. This implies, that the local velocity of the cusp is smaller than the velocity of a flat interface, which means that the cusp is overtaken by the flatter regions. This is illustrated by figure 8.3.
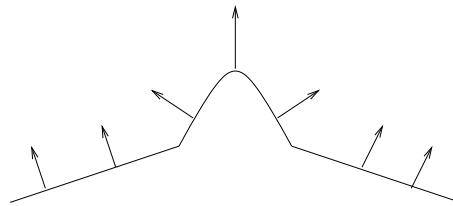

Figure 8.3: Around a cusp, contributions tend to cancel each other.

Originally, I used

$$(v(x))_n = \left(\int K(x - x') E(x')_n dx' \right). \tag{8.34}$$

instead of equation (8.33). Equation (8.34) will decrease the velocity of a cusp, since the field is averaged over a region around the cusp which means that the velocity of a cusp is lowered. By the time I was trying to implement a mechanism like this, I made unfortunately some oversimplications, which led to the (erroneous ?) conclusion that the mechanism could not work, even independently of the implemented dispersion relation. I will point out the correct approach in the following section.

8.4   Implementation of the dispersion relation

In this section I will derive an expression for $K(x - x')$ such that

$$(v(x))_n = \left(\int K(x - x') E(x') dx' \right)_n \tag{8.35}$$

for the planar front. The function $K(x - x')$ will depend on the dispersion relation $s(k)$. Taking the normal component of the field before the integration does not change the derivation; (it does not matter for a planar front). It does change the implementation of the boundary condition in the full problem; I will indicate the change.
Use the same notation as in Section 8.1.1; the perturbed coordinate ζ was introduced

$$\zeta = \xi - \delta e^{ikx+st} + c.c. \tag{8.36}$$

such that the perturbed interface is located at $\zeta = 0$. Solving the Laplace equation in front of the front yields

$$\Phi(\xi) = E_0\xi + ae^{ikx+st}e^{-|k|\xi} + c.c.. \tag{8.37}$$

The constant a can be determined using the fact that the interface, located at $\zeta = 0$ is equipotential and gauged to zero:

$$a = -E_0\delta, \quad \Phi(\xi) = E_0\xi - E_0\delta e^{ikx+st}e^{-|k|\xi}. \tag{8.38}$$

This means that the normal component of the electric field is given by

$$\mathbf{E}_n = -E_0 - \delta|k|E_0 e^{ikx}e^{st} + c.c. \tag{8.39}$$

up to linear order in δ. The normal component of the velocity of the interface is calculated as follows; the interface is defined as $\zeta = 0$, which means

$$\frac{d\zeta}{dt} = \frac{d\xi}{dt} - \delta s e^{ikx}e^{st} + c.c. = 0 \tag{8.40}$$

and we see that

$$v\hat{z} = \frac{dz}{dt}\hat{z} = \left(\frac{d\xi}{dt} + v_0\right)\hat{z} = (E_0 + \delta s e^{ikx+st} + c.c.)\hat{z}, \tag{8.41}$$

and I obtain

$$v_n = E_0 + \delta s e^{ikx+st} + c.c.. \tag{8.42}$$

Any perturbation of the uniformly translating front can be written as a sum a Fourier modes:

$$E_n = -E_0 - E_0 \int |k| e^{s(k)t} \delta_k e^{ikx} dk, \tag{8.43}$$

where $\delta_k = \delta^\star_{-k}$ since $\mathbf{E}$ is real. Expand v_n in the same way:

$$v_n = E_0 + \int_{\mathbb{R}} s(k) e^{s(k)t} \delta_k e^{ikx}. \tag{8.44}$$

It is convenient to take Fourier transforms of the electric field and the velocity. Define

$$\hat{f}(k) = \frac{1}{2\pi} \int_{\mathbb{R}} f(x) e^{-ikx} dx \tag{8.45}$$

and the inverse transformation

$$f(x) = \int_{\mathbb{R}} f(k) e^{ikx} dk. \tag{8.46}$$

Use

$$\hat{E}(k) = \frac{1}{2\pi} \int_{\mathbb{R}} \mathbf{E}_n e^{-ikx} dx = -E_0 \delta(k) - E_0 \delta_k |k| e^{st} \tag{8.47}$$

and similarly for $\hat{v}(k)$:

$$\hat{v}(k) = E_0 \delta(k) + s(k) \delta_k e^{s(k)t} \tag{8.48}$$

which implies

$$\hat{v}(k) = \frac{-s(k)}{|k| E_0} \hat{E}(k) \quad \forall k \neq 0. \tag{8.49}$$

Notice that we can extend $s(k)$ to $k < 0$, since it is symmetric with respect to this transformation: $s(k) = s(-k)$. It is convenient to use a functional form for $s(k)$ which can be substituted in equation (8.49). We want to implement the following properties that we derived from the linear stability analyisis:

$$s(k) \to |k| E_0 \quad \text{as} \quad |k| \to 0 \tag{8.50}$$

and

$$s(k) \to k_0 E_0 \quad \text{as} \quad |k| \to \infty, \ k_0 = \frac{1}{2} e^{-1/E_0}. \tag{8.51}$$

Use the following interpolation for $s(k)$:

$$s(k) = \frac{k_0}{k_0 + |k|} |k| E_0, \tag{8.52}$$

which can be inserted in equation (8.49) to obtain:

$$\hat{v}(k) = \frac{-k_0}{k_0 + |k|} \hat{E}(k). \tag{8.53}$$

(Notice that equation (8.53) also holds for $k = 0$). This means that I can transform equation (8.53) back to real space to derive the desired dynamical condition:

$$v_n(x) = \frac{-1}{2\pi} \left(\int_{\mathbb{R}} dk \int_{\mathbb{R}} dx' \ e^{ik(x-x')} \frac{k_0}{k_0 + |k|} \mathbf{E}(x') \right)_n. \tag{8.54}$$

Notice that the k integral can be rewritten in an integral over $\mathbb{R}^+$.

$$v_n(x) = \frac{-1}{\pi} \left(\int_{\mathbb{R}^+} dk \int_{\mathbb{R}} dx' \ \cos(k(x-x')) \frac{k_0}{k_0 + k} \mathbf{E}(x') \right)_n. \tag{8.55}$$

I will use equation (8.55) as the new boundary condition on the interface.

8.5 Implementation of the new boundary condition in the full problem

The dynamical equation needs to be incorporated in the conformal mapping frame. This means that the integration has to be taken along the interface instead of over all $x \in \mathbb{R}$:

$$\int_{\mathbb{R}} dx' = -\int_{\alpha'=-\pi}^{\pi} |\partial_\alpha f| d\alpha'. \tag{8.56}$$

The minus sign is due to the fact that I reversed the direction of integration. The distance $d(\alpha - \alpha')$ has to be measured along the interface; this means that I have to replace it by

$$d(\alpha - \alpha') = \min \left(\int_{\alpha}^{\alpha'} |\partial_y f| dy, | \int_{\alpha}^{-2\pi+\alpha'} |\partial_y f| dy| \right), \tag{8.57}$$

where $\alpha < \alpha'$. Write the velocity, the normal and the electric field in complex notation instead of vector notation:

$$v = v_x + iv_y, \quad n = n_x + in_y, \quad E = E_x + iE_y. \tag{8.58}$$

The normal component of the velocity reads

$$v_n = v_x n_x + v_y n_y = \text{Re}(n v^\star). \tag{8.59}$$

Substitute this in equation (8.55)

$$\mathbf{v}_n(\alpha) = \frac{1}{\pi} \text{Re} \Big(\int_{\mathbb{R}^+} dk \int_{\alpha'=-\pi}^{\pi} |\partial'_\alpha f| d\alpha' \; \cos(kd(\alpha - \alpha'))$$
$$\frac{k_0}{k_0 + k} n(\alpha)(E_x(\alpha') - iE_y(\alpha'))), \tag{8.60}$$

where $d(\alpha - \alpha')$ is defined in equation (8.57). Rewrite

$$E_x - iE_y = \partial_x \phi - i\partial_y \phi = \partial_x(\phi + i\psi) = \partial_z \Phi(z) = \frac{\partial_\alpha \hat{\Phi}}{\partial_\alpha f}. \tag{8.61}$$

and use the expression for the normal

$$n = \frac{i\partial_\alpha f}{|\partial_\alpha f|} \tag{8.62}$$

to obtain the velocity in terms of the potential and the mapping function:

$$\mathbf{v}_n = \text{Re} \left(\int_{-\pi}^{\pi} d\alpha' |\partial_{\alpha'} f| K(\alpha - \alpha') \frac{\partial_\alpha f}{|\partial_\alpha f|} \frac{i\partial_{\alpha'} \hat{\Phi}}{\partial_{\alpha'} f} \right), \tag{8.63}$$

where

$$K(\alpha - \alpha') = \frac{1}{\pi} \int_{\mathbb{R}^+} dk \frac{k_0}{k_0 + k} \cos k(d(\alpha - \alpha')). \tag{8.64}$$

In my first attempt, I evaluated the normal inside the integral, which means that the argument of the normal becomes α', which simplifies equation (8.63) a bit. The equations (8.57), (8.63) and (8.64) fully specify the velocity of the interface in terms of the mapping function for any given k_0. Notice that the potential is known, since it is the same as in the unregularized case:

$$\hat{\Phi}(\omega) = E_0 a_{-1} \left(\frac{1}{\omega} + \omega \right), \quad \hat{\Phi}(\omega = e^{i\alpha}) = -2iE_0 a_{-1} \sin \alpha. \tag{8.65}$$

It is difficult to make any analytic progress, unless I study the circle as initial condition, which will be done in Section 8.6.
If we want to study the full problem with a general initial condition, the equation of motion of the mapping function becomes

$$\text{Re}(i\partial_t f \partial_\alpha f^\star) = |\partial_\alpha f| v_n(e^{i\alpha}). \tag{8.66}$$

The easiest way to solve equation (8.66) is the introduction of a mode expansion for the mapping function f; higher modes will be generated though, since the right hand side generates all modes $\sim \cos k\alpha$. This can be a line for future research, I will not pursue it here any further.

8.6 Study of the circle

It is possible to show that I can retrieve the unregularized circle if I take the limit $k_0 \to \infty$. Take the circle with radius one as initial condition:

$$f_t(\omega) = \frac{1}{\omega} + vt \Rightarrow |\partial_\alpha f| = 1, \tag{8.67}$$

which simplifies the equations (8.57)-(8.64) a lot. The equation for the velocity becomes

$$v_n(e^{i\alpha}) = 2E_0 \int_{-\pi}^{\pi} \cos(\alpha' - \alpha) \cos \alpha' K(\alpha - \alpha'), \tag{8.68}$$

where I need to be careful with the evaluation of equation (8.57); the distance between α and α' is

$$x - x' = \alpha - \alpha' \quad \text{if} \quad |\alpha - \alpha'| < \pi, x - x' = 2\pi - \alpha + \alpha' \text{ if } |\alpha - \alpha'| > \pi. \tag{8.69}$$

Inserting this allows to calculate the second integral;

$$v_n(e^{i\alpha}) = \frac{2E_0}{\pi} \int_{\mathbb{R}^+} dk \frac{k_0}{k_0 + k} \int_{-\pi}^{\pi} \cos(k(x - x')) \cos(\alpha' - \alpha) \cos \alpha' d\alpha'. \tag{8.70}$$

Evaluating the first integral as well in the limit $k_0 \to \infty$ gives the expected result:

$$v_n(e^{i\alpha}) = 2E_0 \cos \alpha. \tag{8.71}$$

The uniformly translating circle with velocity $2E_0$ is recovered. Studying finite k_0, one might recover the regularized circle as well. This requires a smart 'guess' of the precise form of the interpolation formula though. This could be the subject of further investigation.

8.7 Planar solutions for $D \neq 0$

There were doubts whether a dispersion relation with short wavelength instability as (8.2) would regularize the motion. We therefore derived the dispersion relation for streamers with nonvanishing diffusion numerically. The streamer equations were derived in Chapter 3 as:

$$\partial_t \sigma - \nabla \cdot (\sigma \mathbf{E} + D \nabla \sigma) = \sigma f(\mathbf{E}), \tag{8.72}$$
$$\partial_t \rho = \sigma f(\mathbf{E}), \tag{8.73}$$
$$\nabla \cdot \mathbf{E} = \rho - \sigma, \tag{8.74}$$

where

$$f(\mathbf{E}) = |\mathbf{E}| e^{-1/|\mathbf{E}|}. \tag{8.75}$$

The general idea of this section is as follows; we would like to find the dispersion relation $s(k)$ numerically. In order to do so, we run a 2D-simulation of the full PDE's with an appropriate initial condition. This initial condition has the following form:

$$\mathbf{U}(x,z,0) = \mathbf{U}_0(z) + \delta\mathbf{U}_1(z)e^{ikx}, \tag{8.76}$$

if $\mathbf{U}_1$ is to be an eigenperturbation from the start, the choice of $\mathbf{U}_0$ and $\mathbf{U}_1$ is dictated by the uniformly translating planar solution about which we perturb. If we take δ small enough, $\delta e^{st} \ll \frac{2\pi}{k}$, we will stay in the linear regime and we can find $s(k)$ by comparing the amplitudes of the perturbation at different timesteps. Details and the results of the numerics are given in Section 8.7.1.

8.7.1   Numerical solution of the initial value problem

From the analysis we know that the perturbed solutions read

$$\mathbf{U}(x,z,0) = \mathbf{U}_0(x, z + \delta\cos(kx), 0) + O(\delta^2) \tag{8.77}$$

for small k, where $\mathbf{U}_0$ is the planar front. (Only the coordinate is perturbed, the contribution of the fields is higher order in δ). This gives me a convenient initial condition for the perturbation of the planar front:

$$\mathbf{U}(x,z,0) = \mathbf{U}_0(z, t=0) + \delta\cos(kx)(\partial_z\mathbf{U}_0)(z, t=0), \tag{8.78}$$

which is equivalent to equation (8.76), with $\mathbf{U}_1 = \partial_z\mathbf{U}_0$.
We use an algorithm to solve the full 2D PDE's, which has already been used in [13]. In this case, we have to solve two separate problems; first we use some initial condition which is uniform in x in order to find the planar front $\mathbf{U}_0$ after a sufficiently long integration time. This is relatively easy, since it is a one-dimensional problem. In the next step we take the initial condition (8.78). For all values of k, we choose the length of the domain in the x-direction, L_x, such that exactly 5 cosines fit into the domain:

$$L_x = \frac{10\pi}{k}. \tag{8.79}$$

We also fix the number of points in the x-direction and we impose periodic boundary conditions at $x = 0$ and $x = L_x$, since we want to keep the peridicity of the solution. For $z = 0$ and $z = L_z$, we impose Neumann-conditions on the electrons. Since we have a constant potential behind the front and a constant field in front of the front, we have Dirichlet and Neumann conditions for the electric potential ϕ at $z = 0$ and $y = L_z$ respectively.
In order to find the growth rate of the perturbation, we need to find the maximum of σ in the z-direction for fixed x. The next step is to look at the amplitude of the electron density σ as a function of x at this maximum. I will denote the maximum by z_{max} which means that the desired function, at $t = 50$ is given by $\sigma(x, z_{max}, t = 50)$. This function is plotted in Figure 8.4:
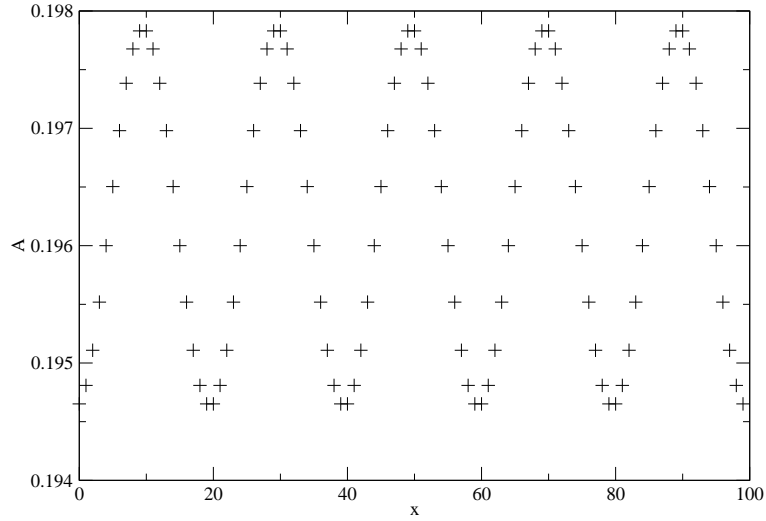
Figure 8.4: The amplitude of the perturbation of σ as a function of x at $t = 50, k = 0.45$ at z_{max}. We still clearly see the cosine shape.

We clearly see, that we still have the five cosines.

It is easy to find the amplitude of $\sigma(x, z_{max}, t)$; in order to prevent lower modes from entering the calculation, we use:

$$A = \frac{-k}{5\pi} \int_0^{\frac{10\pi}{k}} \sigma(x, z_{max}, t) \cos(kx) \, dx. \qquad (8.80)$$

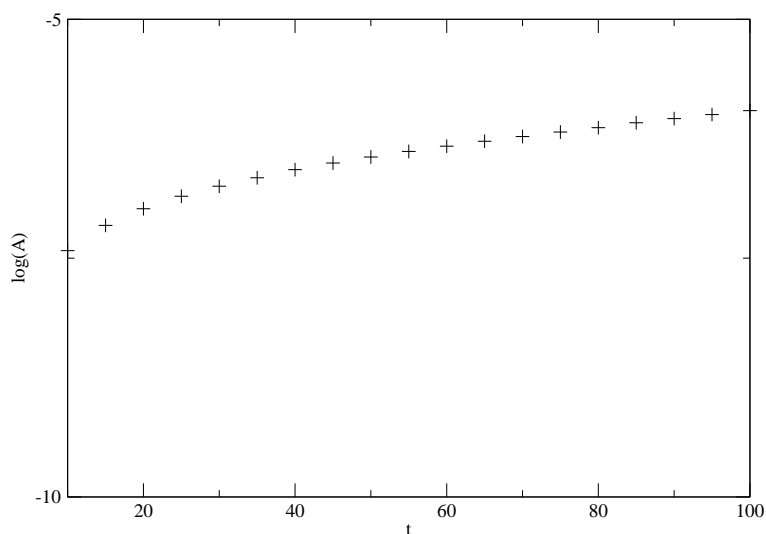In Figure 8.5 we plotted $\log(A)$ as a function of time.

Figure 8.5: $\log(A)$ as a function of time; $k = 0.45$.

Using a least squares algorithm, we can find the inclination of the line through these points, which is the growth rate $s(k)$.
However, in Figure 8.5 we see a transient behaviour before we reach constant growth rate; this is observed for the larger k-values. For small k, the eigenfunction is given by equation (8.78); this is the reason why we have this transient behaviour only for $k > 0.1$. It is more difficult to determine the growth rate in this case; we can not run the simulation longer (the electrode will be reached), so we use the data up to $t = 100$ and use different starting points for the fit, to see whether the inclination of the curve converges to a constant. The uncertainty of the starting point of the fitting procedure is reflected in the error bars in Figure 8.6 which are almost absent for small k and increase for larger k, as expected.
Figure 8.6 shows the dispersion relation from this section together with the curve obtained in Section 8.7.2. Especially for small values of k up to the maximum of $s(k)$, the agreement is very good.
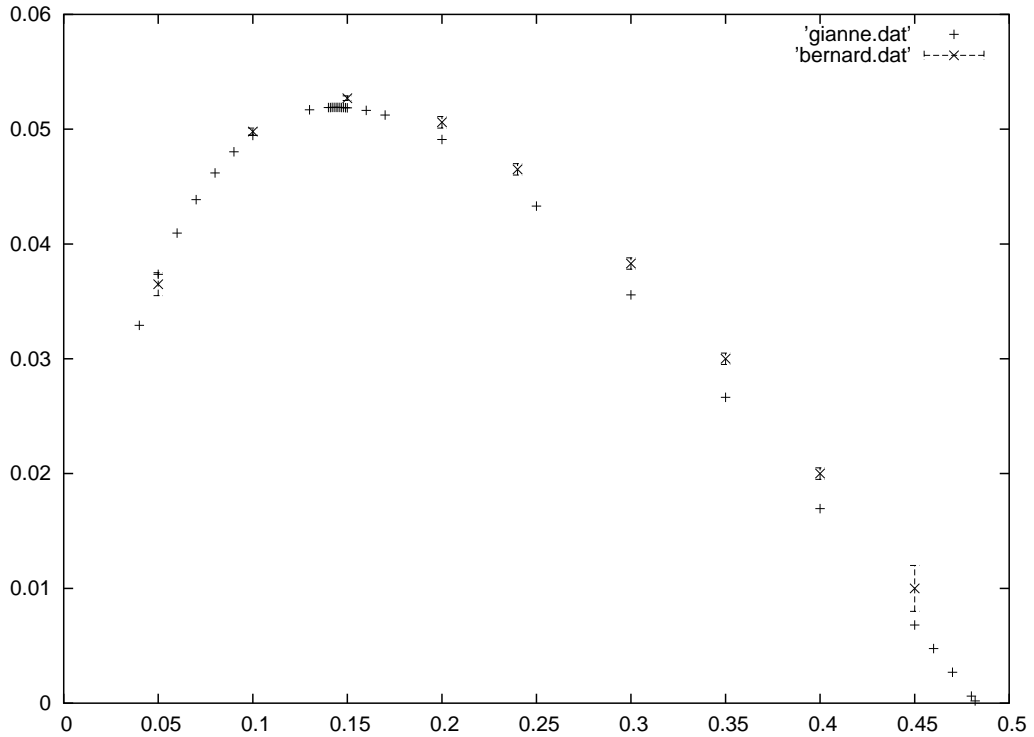
Figure 8.6: The dispersion relation obtained in two different ways; crosses for the intial value problem and plus-signs for the eigenvalue problem, $E_0 = 1$ and $D = 0.1$.

We have to make several approximations which will be discussed; discretization of space and time and choice of the start of the fit. The choice of δ can play a role too. Doubling the number of gridpoints in both spatial directions meant lowering the value of $s(k)$ a few percents, for large k. The timestep does not influence the outcome. We need to chose δ large enough that the perturbation is visible and small enough to stay in the linear regime. For $k > 0.2$, it takes longer to reach the eigenperturbation, which means that the value $s(k)$ picks up some information of the transients and becomes too high. We conclude that the values $s(k), k > 0.2$ can be viewed as upper bounds, which agrees nicely with the results in Section 8.7.2.

8.7.2   Numerical solution of the eigenvalue problem

The dispersion relation $s(k)$ for $D \neq 0$ can also be treated as an eigenvalue problem: it is defined by the ansatz $\mathbf{U}_1(z,t) = \mathbf{U}_k(z)e^{st}$ inserted into the PDE's of the linear perturbation supplemented with the boundary conditions at $z \to \pm\infty$. The problem was solved numerically by Gianne Derks [51]. Denote the 0th order solution as σ_0 etc. and define $f_0 = E_0 e^{-1/E_0}$. Let the vector $\mathbf{w}$ contain the physical fields:

$$\mathbf{w} = \begin{pmatrix} \partial_\zeta \sigma \\ \sigma \\ \rho \\ E \\ \phi \end{pmatrix} \tag{8.81}$$

then the equation

$$\partial_\zeta \mathbf{w} = \mathbf{A}[\zeta; E_0, k, s]\mathbf{w}, \tag{8.82}$$

where the matrix $\mathbf{A}$ is given in terms of the planar solution, k, s, D and $v = E_0 + 2\sqrt{Df_0}$

$$\mathbf{A} = \begin{pmatrix} \frac{E_0-v}{D} & \frac{2\sigma_0-\rho_0-f_0+s+Dk^2}{D} & -\frac{\sigma_0}{D} & -\frac{\partial_\zeta \sigma_0-\sigma_0 f_0'}{D} & 0 \\ 1 & 0 & 0 & 0 & 0 \\ 0 & -\frac{f_0}{v} & \frac{s}{v} & \frac{\sigma_0 f_0'}{v} & 0 \\ 0 & -1 & 1 & 0 & -k^2 \\ 0 & 0 & 0 & -1 & 0 \end{pmatrix} \tag{8.83}$$

defines the eigenvalueproblem. For $\zeta \to -\infty$ two conditions are given: $\rho = \sigma$ and $E = 0$; for $\zeta \to \infty$ three conditions are given: $\rho = \sigma = E = 0$. Together with the gauge invariance of ϕ (the sixth condition), the eigenvalue problem (8.82) is fully specified. For further details on the numerical solution strategy I refer to [51]. The resulting curve $s(k)$ is plotted in figure 8.6.

Chapter 9

Conclusion

A minimal streamer model has been derived; PDE simulations motivated the application of a moving boundary approximation and led to the main question of this thesis: can we analyze streamer propation and branching using a moving boundary approximation. The unregularized problem was analyzed and reduced to a system of ODE's. Unphysical cusps were present in the solutions; this was not surprising, since a regularization mechanism was missing. Cusp formation is inevitable in an unregularized problem; this is known from viscous fingering. A new boundary condition on the interface was derived from the microscopic PDE's, a mixed Dirichet-Neumann condition, which took the width ϵ of the boundary layer into account. From viscous fingering it is known that simulating the regularized problem is a demanding numerical problem. Instead of going into this problem we decided to formulate a different problem first: is the new boundary condition able to regularize the moving boundary problem?

Points where the cusps form on the interface coincide with the points where the mapping function looses its conformality. The dynamics of those points was traced and it was shown in some example that indeed generically cusp formation was inevitable in the unregularized case. The results for the short time dynamics of the regularized case were promising but inconclusive. However, we were able to derive an explicit, analytic solution of the regularized problem: the uniformly translating circle. The next step was the study of the linear stability of the circle. We were able to solve the regularized PDE's analytically for $\epsilon = 1$ in this case. The analytic solutions show that the circle is convectively stable; a perturbation can be amplified initially but is convected away to the back where it dies out. This is exactly the same scenario observed numerically and experimentally in viscous fingering. We can get further, since we have analytic solutions. In particular, we can derive the slow manifold on which the perturbation decays for $t \to \infty$. The stability of the circle is surprising as the planar front is unstable against perturbations of any wavelength. For viscous fingering, the regularization allows only a finite band of wave lengths to destabilize a planar front. For this reason a stronger regularization for the streamer was derived in the last chapter, but this regularization in the end was not needed.

The conservation of the analyticity of the mapping function was solved in a natural way, using a mode expansion. This led to erroneous conclusions on temporal eigenfunctions and might cause erroneous results in the PDE-solutions of the full moving boundary problem. Recent discussions with S. Tanveer showed that these problems are specific to our regularization and do not appear with surface tension regularization. It is possible to conserve the analyticity of a function using the so called Hilbert transform. This would be a logical next step to continue the investigation of both the linear stability of the circle for $\epsilon < 1$ and the full problem. Results of L. Schaefer for the linear stability analysis of the circle for $\epsilon < 1$ show that the convective stability is a generic feature of the problem for all $\epsilon > \frac{1}{20}$. The explicit solutions for $\epsilon = 1$ can be used to test the numerical code; they can serve as a gauge point. Another interesting question is whether other attractors with a different geometry exist, e.g. half infinite finger like streamers.

The answer to the central question of this thesis, can a moving boundary approximation be used to describe streamer propagations and branching, is summarized as follows. The model is able to describe streamer propagation but stays numerically challenging. The scenario for branching can be summarized as follows: the unregularized problem does show the onset of branching for any perturbation, but then develops unphysical cusps. The regularized problem shows that linear perturbations of curved fronts are convected away. Therefore, only a finite perturbation can lead to branching. The bassin of attraction of propagating and branching solutions as well as the size and form of generic physical perturbations need to be determined.

Bibliography

[1] C.T.R. Wilson, Proc. Phys. Soc. London **37**, 32D-37D (1925).

[2] H.T. Su *et al.*, Nature **423**, 974-976 (2003).

[3] V.P. Pasko, Nature **423**, 927-929 (2003).

[4] V.P. Pasko *et al.*, Nature **416**, 152-154, (2002).

[5] E.G. Gerken, U.S. Inana and C.P. Barrington-Leigh, Geophys. Res. Lett. **27**, 2637-2640 (2000).

[6] T.M.P. Briels *et al.*, Branching of streamer type corona discharge, Proc. XIV Int. Conf. Gas Discharges and Appl., (2002)

[7] C. Montijn, Evolution of negative streamers in nitrogen: a numerical investigation on adaptive grids, Ph.D. Thesis, TU Eindhoven, Dec. 05.

[8] U.Ebert, W. van Saarloos and C. Caroli Phys. Rev. Lett. **77**, 4178-4181, (1996).

[9] U.Ebert, W. van Saarloos and C. Caroli Phys. Rev. E **55**, 1530-1549, (1997).

[10] U. Ebert and W. van Saarloos, Phys. Rep. **337**, 139-156 (2000).

[11] D. Bensimon, L.P. Kadanoff, S. Liang, B.I. Shraiman, and C. Tang, Rev. Mod. Phys. **58**, 977-999 (1986).

[12] M. Arrayas and U. Ebert, Phys. Rev. E **69**, 036214 (2004).

[13] A. Rocco *et al.*, Phys. Rev. E **66**, 035102 (2002).

[14] M. Arrays, U. Ebert, W. Hundsdorfer, Phys. Rev. Lett. 88, 174502 (2002),

[15] P.G. Saffman and G. Taylor, Proc.R.Soc. London Ser.A **245**, 312 (1958).

[16] G. Taylor and P.G. Saffman, Quart.J.Mech.and Appl. Math. **12**, 265 (1959).

[17] J.W. McLean and P.G. Saffman, J. Fluid Mech. **102**, 455-469 (1981).

[18] J.-M. Vanden-Broeck, Phys. Fluids **26**, 2033-2034 (1983).

[19] R. Combescot *et al.*, Phys. Rev. Lett. **56**, 2036 (1986).

[20] B. Shraiman and D. Bensimon, Phys. Rev. A **30**, 2840-2842 (1984).

[21] S.K. Sarkar, Phys. Rev.A **31**, 3468-3469, (1985).

[22] D. Bensimon, Phys. Rev.A **33**, 1302-1309, (1986).

[23] D. Bensimon and P. Pelce, Phys. Rev. A **33**, 4477-4478, (1986).

[24] D.A. Kessler and H. Levine, Phys. Rev. A **33**, 2621-2633 (1986).

[25] D.A. Kessler and H. Levine, Phys. Rev. A **33**, 2634-2639 (1986).

[26] A.J. Degregoria, L.W. Schwartz, J. Fluid. Mech. **164**, 383-400 (1986)

[27] P. Tabelling *et al.*, J. Fluid. Mech. **177**, 67-82 (1987).

[28] Y. Couder *et al.*, Phys. Rev. A **34**, 5175-5178 (1986).

[29] E. Ben-Jacob et all, Phys. Rev. Lett. **55**, (1985).

[30] S. Tanveer, Phys. Fluids **29**, 3537-3548 (1986).

[31] S. Tanveer, Phys. Fluids **30**, (3), 651-658 (1987).

[32] M. Siegel and S. Tanveer, Phys. Rev. Lett. **76**, 419 (1996).

[33] S.D. Howison, Proc. Roy. Soc. Edinburgh, **102A**, 141-148 (1986).

[34] S.D. Howison, Eur. J. Appl. Math. **3**, 209-224 (1992).

[35] Y.E. Hohlov and S.D. Howison, Q. Appl. Math. **51**, 777-789 (1993).

[36] K.V. McCloud and J.V. Maher, Phys. Rep. **260**, 139-185 (1995).

[37] G.L. Vasconselos, Phys. Rev. E **50**, R3306-R3309 (1994).

[38] G.L. Vasconselos, Phys. Rev. E **62**, R3047-R3050, (2000).

[39] D.A. Kessler and H. Levine, Phys. Rev. Lett. **86**, 4532-4535 (2001).

[40] J. Casademunt and F.X. Magdaleno, Phys. Rep. **337**, 1-35 (2000).

[41] J. Casademunt, Chaos **14**, 809-823 (2004).

[42] S. Richardson, J. Fluid Mech. **56**, 609-618 (1972).

[43] V. Entov, P.I. Etingof and D.Y. Kleinbock, Eur. J. Appl. Math. **4**, 97-120 (1993).

[44] Q. Nie and F.-R. Tian, SIAM J. Appl. Math. **62**, 385-406 (2001).

[45] B. Meulenbroek *et al.*, Phys. Rev. Lett. **90**, 024502 (2003).

[46] B. Meulenbroek *et al.*, J. Non-Newt. Fluid Mech. **116**, 235 (2004).

[47] B. Meulenbroek *et al.*, Phys. Rev. E **69**, 067402 (2004).

[48] B. Meulenbroek *et al.*, Phys. Rev. Lett. **90**, 195004 (2005).

[49] C. Montijn *et al.*, IEEE Trans. Plasma Science **33**, 260-261 (2005).

[50] U. Ebert *et al.*, Plasma Sources Science and Technology, in print.

[51] G. Derks *et al.*, [in preparation].

[52] U.Ebert en F. van der Lijn, Zenit, 12-15 januari 2005.

[53] Wetenschapsbijlage van de Volkskrant, 7 mei 2005.

[54] Net als Prof. Terwiel, die in zijn eerste college quantummechanica een samenvatting gaf, die te begrijpen was voor de geletterde leek, onder meer gebruik makend van Hilbertruimtes.

[55] Functions of a complex variable, Carrier, Crook and Pearson, McGraw-Hill (1966).

[56] The Schwarz function and its applications, Davis, Mathematical association of America (1974).

[57] Conformal representation, Caratheodory, Cambridge University press London (1932).

[58] Numerical recipes in Fortran, second edition, Cambridge University press (1992).

[59] Pattern formation and dynamics in nonequilibrium systems, Greenside and Cross.

Summary

Patterns occur in nature on all scales; an example on a large scale is the distribution of galaxies in the universe. They are neither clumped together in a massive black hole nor distributed uniformly through space. Denser regions are separated from each other by almost empty regions. A more familiar example can be encountered on the beach: a pattern of regular sand ripples. These exist in a sand desert as well on a larger scale where sand dunes several kilometers from each other are formed. The structure of a snow flake is an example of pattern formation on a very small scale. The patterns I studied are on a scale somewhere in between: electric discharges in the atmosphere. The most familiar example is lightning, but above a thunder cloud a large variety of discharges can be seen as well. Those events were reported only a couple of years ago, which is not surprising, since they tend to be obscured by the much brighter lightning flashes and, of course, by the clouds. Those discharges were named 'transient luminous events' (TLE's) or more fanciful: sprites, jets and elves. An article about those TLE's appeared in Zenit and de Volkskrant [53]. A telescopic image of a sprite shows an inner structure of the sprite: it consists of a number of channels which are believed to be so called 'streamers': an ionized channel with an active, charged head. The basic idea of a discharge is quite simple: when a large electric field is imposed on a nonionized medium (air), free electrons will be accelerated and collide with neutral molecules. This can lead to ionization of the molecules and the release of a new electron, thus leading to an avalanche of electrons: the initially nonionized region becomes ionized. The electrons can not be observed directly, but they excite the molecules as well. The excited molecules emit a photon when returning to their ground state: those photons can be observed.

Our goal is to find a theoretical model which describes propagation and branching of streamers. Physical models are typically reductionistic: one tries to identify the essential mechanisms and investigates whether the correct physics is retrieved. We will follow this line and derive a 'minimal' model for streamers, which incorporates the following ingredients: only one ionization reaction, electrostatic interactions and mobile electrons that carry the current. This results in partial differential equations (PDE's) which in general need to be solved by numerical computation. The numerical results do indeed show streamer propagation and branching, but the accuracy of the numerical scheme was challenged: one may be looking at some numerical artefact instead of some real physical in-

stability. Analysis of the minimal model is required: the numerical analysis did give an idea for an analytic approach. It showed that space was divided in two regions: the ionized tail of the streamer was separated from the nonionized surroundings by a very thin space charge layer. This suggested a moving boundary approximation. I will explain the idea of this method with its application to a different physical system: viscous fingering. (In pattern formation, similar methods can often be applied to systems which are physically quite different. Similar equations have similar solutions.)

Consider two horizontal glass plates which are placed very close to each other with closed side walls. When water flows between the plates, it can be viewed from above; since the plates are close together, this flow can be considered two dimensional. Such a device is called a Hele-Shaw cell. When water is injected in a long stretched empty cell, not much happens and the water simply expels the air. When the experiment is performed the other way around, injection of air in a cell filled with water, something completely different happens: a finger of air forms in the cell which is about half the width of the channel (thus: viscous fingering). This is because a planar interface between water and air is unstable if the air is pushing: small perturbations will grow and disturb the interface. Since the air and the water hardly mix, the problem is fully specified by the position of the interface; subsequently, the temporal evolution is fully determined by the motion of the interface. This reduction of the problem is called a moving boundary approximation. This is even more convenient, because the problem is two dimensional; I will explain this for the more mathematically inclined reader. The pressure has to satisfy the Laplace equation in the water region. Complex analysis can be used since the problem is two-dimensional. Solving the Laplace equation is equivalent to finding an analytic function, the complex potential. The real part of this function corresponds to the pressure and automatically satisfies the Laplace equation. Finding an analytic function on a moving domain is hard as well, though. It is possible to apply the Riemann mapping theorem, which states that (under some conditions) any region in $\mathbb{C}$ can be mapped onto the unit disc. Since a composition of analytic functions is analytic, one only has to find the potential on the unit disc (which is standard) and determine the mapping function. Unfortunately, the Riemann mapping theorem is not constructive; the hard part of the problem is the determination of the mapping function. Once this function is determined, it can be evaluated on the unit circle, which yields the interface.

This gave some remarkable results in viscous fingering; fingers were indeed solutions, but any width of the finger would do; why was the finger whose width was about half of the channel selected? This problem was solved about thirty years later: when surface tension was added to the problem, it turned out that the finger with the appropriate width was selected. This is remarkable, since a microscopic mechanism (surface tension) caused a macroscopic selection. This finger is convectively stable, which means that perturbations of the finger may grow, but are convected away to the back of the finger where they die out. This was observed both numerically and experimentally.

Let me get back to the streamer problem; we can apply this machinery if we

study the streamer in two dimensions. The air region corresponds to the ionized region and the water region to the air region, the pressure needs to be replaced by the electric potential and we have almost the same equations. Conformal mapping can be applied, the equation of motion of the mapping function is the same as in the viscous fingering case. The big problem was the analogue of the surface tension, which is evidently very important. To find the 'surface tension', the so called regularization mechanism, we returned to the original microscopic PDE's and used the width of the charge layer as a regularization parameter. Since solving the regularized moving boundary problem is still challenging, we wondered whether we had the correct regularization: does it indeed stabilize? We were able to show that it causes a convective stabilization, which is similar to viscous fingering. We were able to get further than that, since we were able to derive the temporal evolution of arbitrary perturbations of a particular shape up to time infinity.

Samenvatting

Patronen zijn in de natuur te vinden in allerlei ordes van grootte. Een voorbeeld van een patroon op grote schaal is de verdeling van sterrenstelsels in het universum. Ze zijn noch samengeperst in een groot zwart gat, noch uniform verdeeld in de ruimte. Dichter bevolkte gebieden worden afgewisseld met vrijwel lege gebieden. Een bekender voorbeeld komen we tegen op het strand: een patroon van regelmatige heuveltjes zand. Deze heuvels bestaan ook in een zandwoestijn waar zandduinen enkele kilometers van elkaar gevormd worden. De structuur van een sneeuwvlok is een voorbeeld van een patroon op een heel kleine schaal. De patronen die ik bestudeerd heb, zijn op een schaal hier ergens tussenin: elektrische ontladingen in de atmosfeer. Het bekendste voorbeeld hiervan is bliksem, maar ook boven de onweerswolk kan een aantal verschillende soorten ontladingen waargenomen worden. Pas een aantal jaar geleden zijn deze fenomenen voor het eerst waargenomen en gerapporteerd. Dit is niet zo vreemd, aangezien ze moeilijk te zien zijn door de veel heldere bliksemflitsen en de aanwezigheid van de onweerswolken die het zicht belemmeren. Deze ontladingen werden 'transient luminous events' (TLE's) genoemd, of met wat meer fantasie, sprites, jets en elves. Een artikel over deze TLE's is verschenen in Zenit en de Volkskrant [53]. Een opname met behulp van een telescoop van een sprite onthult de inwendige structuur van de sprite; die bestaat uit een aantal kanalen waarvan men gelooft dat het zogenaamde 'streamers' zijn: een geioniseerd kanaal met een geladen kop. Het basisidee van een gasontlading is vrij eenvoudig: als een niet-geioniseerd medium (zoals lucht) wordt blootgesteld aan een hoog elektrisch veld, zullen vrije electronen versneld worden en botsen met neutrale moleculen. Zo'n botsing kan leiden tot de ionisatie van het molecuul, waarbij een extra electron vrijkomt. Op deze manier ontstaat een lawine van electronen en wordt het medium geioniseerd. Deze electronen zijn niet zichtbaar, maar naast dat ze moleculen ioniseren, slaan ze soms ook moleculen aan en geraken deze in een hogere energietoestand. Wanneer de moleculen weer terugvallen naar de grondtoestand, zenden ze een foton uit. Deze fotonen kan men wel zien.

Het doel van dit proefschrift is het vinden van een model om de propagatie en splitsing van streamers te beschrijven. Natuurkundige modellen zijn meestal reductionistisch van aard: men probeert de essentiele mechanismes de vinden en kijkt of een model met alleen deze mechanismes de correcte natuurkunde beschrijft. We benaderen dit probleem op dezelfde manier en proberen een 'minimaal' model voor streamers te construeren, waar alleen de volgende

ingrediënten in zitten: slechts één ionisatiereactie, elektrostatische interacties
en bewegende electronen die de stroom transporteren. Dit resulteert in partiële
differentiaalvergelijkingen (PDE's) die over het algemeen met een numerieke
code opgelost moeten worden. Deze numerieke resultaten laten inderdaad pro-
pagatie en splitsing van streamers zien, maar de numerieke resultaten werden
ter discussie gesteld: is er hier sprake van een numeriek artefact of is er een
echte fysische instabiliteit? Analyse van het minimale model is noodzakelijk en
de numerieke resultaten gaven een idee voor een analytische aanpak. Deze resul-
taten toonden dat de ruimte verdeeld is in twee gebieden: de geioniseerde staart
van de streamer, gescheiden van de niet-geioniseerde lucht door een dun geladen
laagje. Dit bracht ons op het idee van een zogenaamde moving boundary ap-
proximation. Aan de hand van een ander fysisch probleem, viscous fingering, zal
ik deze methode uitleggen. (Wanneer vorming van patronen bestudeerd wordt,
kunnen vaak gelijksoortige methodes worden toegepast op systemen die fysisch
verschillend zijn.) Neem twee horizontale, parallele platen van glas die dicht bij
elkaar geplaatst worden en maak de zijkanten dicht. Wanneer water tussen de
beide platen stroomt, kan men hier van boven naar kijken en omdat de platen
dicht bij elkaar zijn, is de stroming bijna tweedimensionaal. Een dergelijk appa-
raat wordt een Hele-Shaw cell genoemd. Als water door een lang kanaal geperst
wordt, gebeurt er niet veel bijzonders en wordt de lucht uit het kanaal geduwd.
Wanneer men dit experiment nu andersom doet en probeert water met behulp
van lucht uit het kanaal te persen, gebeurt er iets heel anders. Een vinger
van lucht vormt zich in het kanaal, waarvan de breedte ongeveer de helft van
het kanaal is. Vandaar de naam, viscous fingering. Dit komt omdat een vlak
water-lucht grensvlak instabiel is, wanneer de lucht geperst wordt: kleine ver-
storingen van het grensvlak zullen groeien en de vorm van het grensvlak veran-
deren. Aangezien water en lucht nauwelijks mengen, bepaalt de positie van dit
grensvlak het probleem volledig, dit impliceert dat het tijdsafhankelijke gedrag
van het probleem volledig bepaald wordt door de beweging van het grensvlak.
Een dergelijke vereenvoudiging van het probleem wordt een 'moving bound-
ary approximation' genoemd. Dat is hier nog handiger, aangezien het probleem
tweedimensionaal is: ik zal dit uitleggen voor de lezers met wat meer wiskundige
bagage. In het water moet de druk voldoen aan de Laplacevergelijking. Com-
plexe analyse kan toegepast worden, omdat het probleem tweedimensionaal is.
Oplossen van de Laplacevergelijking is dan equivalent met het vinden van een
analytische functie, de complexe potentiaal. Het reële deel van deze potenti-
aal correspondeert dan met de druk en voldoet automatisch aan de Laplace
vergelijking. Een analytische functie vinden op een bewegend gebied is ook
moeilijk. Het is mogelijk om het Riemann mapping theorem te gebruiken, dat
zegt dat, onder bepaalde voorwaarden, elk gebied in $\mathbb{C}$ afgebeeld kan worden op
de schijf met straal 1. Deze afbeelding is conform en dus analytisch; aangezien
een compositie van analytische functies weer analytisch is, hoeft alleen maar
een analytische functie gevonden te worden op de schijf (en dat is standaard).
Helaas is het Riemann mapping theorem niet constructief: het lastige deel van
het probleem is het bepalen van de mappingfunctie. Wanneer die bepaald is,
kan deze geëvalueerd worden op de eenheidscirkel, wat het grensvlak oplevert.

Deze methode gaf enkele opmerkelijke resultaten in het viscous fingering-probleem: vingers waren inderdaad oplossingen van de vergelijkingen, maar elke willekeurige breedte was een oplossing: waarom werd nu de halve breedte van het kanaal geselecteerd? Dit probleem werd ongeveer dertig jaar later opgelost. Wanneer oppervlaktespanning aan het model werd toegevoegd, werd automatisch de juiste λ geselecteerd. Dit is opmerkelijk, aangezien een microscopisch mechanisme (oppervlaktespanning) zorgt voor een macroscopische selectie. Deze vinger is convectief stabiel, wat betekent dat verstoringen van de vinger wel kunnen groeien, maar tegelijkertijd naar de achterkant weggeconvecteerd worden, waar ze verdwijnen. Dit werd zowel experimenteel als numeriek waargenomen. Nu kom ik terug bij het probleem van de streamer; we kunnen deze hele machinerie gebruiken als we het probleem in twee dimensies bekijken. De lucht correspondeert dan het het geioniseerde gebied en het water met het neutrale gebied (de lucht). De druk moet vervangen worden door de electrische potentiaal. Dit levert dan bijna dezelfde vergelijkingen op. Een conforme afbeelding kan weer gebruikt worden, de bewegingsvergelijking voor de mappingfunctie is dezelfde als die in het geval van viscous fingering. Het grote probleem was het vinden van het analogon van oppervlaktespanning, die zeker een grote rol speelde bij het oplossen van het probleem van viscous fingering. Om onze 'oppervlaktespanning' te vinden, het zogenaamde regularisatiemechanisme, bekeken we opnieuw de microscopische PDE's. We gebruikten de breedte van het laagje met lading als regularisatieparameter. Aangezien het oplossen van een moving boundary-probleem nog steeds erg lastig is, vroegen we ons eerst af of deze parameter het probleem wel kon regulariseren. We hebben aangetoond dat deze regularisatie inderdaad zorgt voor een convectieve stabilisatie, net als bij viscous fingering. We zijn zelfs wat verder gekomen, omdat we de verstoring van een bepaalde vorm willekeurig lange tijd analytisch kunnen berekenen.

Acknowledgements

Curriculum Vitae

De auteur van dit proefschrift werd geboren op 1 mei 1978 te Voorburg. Hij behaalde in 1996 zijn gymnasium diploma aan de Christelijke Scholengemeenschap Walcheren (CSW) te Middelburg en vervolgde zijn opleiding aan de Universiteit Leiden. Daar studeerde hij in 2000 af in de Wiskunde bij prof.dr. B. Peletier op de scriptie 'Periodic solutions of a fourth order equation' en in 2001 in de Natuurkunde bij prof.dr. W. van Saarloos op de scriptie 'On the stability of sheared polymeric flows'.

Het promotieonderzoek verrichtte hij als onderzoeker in opleiding van november 2001 tot mei 2006 aan het Centrum voor Wiskunde en Informatica te Amsterdam; dit onderzoek werd afgesloten met dit proefschrift. Het onderzoek stond onder leiding van prof. dr. U.M. Ebert.